8-2018

Organization and development of cholinergic input to the mouse visual thalamus.

Guela Sokhadze
University of Louisville

ORGANIZATION AND DEVELOPMENT OF CHOLINERGIC INPUT TO THE MOUSE VISUAL THALAMUS

By

Guela Sokhadze

B.S., University of Louisville, 2011

A dissertation submitted to the Faculty of School of Medicine of the University of Louisville in Partial Fulfillment of the Requirements for the Degree of

Doctor of Philosophy in Anatomical Sciences and Neurobiology

Department of Anatomical Sciences and Neurobiology
University of Louisville
Louisville, Kentucky

August 2018

ORGANIZATION AND DEVELOPMENT OF CHOLINERGIC INPUT TO THE MOUSE VISUAL THALAMUS

By

Guela Sokhadze

B.S., University of Louisville, 2011

A Dissertation Approved on 6/14/2018

By the following members of the Dissertation Committee:

_____

William Guido, Ph.D.

_____

Martha Bickford, Ph.D.

_____

Robin Krimm, Ph.D.

_____

Nicholas Mellen, Ph.D.

_____

Bart Borghuis, Ph.D.

_____

Robert Lundy, Ph.D.

DEDICATION

This dissertation is dedicated to my parents

Estate Sokhadze and Eva Lamina

ACKNOWLEDGEMENTS

I would like to thank my advisor Dr. William Guido. I am extremely grateful for his mentorship, advice, patience, and encouragement over the years. I would also like to thank the members of my committee, Dr. Martha Bickford, Dr. Robin Krimm, Dr. Nicholas Mellen, Dr. Bart Borghuis, and Dr. Robert Lundy, for providing important feedback which was essential for the completion of this dissertation. I would like to thank all members of Dr. Guido's Lab, including Peter Campbell, Naomi Charalambakis, Barbara O'Steen, and Govin Govindaiah for all their help, encouragement, and friendship. I would also like to extend my appreciation to members of Dr. Bickford's Lab, especially Sean Masterson, Na Zhou, and Ark Slusarczyk who provided me with valuable training in electrophysiology, immunohistochemistry, and anatomical tracing techniques. Finally, I'd like to thank my parents Estate Sokhadze and Eva Lamina for their love and support, and for giving me an opportunity to pursue an academic career.

ABSTRACT

ORGANIZATION AND DEVELOPMENT OF CHOLINERGIC INPUT TO THE MOUSE VISUAL THALAMUS

Guela Sokhadze

June 14th, 2018

Cholinergic signaling plays a vital role in modulating the flow of sensory information through thalamic circuits in a state-dependent manner. In the dorsal lateral geniculate nucleus (dLGN), the thalamic visual relay, release of acetylcholine (ACh) contributes to enhanced thalamocortical transfer of retinal signal during behavioral states of arousal, wakefulness, and sleep/wake transitions. Moreover, ACh modulates activity of the thalamic reticular nucleus (TRN), a structure which provides inhibitory input to dLGN. While several cholinergic nuclei have been shown to innervate dLGN and TRN, it is unclear how projections from each area are organized. Furthermore, little is known of how or when cholinergic fibers arrive and form functional synapses during development. To address these questions, we used a genetically modified mouse (ChAT-Cre) mouse to selectively visualize cholinergic projections to dLGN and TRN. We conducted anterograde viral tracing, demonstrating a mainly contralateral cholinergic projection from the parabigeminal nucleus to dLGN. In addition, we saw a sparse ipsilateral projection from the rostral pedunculopontine tegmentum to dLGN and TRN. Next, we used a fluorescent reporter line (Ai9) to visualize cholinergic innervation in dLGN and TRN during early postnatal life. In

dLGN, innervation began by the end of the first week, increased steadily with age, and reached an adult-like state by the end of the first month. Furthermore, using a model of visual deafferentation (*math5*$^{-/-}$), we showed that the absence of retinal input resulted in disruptions in the trajectory, rate, and pattern of cholinergic innervation in dLGN. In TRN, innervation began during week 1 in the ventral non-visual sectors, proceeded into the dorsal visual sector during week 2, and reached adult-like levels by week 3. To assess the functional maturation of cholinergic synapses within TRN, we used a channelrhodopsin-2 reporter and selectively stimulated cholinergic afferents while conducting recordings from TRN neurons. Postsynaptic responses appeared in non-visual sectors of TRN during the first postnatal week, and in the visual sector by week 2. By the end of the first month, all sectors of TRN exhibited adult-like biphasic responses. Together, these studies shed light on the organizational pattern and developmental progression of cholinergic input to the visual thalamus.

TABLE OF CONTENTS

LIST OF FIGURES

INTRODUCTION

The flow of sensory information from the thalamus to the cortex is actively gated, with the thalamocortical (TC) transmission of sensory signal depending on the animal's current behavioral state (McCormick et al., 2015). Periods of wakefulness and arousal are accompanied by enhanced transfer of sensory signal, while during sleep and quiescence, sensory transmission is greatly attenuated (Sherman & Guillery, 2002; Lee & Dan, 2012). In the visual system, retinal information is relayed to the cortex via the dorsal lateral geniculate nucleus (dLGN) of the thalamus. While the retinal ganglion cells (RGCs) provide the main excitatory drive to dLGN, nonretinal inputs make up over 90% of the total synapses, and work in concert to modulate the responsiveness of dLGN TC relay neurons to incoming retinal input (Sherman & Guillery, 1996). A major modulatory projection arises from the cholinergic nuclei of the brainstem, accounting for up to ~25% of all dLGN synapses in some species (Erisir et al., 1997b). In addition, cholinergic projections target the thalamic reticular nucleus (TRN), a sheet-like structure of GABAergic neurons which send inhibitory projections to dLGN, as well as other nuclei of the dorsal thalamus (Hallanger et al., 1987; Pinault, 2004; Jones, 2007; Beierlein, 2014). While the role of cholinergic signaling within visual thalamic circuits has been thoroughly explored

in rodents and other species (Prince & McCormick, 1986; McCormick, 1992; Uhlrich, 1997; Zhu & Uhlrich, 1998; Zhu & Heggelund, 2001; Yang et al., 2015), less is known of the pattern of connectivity between the distinct cholinergic nuclei and the visual thalamus. Furthermore, little is known of when or how these cholinergic inputs arise during early life, or whether their development is regulated by retinal input. Here we address these questions by using the mouse visual system as a model to examine the organization and development of cholinergic projections to dLGN, TRN, and other nuclei of the visual thalamus.

In the past decade, the mouse has become a popular model for studying the form and function of visual thalamic circuits (Guido, 2008; Bickford et al., 2010; Hong and Chen, 2011; Seabrook et al., 2013; Kerschensteiner & Guido, 2017). The numerous genetic manipulations available in mice allow for novel experimental approaches in the research of sensory circuit organization and function. For example, specific populations of neurons can be selectively visualized using fluorescent proteins, and/or activated using optogenetic constructs (Madisen et al., 2010 & 2012; Zhao et al., 2011). Moreover, genetic knock-out mouse lines can be used to conduct loss-of-function studies (Bouabe & Okkenhaug, 2013). Since many aspects of the visual system are conserved across mammalian species, studies in mice are useful for understanding of fundamental organizing principles of mammalian visual circuits.

In mouse, like all mammals, visual signal is carried centrally by the axons of retinal ganglion cells (RGCs). After partially crossing at the optic chiasm (OX), retinal axons from each eye arrive in the dLGN. The diagram in Figure 1 outlines

the thalamocortical circuit, as well as the ascending modulatory inputs to dLGN and TRN. The TC relay neurons of dLGN transmit information to the primary visual cortex (V1), which in turn sends descending corticothalamic (CT) projections back to dLGN (Sherman & Guillery, 2002; Jones, 2007; Jones, 2009). Furthermore, dLGN receives inhibitory projections from GABAergic neurons of TRN (Coleman & Mitrofanis, 1996; Guillery et al., 2003). TRN itself is innervated chiefly by the collaterals of TC and CT axons (Pinault, 2004). In addition to cortical and thalamic connections, dLGN and TRN receive ascending innervation arising from multiple sources. The main ascending projections to dLGN include superior colliculus (SC), pretectum (PT), and the brainstem (Montero, 1991; Van Horn et al., 2000; Sherman & Guillery, 2002). The TRN receives ascending innervation from the brainstem, as well as globus pallidus, hypothalamus, and basal forebrain (Hallanger et al., 1987; Bickford et al., 1994; Sun et al., 2012; Herrera et al., 2016). While the brainstem and basal forebrain nuclei contain populations of neurons which use various neurotransmitter systems (acetylcholine, glutamate, & GABA), the projection to the thalamus is mainly cholinergic (Do et al., 2016; Kroeger et al., 2017).

In dLGN, cholinergic projections target both cell types of dLGN, the TC relay neurons and intrinsic inhibitory interneurons (Ahlsen et al., 1984; Hallanger et al., 1990; Erisir et al., 1997b; Uhlrich, 1997; Zhu & Heggelund, 2001). The TC relay neurons are glutamatergic, have large somata, radial dendrites, and a myelinated axon which projects to the visual cortex (Sherman & Guillery, 2001; Budd, 2004). The inhibitory interneurons are GABAergic, with small somata, and

long bipolar processes which contact TC relay neurons (Webster & Rowe, 1984; Sherman, 2005). TC relay neurons and inhibitory interneurons express different subtypes of cholinergic receptors, and therefore exhibit distinct responses to acetylcholine (ACh). In TC relay neurons, ACh evokes depolarization through nicotinic ACh receptors (nAChRs), a ligand-gated mixed cation channel (Prince & McCormick, 1986; Uhlrich, 1997). Moreover, TC relay neurons express M1 muscarinic acetylcholine receptors (mAchRs), a G protein-coupled metabotropic receptor which mediates slow depolarization through regulation of potassium channels (Zhu & Uhlrich, 1998). By contrast, interneurons express M2 mAChRs, and respond to ACh with slow metabotropic hyperpolarization (Ahlsen, 1984; McCormick & Pape, 1988; Antal et al., 2010). Thus, the overall effect of ACh on dLGN is excitatory, mediated by combined depolarization of TC relay neurons and hyperpolarization of intrinsic interneurons.

Cholinergic inputs, like other nonretinal modulatory projections to dLGN, have been shown to facilitate the switch between tonic and burst firing mode in TC relay neurons (McCormick & Feeser, 1990; Steriade, 1990; Lu et al., 1993; Godwin et al., 1996; Sherman, 2001; Bista et al., 2012). At a relatively depolarized resting membrane potential (RMP), TC relay neurons exhibit tonic firing, meaning their action potential firing closely approximate the frequency of retinal input in a linear manner (Lo et al., 1991; McCormick, 1992; Lu et al., 1993). At hyperpolarized RMP (V_M < - 70 mV) TC neurons fire in burst mode, with multiple action potentials riding on a calcium spike mediated by low-threshold T-type Ca^{2+} channels (Deschenes et al., 1984; Crunelli et al., 1989). Burst firing is

a non-linear response mode, associated with sleep states, and also during initial stimulus detection (Sherman & Guillery, 1998; Zhan et al., 1999; Sherman, 2001). Generally, increased cholinergic tone during periods of arousal and wakefulness promotes tonic firing in TC relay neurons, while decreased ACh release during sleep and quiescence facilitates the switch to burst firing.

Unlike dLGN, TRN neurons respond homogenously to ACh, exhibiting a biphasic excitation-inhibition response (E-I; Beierlein, 2014). The excitatory component consists of fast ionotropic depolarization mediated by nAChRs, while the inhibitory component is slow metabotropic hyperpolarization mediated by M2 mAChRs (Sun et al., 2013; Beierlein, 2014). Classically, the role of these cholinergic inputs was considered to be the slow muscarinic hyperpolarization of TRN neurons, which results in the disinhibition of dLGN TC relay neurons (Hu et al., 1989). However, recent evidence suggests that cholinergic signaling, arising from the basal forebrain, can also control TRN neuron activity in a temporally-precise manner, modulating the oscillatory rhythms generated by TRN during certain behavioral states (Sun et al., 2013; Beierlein, 2014; Pita-Almenar et al., 2014).

In Figure 2, a simplified diagram depicts how cholinergic brainstem and basal forebrain regions innervate the visual thalamus. The dLGN receives cholinergic innervation exclusively from the brainstem, specifically the mesopontine tegmental nuclei, including laterodorsal (LDTg), and pedunculopontine tegmentum (PPTg) (Woolf & Butcher, 1986; Fitzpatrick et al., 1988; Steriade et al., 1988; Fitzpatrick et al., 1989). The activity of these neurons

has been shown increase during transition from sleep to wakefulness, and periods of heightened arousal (Mesulam et al., 1983; Steriade, 1993; Gut & Winn, 2016; Mena-Segovia & Bolam, 2017; Kroeger et al., 2017). In addition, dLGN receives input from the parabigminal nucleus (PBG), a cholinergic visuo-motor nucleus associated with generation of eye movements and escape behaviors (Graybiel, 1978; Watanabe & Kawana, 1979; Cui & Malpeli 2003; Ma et al., 2013; Shang et al., 2015; Shang et al., 2018). By contrast, TRN receives converging cholinergic innervation from the brainstem and basal forebrain. This includes the mesopontine tegmentum (LDTg & PPTg) of the brainstem, and several cholinergic basal forebrain nuclei, including the Nucleus of the Horizontal Diagonal Band (HDB), Substantia Innominata (SI), and Nucleus Basalis of Myenert (NBM) (Hallanger et al., 1987). These basal forebrain regions are also the source of cholinergic innervation to the neocortex, including the primary sensory cortical areas (Bigl et al., 1982; Woolf et al., 1986; Arroyo et al., 2014).

The mouse dLGN has been widely utilized as a model for studying the formation and refinement of sensory thalamic circuits (Guido, 2008; Hong & Chen, 2011; Kerschensteiner & Guido, 2017; Guido, 2018). To date, studies have primarily focused on the development of the retinogeniculate pathway during early postnatal life (Bickford et al., 2000; Chen and Regehr, 2000; Lo et al., 2002; Jaubert-Miazza et al., 2005; Ziburkus & Guido, 2006; Dilger et al., 2011). Retinal axons reach dLGN at perinatal ages, with contralateral axons entering the nucleus at embryonic day 15-16, and the ipsilateral axons arriving by postnatal day (P) 0-2 (Godement et al., 1984). Eye-specific patterning, whereby

contralateral and ipsilateral retinal projections target specific areas of dLGN, begins to appear by P7 and is largely complete by the time of natural eye opening (P12-14; Chen & Reghr, 2000; Jaubert-Miazza et al., 2005; Ziburkus & Guido, 2006). Recently, several studies have explored the time course of the nonretinal innervation in dLGN, showing that these inputs arrive and make functional connections at later ages compared to the retinogeniculate pathway (Jacobs et al., 2007; Bickford et al., 2010; Seabrook et al., 2012). Corticogeniculate projections, from layer VI of the primary visual cortex, arrive in dLGN at around P3, and innervate the entire nucleus by the end of the second postnatal week (Jacobs et al., 2007; Seabrook et al., 2012). Similarly, intrinsic interneurons of dLGN begin to make functional connections with TC relay neurons by the end of the second postnatal week (Bickford et al., 2010). The observation that retinal innervation precedes nonretinal innervation suggests that retinal inputs play a regulatory role. Indeed, studies in a mouse model of visual deafferentation (*math5*$^{-/-}$) have shown that in the absence of retinal input, corticogeniculate inputs arrive prematurely in dLGN (Seabrook et al., 2013). Moreover, another study has demonstrated that arrival of retinal projections leads to changes in expression of aggrecan, an extracellular matrix molecule which normally acts to inhibit the growth of corticogeniculate axons into the dLGN (Brooks et al., 2011). Together, these findings suggest that the formation of dLGN circuits follows a conserved developmental plan, wherein retinal input arrive first and orchestrate the timing of arrival for nonretinal projections. While previous immunohistochemical studies indicate that cholinergic projections arrive

well after eye-specific segregation is complete (Carden et al., 2000; Ballesteros et al., 2005), it remains to be seen whether cholinergic inputs to dLGN are regulated by retinal input like other nonretinal projections.

In this dissertation, we explore the organization and development of cholinergic projections to the visual thalamus, focusing primarily on dLGN and TRN. In Chapter I, we perform retrograde viral tracing experiments to identify the brainstem regions which project to dLGN. We also conduct Cre-dependent anterograde tracing of brainstem and basal forebrain projections in a mouse line that selectively expresses Cre recombinase in cholinergic neurons (ChAT-Cre). This approach allowed to examine the innervation pattern in the visual thalamus arising from each cholinergic locus. In Chapter II, we cross the ChAT-Cre mouse line to a fluorescent reporter line (ChAT-Cre x Ai9) to express tdTomato in cholinergic neurons from an early age, and track the time course of postnatal cholinergic innervation in dLGN. In addition, we make use of a model of visual deafferentation (*math5*$^{-/-}$ mouse) to examine whether retinal input regulates the developmental timing of cholinergic innervation. Finally, in Chapter III we explore the development of cholinergic input to the visual and nonvisual sectors of TRN using ChAT-Cre x Ai9 mice. Moreover, we take an optogenetic approach to assess the functional development of cholinergic synapses in TRN during postnatal development.

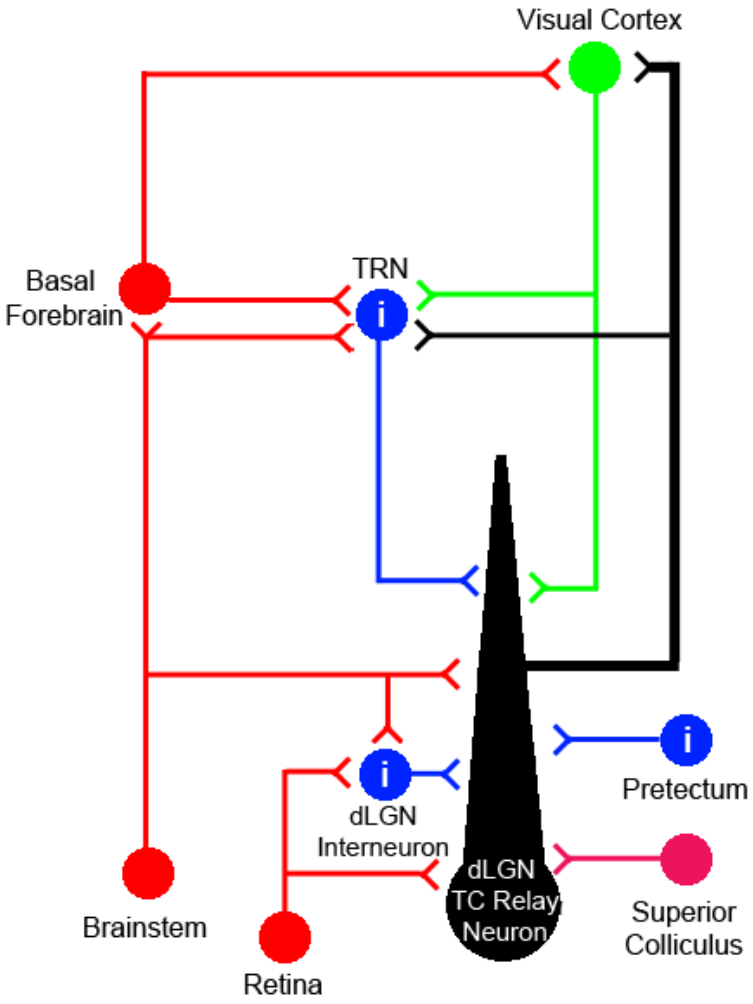

Figure 1. Wiring diagram of retinal and nonretinal inputs onto the thalamocortical (TC) neurons of the dorsal lateral geniculate nucleus (dLGN) in mouse. TRN: Thalamic reticular nucleus. Inhibitory projections are indicated with the letter i.

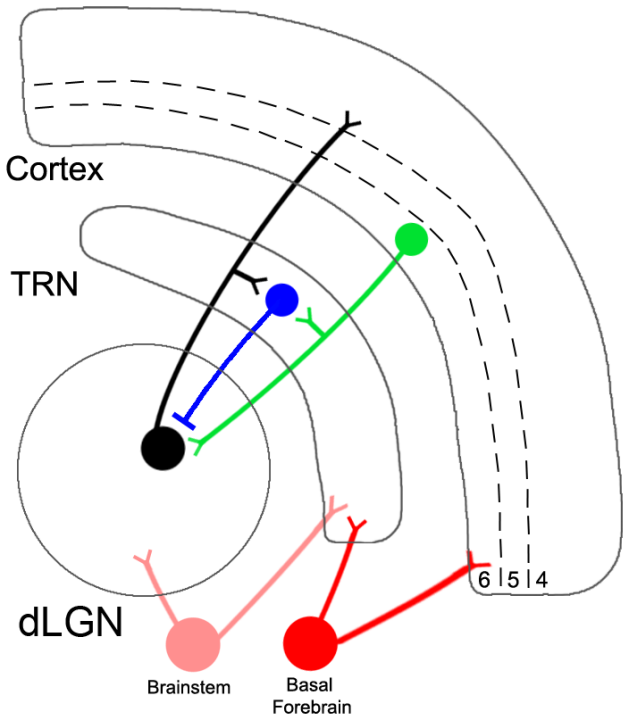

Figure 2. Simplified schematic of cholinergic brainstem and basal forebrain projections to the visual thalamus. TC neurons of dLGN project to layer IV of the visual cortex, and receive projections from layer VI. TRN neurons receive input from axon collaterals of TC relay neurons and corticothalamic neurons. The brainstem provides cholinergic innervation to dLGN and TRN. The cholinergic nuclei of the basal forebrain innervate TRN and cortex.

CHAPTER I

THE ORGANIZATION OF CHOLINERGIC INPUT TO THE DORSAL LATERAL GENICULATE NUCLEUS AND THALAMIC RETICULAR NUCLEUS OF THE MOUSE VISUAL THALAMUS

Introduction

Ascending brainstem cholinergic projections play an important role in modulating thalamocortical (TC) sensory transmission in a state-dependent manner (Steriade 1990; Steriade 1993; Okazi & Kaplan, 2006; Yang et al., 2015). In the dorsal lateral geniculate nucleus (dLGN), the thalamic relay for vision, the release of acetylcholine (Ach) leads to excitation of TC neurons and inhibition of intrinsic GABAergic interneurons (Ahlsen et al., 1984; McCormick & Prince, 1987; McCormick & Pape, 1988; Curro Dossi et al., 1991; Zhu & Uhlrich, 1997; Zhu & Ulrich, 1998; Zhu et al., 1999; Zhu & Heggelund, 2001). Activation of these cholinergic inputs increases the visual responsiveness of dLGN TC neurons, facilitates the switch from burst to tonic firing, and enhances the gain of signal transmission to the visual cortex (McCormick & Prince 1986; Steriade & Dechenes, 1989; Steriade et al., 1990; Uhlrich et al., 1990; Lu et al. 1993; Ozaki & Kaplan, 2006). Anatomical tracing studies in a variety of mammalian species

reveals that dLGN receives a substantial cholinergic projection from the mesopontine tegmentum, including the pedunculopontine (PPTg) and laterodorsal (LDTg) tegmental nuclei (Woolf & Butcher, 1986; Fitzpatrick et al., 1988; Steriade et al., 1988; Fitzpatrick et al., 1989; Zeater et al., 2018). The activity of tegmental neurons has been linked to the regulation of different behavioral states such as arousal, attention, and sleep/wake transitions (Mesulam et al., 1983; Steriade, 1993; Gut & Winn, 2016; Kroeger et al., 2017; Mena-Segovia & Bolam, 2017).

In addition to tegmental projections, dLGN receives cholinergic innervation from the parabigeminal nucleus (PBG), a visuo-motor structure involved in the coordination of eye movements and visually-evoked escape behaviors (Graybiel, 1978; Watanabe & Kawana, 1979; Cui & Malpeli 2003; Ma et al., 2013; Shang et al., 2015; Shang et al., 2018). Unlike tegmental projections, those from the PBG nucleus have a distinct pattern of innervation in dLGN, largely targeting the C-laminae of the cat, and the koniocellular layers primate dLGN (Fitzpatrick et al. 1989; Harting et al., 1991; Zeater et al. 2018). Neurons in these regions are known have unconventional receptive field properties, with many showing a preference for the direction of stimulus motion and orientation (Levay & Ferster, 1977; Stanford et al., 1983; Masland & Martin, 2007; Anderson et al., 2009). These regions also receive input from superior colliculus (Harting et al., 1978; Fitzpatrick et al., 1980; Harting et al., 1986; Harting et al., 1991), suggesting they form part of a specialized visual channel that provides the visual cortex with convergent information about stimulus motion and eye movements.

While rodents have a homologous area in dLGN, known as the dorsolateral shell (Reese et al., 1988; Grubb & Thompson, 2003; Huberman et al., 2009; Cruz-Martin et al., 2014; Bickford et al., 2015; Sun et al., 2016), it is unclear whether PBG projections target this region in a preferential fashion (Harting et al., 1986; Hashikawa et al., 1986; Smith et al., 1988; Harting et al., 1991). The visual thalamus of the mouse has emerged as a model system to study the organization and function of thalamic circuitry (Seabrook et al., 2013; Kerschensteiner & Guido, 2017), yet little is known about the pattern of cholinergic innervation to dLGN or other visual thalamic nuclei.

In the present study, we examined the source, route, and pattern of cholinergic projections to the mouse dLGN by performing retrograde and anterograde tracing experiments. A retrograde virus was used to identify the location of dLGN-projecting tegmental and PBG neurons within the brainstem. To visualize the axonal arbors in dLGN originating from each area, we used a Cre-dependent anterograde virus (Madisen et al., 2010 & 2012) to fluorescently label LDTg, PPTg, and PBG projections in a mouse strain which selectively expresses Cre recombinase in cholinergic neurons (ChAT-Cre). Moreover, we characterized the route of axonal projections from each area, as well as the pattern of cholinergic innervation in other areas of the visual thalamus, including lateroposterior nucleus (LP), ventral lateral geniculate nucleus (vLGN), and thalamic reticular nucleus (TRN).

Materials and Methods

Subjects

All breeding and experimental procedures were approved by the University of Louisville Institutional Animal Care and Use Committee. Mouse strains ChAT-IRES-Cre (Jackson Labs, stock #006410, strain B6;129S6-Chat$^{tm2(cre)Lowl}$/J), and Ai9 (Jackson Labs, stock #007909, strain B6.CgGt(ROSA)26Sor$^{tm9(CAG-tdTomato)HZe}$/J), of either sex were used for breeding or for experiments. Homozygous ChAT-Cre mice were bred with homozygous Ai9 mice to generate ChAT-Cre x Ai9 offspring.

Viral tracer injections

A Cre-containing retrograde Herpes Simplex Virus (hEFα1-HSV-Cre) was used in a Cre-dependent reporter line expressing tdTomato (Ai9). Unilateral injections were made dLGN of adult (P60-P120) Ai9 mice using the following procedure. Prior to surgery, mice were anesthetized deeply using a ketamine/xylazine mixture and head-fixed in a stereotaxic apparatus. An incision was made along the scalp, and a hole was drilled in the skull above the injection site (dLGN; -2.3 mm AP, 2.2 mm ML, -2.8 mm DV from bregma). A Hamilton syringe (World Precision Instruments) was guided by a stereotaxic apparatus and used to deliver 15-40 nL of virus to the target site. Animals were monitored during recovery from the surgical procedure and, after a 21-day incubation period, brains were collected for histology. For anterograde tracing, a Cre-dependent tracer Flex-rev-oChIEF-tdTomato (Addgene plasmid #30541, serotype 9) was used in adult ChAT-Cre mice using aforementioned surgical

procedures. A 15-60 nL bolus of virus was injected into either PBG (-4.2 mm AP, -1.7 mm ML, -3.7 mm DV), PPTg (-4.7 mm AP, 1.2 mm ML, -3.8 mm DV), and LDTg (-5.0 mm AP, 0.6 mm ML, -3.5 mm DV). In some cases, the injection was large enough to label more than one region (e.g., PBG and rostral PPTg). The brains were collected for histology after a 21-day incubation period.

Histology

To collect brain tissue, mice were deeply anaesthetized by isoflurane vapors (2-4%), and transcardially perfused with phosphate-buffered saline (PBS, 0.01 M phosphate buffer with 0.9% NaCl) followed by 4% paraformaldehyde (PFA) in 0.1 M phosphate buffer. Brains were postfixed overnight in 4% PFA, then transferred to PBS. A vibratome (Leica VT1000S) was used to make 70 µm-thick sections in the coronal plane. To amplify tdT fluorescence signal and prevent photobleaching during imaging, DsRed (Clontech) antibody was applied using the following procedure: Sections were placed in blocking medium (10% normal goat serum (NGS), and 0.3% Triton X-100 in PBS) for 1 hour, and then incubated for 12 hours in rabbit anti-DsRed (1:1000) with 1% NGS in PBS. Next, tissue was incubated for 1 hour in 1:100 biotinylated goat anti-rabbit IgG antibody (Vector Labs) with 1% NGS in PBS, followed by 1 hour in 1:100 streptavidin Alexa Fluor (AF) 546 (Life Technologies) in PBS. Sections were mounted onto gelatin subbed glass slides using ProLong mounting medium containing DAPI (Life Technologies).

Imaging and analysis

Images were acquired on a confocal microscope (Olympus FV12000BX61) using Fluoview software (Olympus) or on an epifluorescence microscope (Olympus BX43) using MetaMorph software (Molecular Devices). Acquisition parameters were calibrated using samples with highest and lowest levels of fluorescence to avoid oversaturation while maximizing detection. All monochromatic images used in figures were inverted and contrast-enhanced for clarity.

To reconstruct the location of retrogradely labeled brainstem neurons, consecutive coronal sections of the brainstem (AP – 5.4mm to -4.0 mm from bregma) were imaged using an epi-fluorescence stereo zoom microscope (Olympus). Analysis was limited to cases where success of injection was confirmed by presence of tdT-labeling in ipsilateral SC, visual sector of TRN, and layer 6 of the visual cortex. The images were imported into Neurolucida 360 software (MBF Bioscience) where the contours of the brainstem, fourth ventricle, and cerebral aqueduct were outlined in each section. Next, the location of each tdT-labeled soma was marked. The resulting traces were aligned and merged to create a 3-dimensional representation of the brainstem.

Results

To identify the source of all ascending brainstem projections to dLGN, we conducted retrograde tracing experiments by using a herpes simplex virus containing cre recombinase (hEF1a-HSV-Cre). When injected into the brain of a Cre-dependent fluorescent reporter line (Ai9), HSV-Cre virus is retrogradely transported from the terminals to the soma, and results in the expression of tdTomato (tdT) in the projecting neuron. We made unilateral injections into the right dLGN of HSV-Cre in three adult (>P60) Ai9 mice. In each case, neuronal labeling was apparent in a number of structures that project to dLGN including visual cortex, TRN, superior colliculus, and several brainstem regions. Figure 3 shows an example of tdT labeling in dLGN after an injection of HSV-Cre (Fig. 3A), and the pattern of retrograde labeling within brainstem. Figure 3B illustrates the pattern of retrogradely labeled neurons within LDTg, PPTg, and PBG, while the corresponding composite plot in Figure 3C depicts the location of these neurons throughout the caudo-rostral extent of the tegmentum and PBG. In all cases (n = 3), a unilateral injection in dLGN led to bilateral retrograde labeling in the tegmental nuclei and PBG. The majority of labeled neurons in the tegmentum were ipsilateral to the injected hemisphere, whereas the vast majority of PBG neurons were contralateral (Fig. 3C).

Since brainstem nuclei contain heterogeneous populations of neurons (Scarnati et al., 1987; Hallanger & Wainer, 1988; Wang & Morales, 2009; Kroeger et al, 2017), we utilized a mouse line which selectively expresses Cre in cholinergic neurons (ChAT-Cre). Figure 4 shows the pattern of tdT labeling in the

brainstem and thalamus of an adult ChAT-Cre crossed to the Ai9 reporter. Figure 4A shows three caudo-rostral levels of the brainstem, demonstrating that tdT labeling was present in LDTg (Fig 4A, left), PPTg (Fig. 4A, middle), and PBG (Fig 4A, right). Figure 4C illustrates the pattern of cholinergic innervation within the dorsal thalamus. While dLGN, intergeniculate leaflet (IGL), and ventral geniculate nucleus (vLGN) were densely innervated by tdT-labeled cholinergic fibers, innervation in lateral posterior nucleus (LP) was relatively sparse (Fig. 4C, left). At more rostral regions of the thalamus, cholinergic fibers were found throughout TRN, forming a reticular pattern within the nucleus (Fig. 4C, right). Furthermore, there was a dense plexus of cholinergic fibers within the adjacent ventrobasal nucleus (VB; Fig. 4C, right).

To visualize cholinergic brainstem neurons and their processes, we made injections of a Cre-dependent anterograde adeno associated virus (FLEX-AAV-ChIEF-tdT) in adult ChAT-Cre mice. Examples of unilateral injections in PBG (*n* = 3), PBG & rostral PPTg (*n* = 1), PPTg (*n* = 2) and LDTg (*n* = 2), as well as the pattern of tdT labeling in the dorsal thalamus is shown in Figures 5-8. In all three cases, an injection of AAV-ChiEF-tdT into PBG resulted in extensive tdT labeling of arbors within the contralateral dLGN (Fig. 5B). In addition, there was a projection to the ipsilateral dLGN which was much smaller, and in all cases limited to a small strip within the dorsomedial edge of the nucleus (Fig. 5C; a detailed analysis of PBG arbor distribution within dLGN is presented in Chapter 2). While a small bilateral patch of tdT-labeled fibers was present in the caudo-medial region of LP, no labeling was seen in other regions of the dorsal

thalamus, including ventral lateral geniculate nucleus (vLGN), LP, IGL, VB, TRN, or other nuclei of the dorsal thalamus (Fig. 5B & C). We also noted the presence of PBG axons in the supraoptic decussation (SOX) and optic tract (OT). PBG axons coursed within the ipsilateral supraoptic decussation toward the optic chiasm (OX; Fig. 5D, right), crossing the ventral midline (Fig. 5E), and running dorsally within the optic tract en route to dLGN (Fig. 5D, left).

Figure 6 shows the result of an injection restricted to PPTg (Fig 6A). In the dorsal thalamus, cholinergic PPTg fibers were present in VB and TRN. While the projection to the thalamus was bilateral, the density of arbors was always greater in the ipsilateral hemisphere. The axons of PPTg were present within the ipsilateral SOX (Fig. 6D), but unlike PBG axons, ran dorso-medially toward substantia nigra, rather than ventrally toward OX (Fig. 6D, right). Moreover, PPTg axons did not traverse within OT and did not cross at the ventral midline (Fig. 6D & E). Interestingly, in 2 cases, dLGN and LP were devoid of labeled fibers after an injection restricted to PPTg. However, in another case where the injection site included PBG and rostral PPTg (Fig. 7), we noted a sparse projection to the ipsilateral dLGN, vLGN, IGL, LP, VB, and TRN, along with a small projection to the dorso-medial edge of dLGN. The projection pattern of LDTg, depicted in Figure 8, was similar to that of caudal PPTg. In both cases the projection was bilateral, mostly targeting VB and TRN of the ipsilateral hemisphere, with little or no labeling in dLGN or LP (Fig. 8B & C). While LDTg axons were seen traveling within the ipsilateral SOX (Fig. 8D, right), these axons did not traverse within OT (Fig. 8D & E).

In addition to ascending brainstem projections, in many species the thalamus receives cholinergic input from the basal forebrain, a projection which is restricted to TRN (Woolf, et al., 1986). To confirm this, we performed an injection of FLEX-AAV-ChIEF-tdT in basal forebrain of a ChAT-Cre mouse (*n* = 1). Figure 9A depicts an injection of FLEX-AAV-ChIEF-tdT restricted to HDB and SI, the nuclei of cholinergic basal forebrain which have been shown to project to TRN, as well as sensory cortices (Bigl et al., 1982; Woolf et al., 1986; Arroyo et al., 2014). In TRN, tdT-labeled fibers found bilaterally, with the label restricted to the dorsal “head” of TRN (Fig. 9B & C, right). No other regions of the dorsal thalamus received cholinergic basal forebrain innervation (Fig. 9B & C, left).

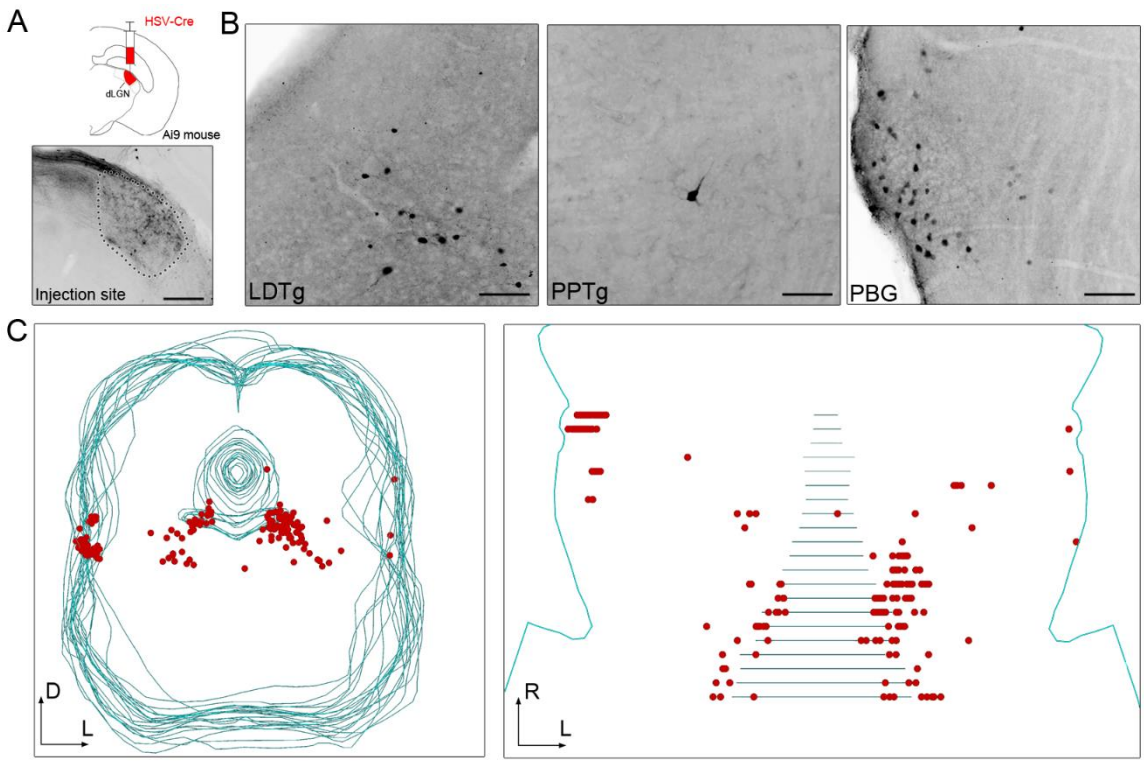

Figure 3. Identification of brainstem nuclei that project to dorsal lateral geniculate nucleus (dLGN). **A.** *Top:* Retrograde virus HSV-Cre was injected into the dLGN of an Ai9 mouse. *Bottom:* Example case showing the resulting tdTomato (tdT) labeling within dLGN after injection of HSV-Cre. Scale = 1 mm. **B.** Coronal views of retrograde tdT labeling of neurons in laterodorsal tegmentum (LDTg, left), pedunculopontine tegmentum (PPTg, middle), and parabigeminal nucleus (PBG, right). Scale = 100 µm. **C.** Composite 3D plots showing the locations of all tdT-labeled brainstem neurons in a coronal (left) and horizontal (right) views. Each red dot represents the location of a tdT-labeled soma, while teal traces outline the borders of the brainstem, 4th ventricle, and cerebral aqueduct.

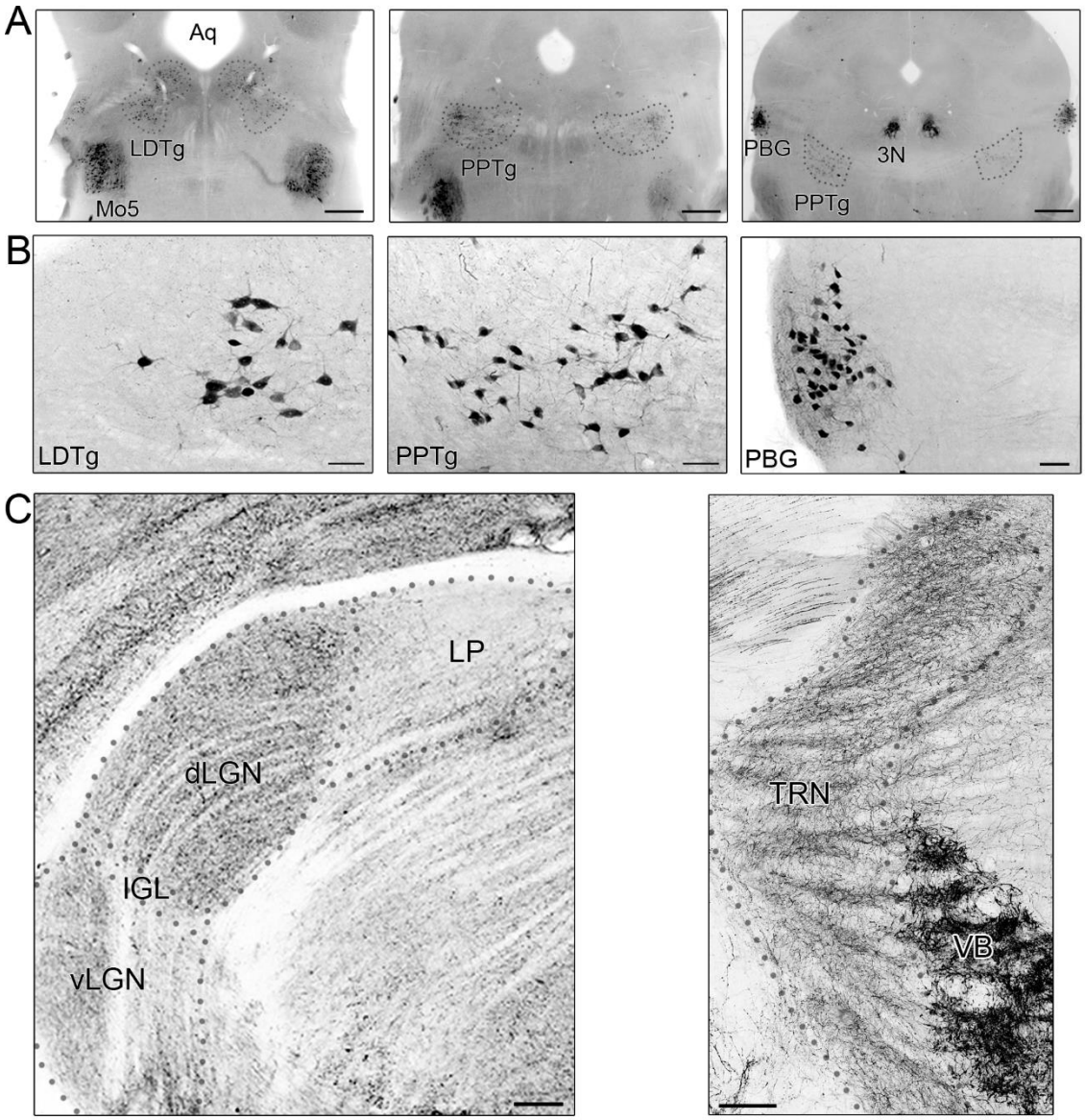

Figure 4. Pattern of tdT labeling in the brainstem, dorsal thalamus, and thalamic reticular nucleus (TRN) of a ChAT-Cre x Ai9 mouse. **A.** Coronal sections at the different caudo-rostral levels of the brainstem show tdT labeling in LDTg (left), PPTg (right), and PBG (right). Additionally, tdT labeling was seen in other cholinergic nuclei including motor nucleus of the trigeminal nerve (Mo5, left & middle), and oculomotor nucleus (3N, right). Dotted lines delineate estimated

boundaries of LDTg, PPTg, and PBG. Scale = 500 µm. **B.** High power views of LDTg, PPTg, and PBG showing robust somatic tdT-labeling. Scale = 50 µm. **C.** Coronal section through the dorsal thalamus, showing tdT-labeled fibers in dLGN, LP, and vLGN. Scale = 100 µm. **D.** Coronal section showing the pattern of tdT labeling within TRN and ventrobasal nucleus (VB). Dotted lines delineate the boundaries of dLGN and TRN. Scale = 100 µm. vLGN: ventral lateral geniculate nucleus. IGL: Intergeniculate leaflet, Aq: Cerebral aqueduct.

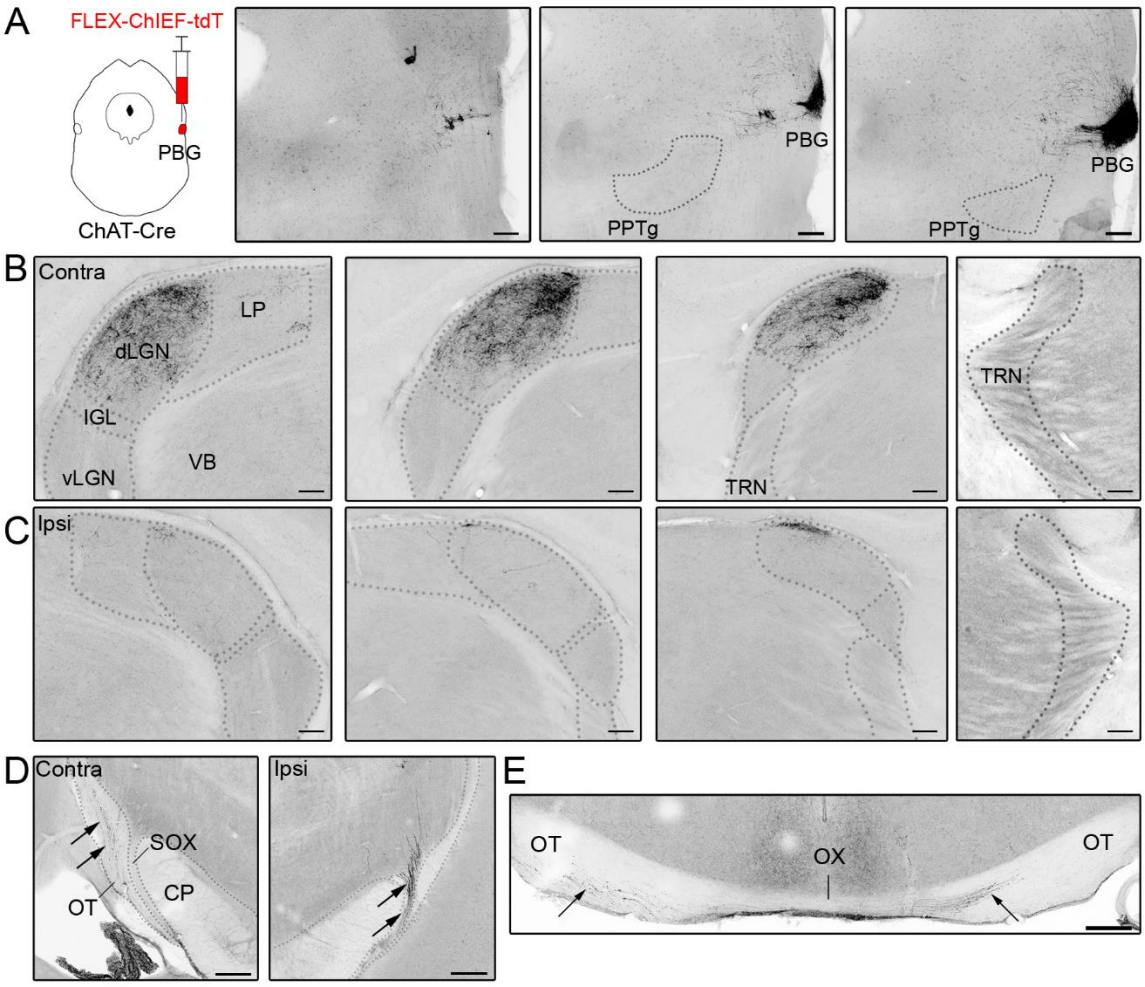

Figure 5. Anterograde viral tracing of PBG projections to the dorsal thalamus. **A.** Coronal views of the brainstem at different caudo-rostral levels showing restricted tdT labeling in PBG after a unilateral injection of FLEX-AAV-ChIEF-tdT virus. Scale = 200 µm. Dotted lines delineate the borders of LDTg, PPTg, and PBG. **B.** Coronal views of the contralateral dorsal thalamus, showing extensive innervation of dLGN by tdT-labeled PBG axonal arbors. Additionally, a small cluster of fibers was seen in the caudo-medial region of lateral posterior nucleus (LP). Scale = 100 µm. **C.** In the ipsilateral thalamus, fibers were restricted to a small area in the dorso-medial dLGN, adjacent to the optic tract (OT). Scale =

100 µm. Dotted lines delineate the borders of dLGN, vLGN, IGL, LP, and TRN. **D.** Coronal views of the contralateral (left panel) and ipsilateral (right panel) cerebral peduncle (CP), supraoptic decussation (SOX), and OT show PBG axons traveling within the contralateral OT (left) and within the ipsilateral SOX (bottom right). Scale = 200 µm. Dotted lines delineate the borders of CP, SOX, and OT. **E.** Coronal view of the ventral midline shows PBG crossing the midline near the optic chiasm (OX), and entering the contralateral OT. Scale = 200 µm. In each panel, arrows indicate the location of tdT-labeled axonal tracts.

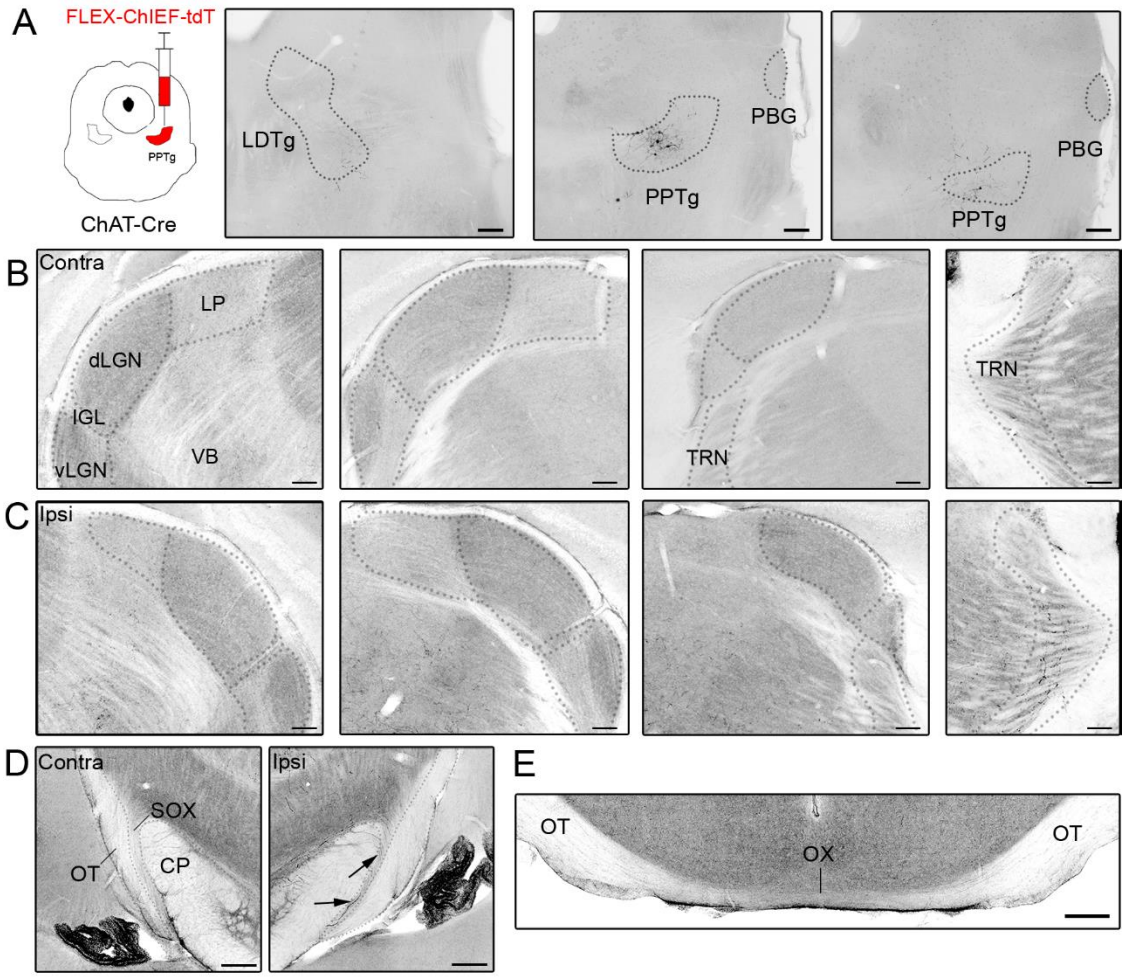

Figure 6. Anterograde viral tracing of PPTg projections to the dorsal thalamus. **A.** Coronal views of the brainstem at different caudo-rostral levels showing tdT labeling restricted to PPTg after an injection of FLEX-AAV-ChIEF-tdT virus. Scale = 200 µm. **B.** Coronal views of the contralateral dorsal thalamus, showing diffusely distributed cholinergic axonal arbors within VB. Scale = 100 µm. Dotted lines delineate the borders of LDTg, PPTg, and PBG. **C.** In the ipsilateral thalamus, tdT-labeled fibers are seen through VB, and ventral TRN. Scale = 100 µm. Dotted lines delineate the borders of dLGN, vLGN, IGL, LP, and TRN. **D.** Coronal views of the contralateral (left panel) and ipsilateral (right panel) CP,

SOX, and OT show PPTg axons traveling within the ipsilateral SOX (right) and veering medially toward substantia nigra. Scale = 200 µm. Dotted lines delineate the borders of CP, SOX, and OT. **E.** Coronal view of the ventral midline shows OX and OT, which are devoid of tdT-labeled axons. Scale = 200 um. In each panel, arrows indicate the location of tdT-labeled axonal tracts.

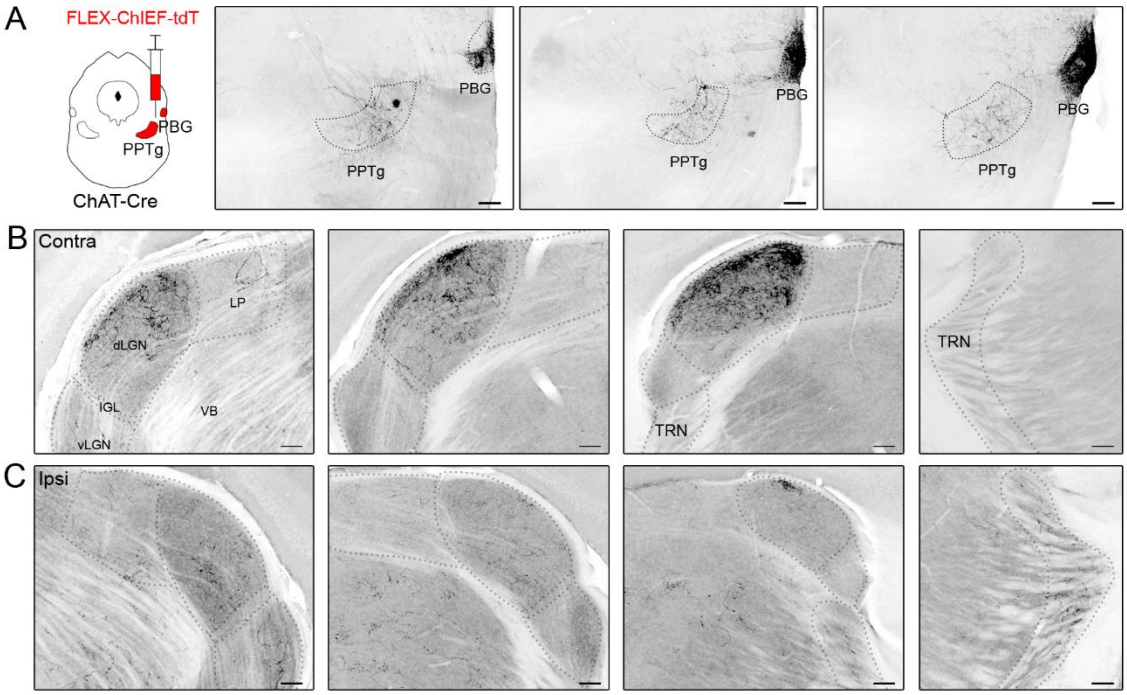

Figure 7. Anterograde viral tracing of PBG and rostral PPTg projections to the dorsal thalamus. **A.** Coronal views of the brainstem at different caudo-rostral levels showing tdT labeling in PBG and rostral PPTg after an injection of FLEX-AAV-ChIEF-tdT virus. Scale = 200 µm. Dotted lines delineate the borders of PPTg and PBG. **B-C.** Coronal views of the contralateral (top) and ipsilateral (bottom) dorsal thalamus showing tdT-labeled fibers in dLGN, vLGN, IGL, LP, VB, and TRN. Scale = 100 µm. Dotted lines delineate the borders of vLGN, dLGN, IGL, LP, and TRN.

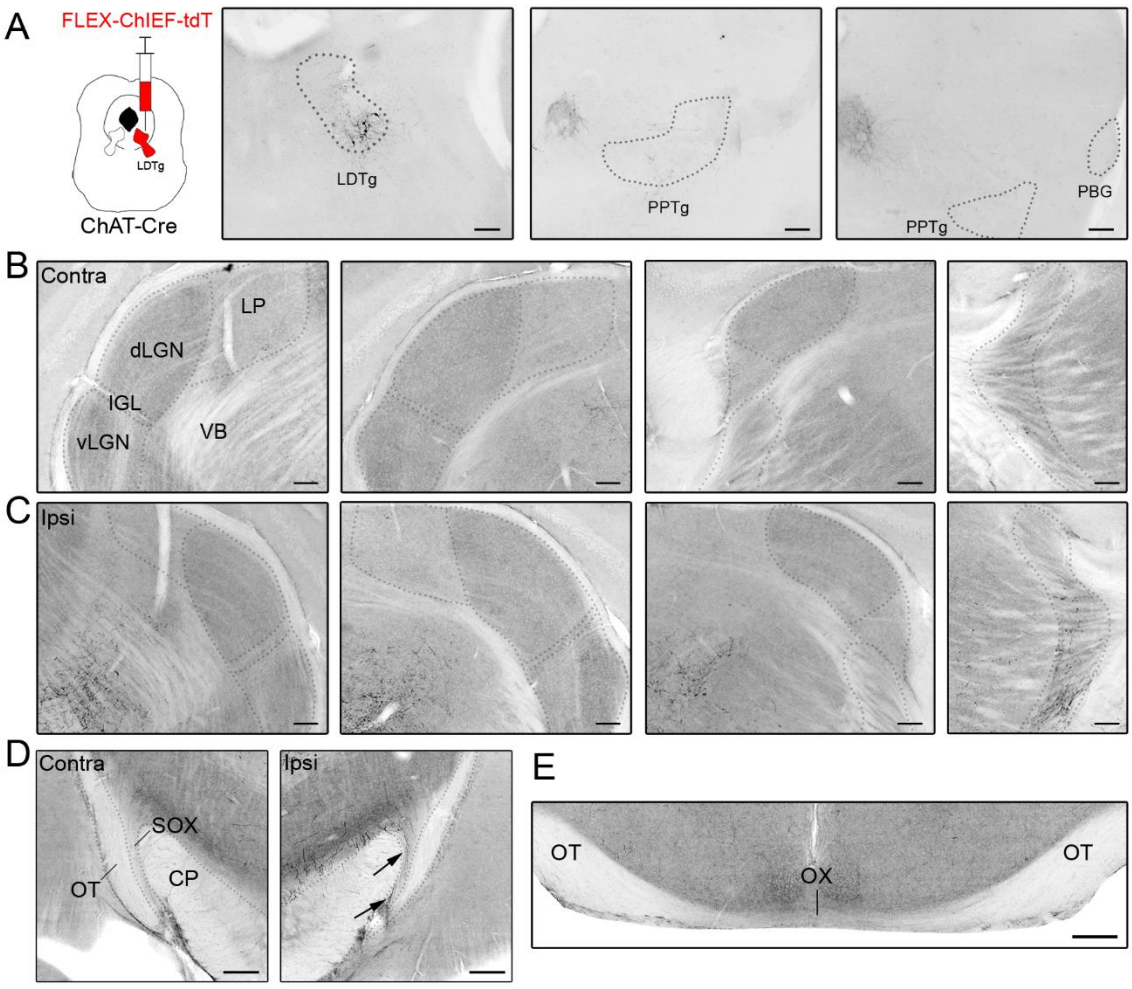

Figure 8. Anterograde viral tracing of LDTg projections to the dorsal thalamus. **A.** Coronal views of the brainstem at different caudo-rostral levels showing tdT labeling restricted to LDTg after an injection of FLEX-AAV-ChIEF-tdT virus. Scale = 200 µm. Dotted lines delineate the borders of LDTg, PPTg, and PBG. **B.** Coronal views of the contralateral dorsal thalamus, showing diffusely distributed cholinergic axonal arbors within VB. Scale = 100 µm. **C.** In the ipsilateral thalamus, tdT-labeled fibers are seen in VB, and ventral TRN. Scale = 100 µm. Dotted lines delineate the borders of vLGN, dLGN, IGL, LP, and TRN. **D.** Coronal views of the contralateral (left panel) and ipsilateral (right panel) CP, SOX, and OT show LDTg axons traveling within the ipsilateral SOX (right) and coursing

medially toward substantia nigra. Scale = 200 µm. Dotted lines delineate the borders of CP, SOX, and OT. **E.** Coronal view of OX and OT at the ventral midline. Scale = 200 µm. In each panel, arrows indicate the location of tdT-labeled axonal tracts.

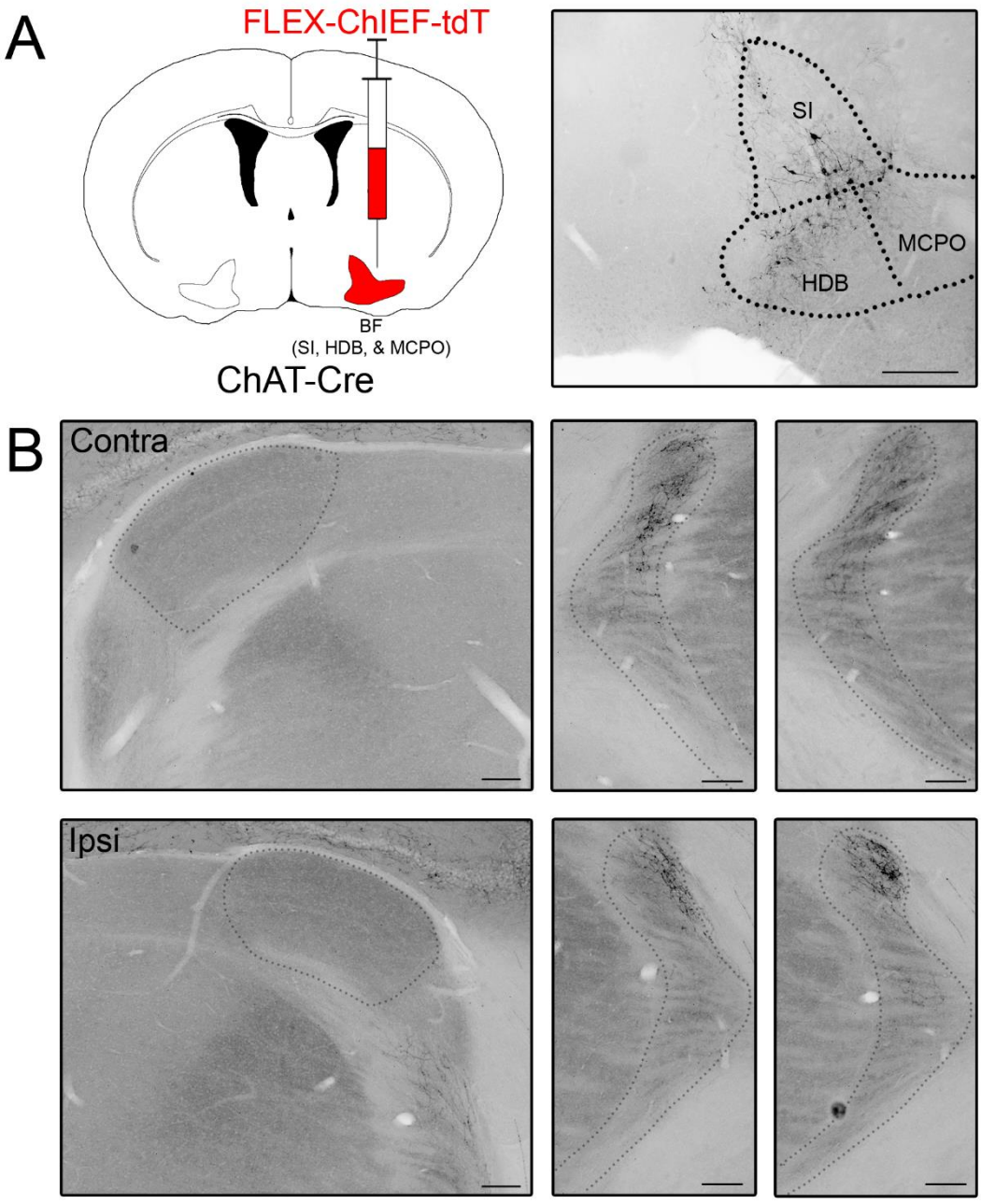

Figure 9. Anterograde tracing of cholinergic basal forebrain (BF) projections to the dorsal thalamus. **A.** Injection of FLEX-AAV-ChIEF-tdT into the basal forebrain of a ChAT-Cre mouse resulted in labeling restricted to the nucleus of the horizontal diagonal band (HDB) and substantia innominata (SI). Scale = 100 µm. Dotted lines delineate the borders of SI, HDB, and magnocellular preoptic

nucleus (MCPO). **B.** Coronal views of the contralateral (top) and ipsilateral (bottom) dorsal thalamus show bilateral labeling of cholinergic fibers in dorsal regions of TRN. No labeling was seen in dLGN or other nuclei of the dorsal thalamus. Scale = 100 µm. Dotted lines delineate the borders of dLGN and TRN.

	dLGN		vLGN		LP		VB		TRN		OT	
	Ipsi	Contra	Ipsi	Contra	Ipsi	Contra	Ipsi	Contra	Ipsi	Contra	Ipsi	Contra
PBG (n = 3)	+*	+++	-	-	+*	-	-	-	-	-	-	+
PBG & rostral PPTg (n = 1)	++	+++	+	-	+	+	++	+	++	-	-	+
LDTg (n = 2)	-	-	-	-	-	-	++	+	++	-	-	-
PPTg (n = 2)	-	-	-	-	-	-	++	+	++	-	-	-

Table 1. Estimated density of cholinergic projections: dense +++; moderate ++; sparse +; +*: dense projection restricted to a small area; none -. dLGN dorsal lateral geniculate nucleus, LP lateroposterior nucleus, TRN thalamic reticular nucleus, VB ventrobasal nucleus, OT optic tract, IGL intergeniculate leaflet, vLGN ventral geniculate nucleus.

Discussion

In this study we used retrograde and anterograde viral tracers in genetically modified mice to visualize the source and projection of ascending brainstem projections to dLGN and other regions of the thalamus. Consistent with reports in other mammals, our retrograde tracing experiments showed that mouse dLGN receives ascending brainstem input from the mesopontine tegmentum (LDTg & PPTg), as well as PBG nucleus (Woolf & Butcher, 1986; Fitzpatrick et al., 1988; Steriade et al., 1988; Fitzpatrick et al., 1989). As summarized in Table 1, many of these are cholinergic in origin. For example, our Cre dependent anterograde tracing experiments done in ChAT-Cre mice revealed an extensive cholinergic PBG innervation throughout the contralateral dLGN, and a small patch of termination in the ipsilateral dLGN restricted to the dorsomedial pole. However, in one case where we labeled PBG and the rostral end of PPTg, we noted a diffuse but sparse ipsilateral projection to dLGN, vLGN, IGL, LP, TRN, and VB. In cases where injections targeted tegmental nuclei LDTg or the middle to caudal aspects of PPTg, we observed a bilateral projection to VB and TRN, and no labeled fibers in dLGN, vLGN, IGL, or LP. This suggests that cholinergic tegmental projections are spatially organized, with the rostral tegmentum projecting to the visual regions of the thalamus, and caudal tegmentum to somatosensory ones.

While our retrograde tracing experiments revealed a projection to dLGN from the tegmentum, our Cre-dependent anterograde injections reveal that much of this projection is not cholinergic. Instead, it likely to involves a heterogeneous

population of glutamatergic and/or histaminergic brainstem neurons (Scarnati et al., 1987; Hallanger & Wainer, 1988; Wang & Morales, 2009). Together these groups contribute to behavioral state-dependent modulation of thalamic circuits (Kroeger et al., 2017).

Tracing studies in a number of species demonstrate that cholinergic projections of PBG exhibit a distinct pattern of innervation within dLGN. In cats, tree shrews, and some primates, PBG axons largely innervate regions of dLGN associated with a small-celled visual pathway that resides in the C-laminae or koniocellular layers (Langer & Colby, 1979; Harting et al., 1986; Fitzpatrick et al., 1988; Harting et al. 1991). In many rodent species, the pattern of PBG projections seems to follow a similar trajectory, targeting the homologous dorsolateral shell region of dLGN (Harting et al., 1991; but see Watanabe & Kawana, 1979; Stevenson & Lund, 1982; Sefton & Martin, 1984).

Our studies are the first to demonstrate a large, mostly contralateral cholinergic PBG projection to dLGN in the mouse. Much like other mammals (Baleydier & Magnin, 1979; Watanabe & Kawana, 1979; Fitzpatrick et al., 1988; Fitzpatrick et al., 1989), we found cholinergic PBG axons travel toward the ventral midline within SOX, cross to the contralateral hemisphere, and traverse within the optic tract en route to dLGN. However, the contralateral projections to dLGN appear more extensive, extending well beyond the boundaries of the dorsolateral shell. Interestingly, we discovered a small ipsilateral projection that was restricted to the dorsolateral shell, in a region that represents upper nasal visual fields. The functional significance of these projections to dLGN remains

unclear, however it is worth noting they overlap with input from direction selective retinal ganglion cells (DSGCs), as well as the superior colliculus (Harting et al., 1986; Fitzpatrick et al., 1988). In mouse, the prevalence of direction selectivity and orientation selectivity is quite high among dLGN neurons, with a number of identified DSGCs projecting beyond the boundaries of the dorsolateral shell (Kay et al., 2011). Thus, such convergence suggests that PBG projections may play a unique role in the state-dependent amplification of signals related to stimulus motion and eye movements (Cui & Malpeli, 2003; Ma et al., 2013).

CHAPTER II

THE ABSENCE OF RETINAL INPUT DISRUPTS THE DEVELOPMENT OF CHOLINERGIC BRAINSTEM PROJECTIONS IN THE MOUSE DORSAL LATERAL GENICULATE NUCLEUS

Introduction

The dorsal lateral geniculate nucleus (dLGN) of the mouse has become a model system to study the development of thalamic circuits (Guido, 2008; Hong & Chen, 2011; Huberman et al., 2008). Much of our present understanding is based on studies focused on the retinogeniculate pathway, the connections between retinal ganglion cells (RGCs) and dLGN neurons. While retinal projections provide the primary excitatory drive for relay neurons of dLGN, the vast majority of input is nonretinal in origin (Bickford et al., 2010), and acts to modulate the gain of retinogeniculate transmission in a state-dependent manner (Sherman & Koch, 1986; Sherman, 1996). The primary sources of nonretinal input to dLGN include glutamatergic neurons of visual cortex layer VI, GABAergic neurons of the thalamic reticular nucleus, and the cholinergic neurons from different brainstem nuclei. Despite the fact that over 90% of all synapses in dLGN arise from nonretinal sources, we know little about how and when these projections innervate dLGN, or how they interact with the arrival and refinement of retinal projections. What little we do know is based on the corticothalamic

pathway (Jacobs et al., 2007; Seabrook et al., 2013; Grant et al., 2016). Layer VI neurons of the neocortex begin to innervate the dorsal thalamus at perinatal ages, but corticogeniculate innervation occurs largely after the first postnatal week, after the arrival of retinal axons and their refinement into non-overlapping eye-specific domains (Seabrook et al., 2013). Moreover, retinal input orchestrates the timing of corticogeniculate innervation by regulating the levels of aggrecan, a repulsive extracellular matrix molecule (Brooks et al., 2013). What remains to be tested is whether such sequencing and reliance on retinal input is part of a conserved developmental plan that governs the arrival of other nonretinal inputs to dLGN.

To address this, we examined another major nonretinal projection to dLGN, the ascending cholinergic input from the brainstem. Estimates reveal that about 25% of all synapses in dLGN arise from brainstem cholinergic nuclei (Erisir et al., 1997). These projections have a substantial influence on retinogeniculate transmission, regulating the firing mode of dLGN neurons (Lu et al., 1993), establishing network states during sleep, wakefulness, and arousal (Gut & Winn, 2016; Mena-Segovia & Bolam, 2017), as well as modulating visuo-motor interactions (Cui & Malpeli, 2003). Previous immunohistochemical studies have shown a late postnatal onset for the labeling of acetylcholine-synthesizing enzyme choline acetyltransferase (ChAT) in dLGN, which increases in density over a protracted period of development (Carden et al., 2000; Ballesteros et al., 2005). However, little is known about the source, trajectory, and pattern of cholinergic innervation in the developing mouse dLGN. In several mammalian

species, ascending cholinergic projections to dLGN originate from two distinct brainstem groups, the pedunculopontine and laterodorsal tegmental nuclei (PPTg, & LDTg), as well as the parabigeminal nucleus (PBG) (Hallanger et al., 1987; Harting et al., 1991; Fitzpatrick et al., 1988). The projection from PBG is especially notable since these axons course within the optic tract en route to dLGN and superior colliculus (Harting et al., 1991; Sefton & Martin, 1984; Hashikawa et al., 1986), raising the possibility that retinal axons participate in the guidance of PBG axons.

Here, we examined the postnatal development of cholinergic input to dLGN and tested whether the absence of retinogeniculate projections affects the timing and patterning of cholinergic innervation. To visualize ascending cholinergic projections, we crossed a ChAT-Cre knock-in mouse line with a Cre-dependent reporter strain (Ai9) to selectively drive expression of the fluorescent protein tdTomato (tdT) in cholinergic neurons (Madisen et al., 2010). To evaluate the development of cholinergic innervation of dLGN in the absence of retinal projections, we utilized a mutant mouse that lacks *math5*, a transcription factor necessary for RGC progenitor cell differentiation (Wang et al., 2001). *Math5*$^{-/-}$ mice exhibit a $\geq$95% loss of RGCs, and the surviving RGCs fail to form an optic nerve, thus leaving the brain devoid of retinal input (Brown et al., 1998; El-Danaf et al., 2015). Furthermore, we used Cre-dependent viral tracing techniques to assess whether the trajectory of optic tract-associated PBG axons to dLGN was disrupted in a brain lacking retinofugal projections.

Materials and Methods

Subjects

All breeding and experimental procedures were approved by the University of Louisville Institutional Animal Care and Use Committee. Transgenic mouse strains ChAT-IRES-Cre (Jackson Labs, stock #006410, strain B6;129S6-Chat$^{tm2(cre)Lowl}$/J), Ai9 (Jackson Labs, stock #007909, strain B6.CgGt(ROSA)26Sor$^{tm9(CAG-tdTomato)HZe}$/J), and *math5*$^{-/-}$ (on a mixed C57B6/J and 129/SvEV background) of either sex were used for breeding or for experiments. Homozygous ChAT-Cre mice were bred with homozygous Ai9 mice to generate ChAT-Cre x Ai9 offspring. ChAT-Cre$^{+/+}$ x *math5*$^{-/-}$ mice were bred with Ai9$^{+/+}$ x *math5*$^{-/-}$ mice to generate ChAT-Cre$^{+/-}$ x Ai9$^{+/-}$ x *math5*$^{-/-}$ offspring.

To genotype for Cre, the following primers were used in polymerase chain reaction reactions (PCR): Cre-F (CCTTCTATCGCCTTCTTGACG), Cre-R (AGATAGATAATGAGAGGCTC), WT-F (GTTTGCAGAAGCGGTGGG), WT-R (AGATAGATAATGAGAGGCTC). PCR amplification was performed in 28 cycles by denaturation at 94°C for 15 s, annealing at 60°C for 15 s, and elongation at 72°C for 10 s. To genotype for *math5*, the following primers were used: Neo-F (GCCGGCCACAGTCGATGAATC), Neo-R (CATTGAACAAGATGGATTGCA), *math5*-F (ATGGCGCTCAGCTACATCAT), and *math5*-R (GGGTCTACCTGGAGCCTAGC). PCR amplification was performed in 35 cycles by denaturation at 94°C for 30 s, annealing at 59°C for 30 s, and elongation at 72°C for 45 s.

Histology

To collect brain tissue for analysis, mice were deeply anaesthetized by hypothermia (<P5) or isoflurane vapors, and transcardially perfused with phosphate-buffered saline (PBS, 0.01 M phosphate buffer with 0.9% NaCl) followed by 4% paraformaldehyde (PFA) in 0.1 M phosphate buffer. Brains were postfixed overnight in 4% PFA, then transferred to PBS. A vibratome (Leica VT1000S) was used to make 70 µm-thick sections in the coronal plane. To amplify tdT fluorescence signal and prevent photobleaching during confocal imaging, DsRed (Clontech) antibody was applied using the following procedure: Sections were placed in blocking medium (10% normal goat serum (NGS), and 0.3% Triton X-100 in PBS) for 1 hour, and then incubated for 12 hours in rabbit anti-DsRed (1:1000) with 1% NGS in PBS. Next, tissue was incubated for 1 hour in 1:100 biotinylated goat anti-rabbit IgG antibody (Vector Labs) with 1% NGS in PBS, followed by 1 hour in 1:100 streptavidin Alexa Fluor (AF) 546 (Life Technologies) in PBS. To stain tissue for choline acetyltransferase, sections containing the brainstem were placed in blocking medium for one hour and then incubated overnight in 1:100 goat anti-ChAT antibody (AB144P, Millipore). Next, tissue was incubated in 1:300 anti-goat AF 488 (Life Technologies) in PBS for one hour. All sections were mounted onto gelatin subbed glass slides using ProLong mounting medium containing DAPI (Life Technologies).

CTB injection

Intravitreal binocular eye injections of the anterograde tracer cholera toxin subunit B (CTB) conjugated to Alexa Fluor 488 (Invitrogen) were done in an adult

(P60) ChAT-Cre x Ai9 mouse. Under anesthesia (a mixture of ketamine, 120-140 mg/kg, and xylazine, 12-14 mg/kg), the sclera was pierced with a sharp-tipped glass pipette in order to drain excess vitreous. Another pipette, filled with 1% solution of CTB-AF-488 dissolved in distilled water, was inserted into the opening created by the first pipette. A picospritzer attached to the pipette was used to deliver approximately 2-3 µl of the CTB solution into the vitreous of the eye. After a 48-hour survival period, brain tissue was harvested using the methods describe above.

Viral tracer injection

Intracranial injections of a Cre-dependent adeno-associated viral tracer FLEX-rev-oChIEF-tdTomato (Addgene plasmid #30541, serotype 9) were made in the left PBG of adult (>P60) ChAT-Cre and ChAT-Cre x *math5*$^{-/-}$ mice. Prior to surgery, mice were deeply anesthetized using a mixture of ketamine/xylazine and head-fixed in a stereotaxic apparatus. An incision was made along the scalp, and a hole was drilled in the skull above the injection site (-4.2 mm AP, -1.75 mm ML from Bregma). A Hamilton syringe (World Precision Instruments) was guided by a stereotaxic apparatus, and used to deliver 15 nL of virus into the left PBG. After a 14-17 day incubation period, brain tissue was collected for histology using aforementioned procedures. In all cases including WT and mutants, 24-32 tdT-positive neurons were found throughout the rostrocaudal extent of PBG.

Imaging and analysis

All images were acquired on a confocal microscope (Olympus FV12000BX61) using Fluoview software. The boundaries of dLGN was identified with the aid of DAPI staining. To acquire images of dLGN, a 20x objective lens (0.75 NA) was used to scan successive optical sections (1.14 μm step size), which were then collapsed to generate a Z-stacked image. In cases where the dLGN was larger than the area that could be captured using the 20x objective, two images were digitally stitched together to generate a single composite image (e.g. Fig. 4 WT P21 & P30). Acquisition parameters were calibrated using samples with highest and lowest levels of fluorescence to avoid oversaturation while maximizing detection. Black and white confocal images were inverted for clarity (e.g., Figs. 10, 12, 13, 15, 16, 17 and 18). The heat maps depicted in Figure 6 were generated using ImageJ (NIH) “thermal” lookup table function. When acquiring images to be used for quantitative analyses, acquisition parameters were kept consistent across samples. To quantify the degree of cholinergic innervation in dLGN, confocal images were imported into Photoshop (Adobe) and the area of dLGN was outlined with the aid of DAPI staining. A threshold value was chosen on the histogram (pixel intensity of 60 on a scale of 0-255) to create a binarized image consisting of signal and background (Jaubert-Miazza et al., 2005; Demas et al., 2006; Seabrook et al.,2013; Dilger et al., 2015; Sokhadze et al., 2018). The ImageJ software (NIH) was used to count the number of pixels comprising the signal, and the total area of dLGN. For each section of dLGN, the values representing the degree of innervation (Fig. 14) were

expressed as a percentage of the fluorescence signal in relation to the total area. For each hemisphere, 3-5 successive sections through the middle of dLGN were averaged to obtain the final value. For each age/group, 4-6 hemispheres were analyzed from 3 animals.

To quantify the distribution of anterogradely labeled PBG projections, sections containing dLGN were imaged and binarized using the thresholding procedure described above. In each section, two lines were drawn through the middle of dLGN, dividing the nucleus into 4 equal quadrants (dorsolateral - DL, dorsomedial - DM, ventrolateral - VL, and ventromedial - VM; see Fig. 19 inset). The number of pixels comprising the fluorescence signal in each quadrant was counted. Final values for each hemisphere (based on 4-5 sections) were expressed as the percentage of pixels in each quadrant compared to the total number of pixels.

Results

To visualize brainstem cholinergic neurons and their projections to dLGN, we crossed ChAT-Cre mice with an Ai9 reporter line. Figure 10A shows the pattern of tdTomato (tdT) labeling in the brainstem in an adult (P60) ChAT-Cre x Ai9 mouse. Somatic labeling of tdT was seen in cholinergic neurons of brainstem nuclei reported to project to dLGN (Sefton & Martin, 1984; Fitzpatrick et al., 1989; Harting et al., 1991; Carden et al., 2000) including laterodorsal tegmentum (LDTg, Fig. 10A, left), pedunculopontine tegmentum (PPTg, Fig. 10A, left & right), and parabigeminal nucleus (PBG, Fig. 10A, right). High power views of these nuclei (Fig. 10B) showed that tdT-labeled somata were present in the adult (P60) and at birth (P0), and comparable numbers of neurons were labeled. In adults, labeled projections were evident throughout the dorsal thalamus, including the ventral (vLGN) and dorsal lateral geniculate nuclei (dLGN), lateral posterior nucleus (LP), and in the pretectum (PT) (Fig. 10C, left). At P0, cholinergic innervation was sparse in these regions, and entirely lacking in dLGN (Fig. 10C, right).

Consistent with observations made in other mammalian species (Hashikawa et al., 1986; Harting et al., 1991), in mouse we noted that (tdT-labeled) cholinergic axons traversed through the supraoptic decussation and the optic tract (Fig. 11). The supraoptic decussation contains multiple axonal tracts of nonretinal origin, lies adjacent to the optic tract near the cerebral peduncle, and crosses midline along the ventral border of the hypothalamus just caudal and ventral to the optic chiasm (Broadwell & Bleier, 1976). To distinguish between

tdT-labeled cholinergic brainstem axons and retinal axons in the optic tract, we made binocular intravitreal injections of anterograde tracer cholera toxin subunit B (CTB) conjugated to Alexa Fluor 488 (green) in an adult ChAT-Cre x Ai9 mouse. Figure 11 provides coronal views of the optic tract at the level of dLGN (Fig. 11A), cerebral peduncle (Fig. 11B), and optic chiasm (Fig. 11C). At all levels, tdT-labeled cholinergic (red) and CTB-labeled retinal (green) axons shared similar trajectories. In the dorsal thalamus (Fig. 11A), cholinergic and retinal axons coursed together in the optic tract along the dorsolateral boundary of dLGN. At more ventral levels, cholinergic axons were found within the supraoptic decussation along the lateral edge of the cerebral peduncle, as well as in the adjacent optic tract (Fig. 11B). At the base of the brain, at the level of the optic chiasm, cholinergic axons were present along midline in the supraoptic decussation and more laterally where they comingled with retinal axons in the optic tract (Fig. 11C, Fig. 17).

To determine whether retinal input is involved in regulating the development of cholinergic projections to dLGN, we compared the pattern and time course of innervation in ChAT-Cre x Ai9 mice (wild type, WT) with age-matched ChAT-Cre x Ai9 mice bred on a *math5*-null background (*math5*$^{-/-}$), a mutant strain that lacks an optic nerve as well as central retinal projections (Brown et al., 1998; El-Danaf et al., 2015). In both WT and *math5*$^{-/-}$ mice, cholinergic fibers began to innervate dLGN by P5 (Fig. 12A & B). In WTs, cholinergic axons closely followed the optic tract, innervating dorsolateral edge of dLGN (Fig. 12A & A'). However in dLGN of *math5*$^{-/-}$ mice, aggregation of

cholinergic axons along the dorsolateral edge was less striking (Fig. 12B & B'). Figure 13 shows the progression of cholinergic innervation in WT and *math5*$^{-/-}$ at different postnatal ages (P5, P9, P11, P14, P21, and P30). As reported previously, there was a reduction in total size of dLGN in *math5*$^{-/-}$ mice, compared to WTs (El-Danaf et al., 2015). In WTs between P5-P30, cholinergic innervation progressed steadily in a dorsolateral to ventromedial manner so that by P30 the entire nucleus contained a diffuse arrangement of cholinergic arbors. *Math5*$^{-/-}$ mice also showed an age-related increase in cholinergic innervation. However, compared to WT, *math5*$^{-/-}$ mice exhibited alterations in the rate and route of innervation, as well as in the patterning of their axon arbors.

To compare the rate of cholinergic innervation in the WT and *math5*$^{-/-}$ mice, we quantified the degree of cholinergic innervation in dLGN as a function of postnatal age. Figure 14 presents mean values for WT and *math5*$^{-/-}$ mice between P3-P60. While both groups showed a progressive increase with age between P5-30, the rate of innervation was slower for *math5*$^{-/-}$ between P9 and P21. At these ages, the degree of innervation was significantly lower in *math5*$^{-/-}$ compared to age-matched WTs (two-way ANOVA, $F = 2.49$, Bonferroni *post-hoc* test, P9, $p < 0.05$; P11, $p < 0.01$; P14, $p < 0.01$; P18, $p < 0.01$; P21, $p < 0.05$). At P30, the degree of innervation was similar in both groups and remained stable into adulthood (P30-60).

The architecture of cholinergic arbors in dLGN of *math5*$^{-/-}$ mice also differed from WT. Examples of these differences are illustrated in Figure 15 which depicts low and high power views of cholinergic projections in WT (Fig.

6A1 & A2) and *math5*$^{-/-}$ (Fig. 15B1 & B2) mice at P14 and P30. In WT, low power images along with a corresponding “heat map” that plots the intensity of tdT fluorescence, revealed a diffuse and homogeneous intensity profile for areas of cholinergic innervation. High power views of these regions showed an orderly arrangement of fine-caliber axonal processes. By contrast, *math5*$^{-/-}$ mice exhibited ectopic patches of intense fluorescence consisting of a dense tangled plexus of processes.

Another salient phenotype in *math5*$^{-/-}$ mice was the alteration in the route taken by cholinergic axons to arrive in dLGN, especially those which normally traverse through the dorsal thalamus along the optic tract. Figure 16 shows coronal sections of the thalamus in WT and *math5*$^{-/-}$ mice (P14) at a caudal (Fig. 16A & B) and rostral (Fig. 16C & D) level of dLGN. In WTs (Fig. 16A & C), at both levels a large number of cholinergic axons were seen traveling along the outer border of the thalamus. High power views show these projections arise with the optic tract near the cerebral peduncle (Fig. 16A’’ & C’’), and run dorsally along the lateral border of vLGN and dLGN (Fig. 16A’ & C’). However, in *math5*$^{-/-}$ mice, cholinergic axons were displaced medially at caudal dLGN (Fig. 16B & B’), and were not readily apparent at a more rostral level (Fig. 16D & D’). Moreover, while cholinergic axons were present near the cerebral peduncle (Fig. 16B’’), they failed to fasciculate into separate bundles (Fig. 16D’’), that in WT course in the supraoptic decussation and in the optic tract.

Previous studies in rodents indicate that cholinergic axons within the optic tract arise from PBG (Watanabe & Kawana, 1979; Harting et. al., 1991). To

determine whether PBG is the source of the misrouted cholinergic axons observed in *math5*$^{-/-}$, we selectively labeled PBG neurons in adult ChAT-Cre (WT, *n* = 3) and ChAT-Cre *x math5*$^{-/-}$ (*math5*$^{-/-}$, *n* = 4) mice using injections of Cre-dependent anterograde adeno-associated viral tracer FLEX-AAV-ChIEF-tdTomato. Figure 17 shows the pattern of axonal projections following a unilateral labeling of PBG in a WT (Fig. 17A) and *math5*$^{-/-}$ (Fig. 17D) mouse. Examples of the injection site in PBG for WT and math5 null are shown in Figs. 17A' and 17D', along with high power views of tdT expression in PBG neurons in Figs 17A'' and 17D''. In WT, PBG axons coursed within the ipsilateral supraoptic decussation near the cerebral peduncle (Fig. 17B), crossed to the contralateral hemisphere at ventral midline (Fig. 17C), and ascended along the lateral aspect of thalamus with the optic tract (Fig. 17B'). In *math5*$^{-/-}$, PBG axons followed a similar trajectory (Fig. 17E & F) until reaching contralateral ventral thalamus, where they veered in a medial direction traversing dorsally through the medial geniculate nucleus and vLGN (Fig. 17E'). Figure 18 illustrates the patterning of cholinergic arbors within dLGN of WT and *math5*$^{-/-}$ mice after a unilateral injection into PBG. In WTs, the projection to the ipsilateral dLGN was restricted to a small strip of arbors in the dorsomedial pole (Fig. 18A, A1, & A1'). By contrast in *math5*$^{-/-}$ mice, the ipsilateral projection was expanded, occupying a greater area and extending beyond the dorsolateral region of the nucleus (Fig. 18B, B1, & B1'). Despite the expansion of ipsilateral projections, there was no evidence of PBG arbors ectopically innervating areas outside of dLGN (Fig. 18A & B). The projections to contralateral dLGN appeared to be similar in both WT and *math5*$^{-/-}$, with arbors

occupying more territory and distributed throughout the entire nucleus (Fig. 18C, & Fig 18D).

To compare the pattern of PBG projections in WT (n = 3) and *math5*$^{-/-}$ (n = 4) ChAT-Cre mice, we quantified the distribution of tdT-labeled arbors within dLGN. Figure 19 shows a scatter plot quantifying the spatial distribution of td labeled PBG fibers in the ipsilateral (left) and contralateral (right) dLGN. Values represent the percentage of fluorescence in each quadrant (dorsolateral, DL; dorsomedial, DM; ventrolateral, VL; and ventromedial, VM; see Fig 19 inset) as a function of total fluorescence. In the ipsilateral dLGN of WT, we found a significant difference in fiber distribution between quadrants (Kruskal-Wallis, H = 8.23, p = 0.014), with the DL quadrant exhibiting the highest proportion (mean=72.9%). In the ipsilateral dLGN of *math5*$^{-/-}$, labeling either exhibited a variable distribution (n = 2), or was absent altogether (n = 2, not shown). It is important to note that we did observe tdT labeled PBG neurons and their projections throughout the contralateral dLGN. This suggests targeted injections were successful and the absence of label reflects inherent variability in ipsilateral projections. In the contralateral dLGN of WT mice, we noted a significant difference in distribution between quadrants (K-W, H = 9.97, p = 0.0003), with values in DL higher than VM quadrant (Dunn's *post-hoc* test, DL vs. VM, p = 0.013). A similar pattern was seen in contralateral dLGN of *math5*$^{-/-}$ (K-S, H = 14.12, p < 0.0001, Dunn's *post-hoc* test, DL vs. VM; p = 0.002). Finally, we found that arbor distribution in the contralateral dLGN between WT and *math5*$^{-/-}$ were not significantly different from each other (two-way ANOVA, F = 0.87, p = 0.47).

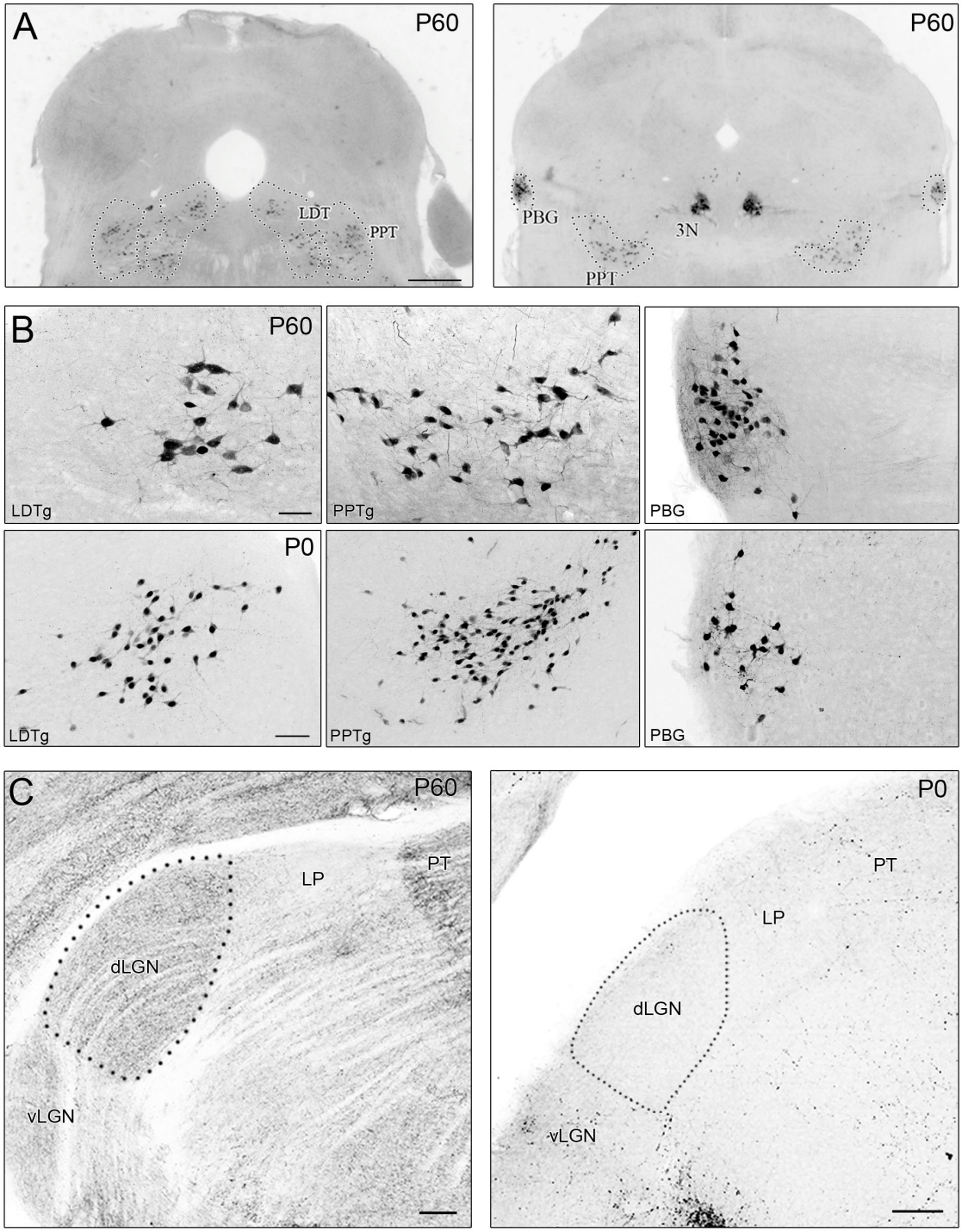

Figure 10. Pattern of tdTomato (tdT) labeling in brainstem and thalamus of ChAT-Cre x Ai9 mouse. **A.** Coronal sections of the brainstem showing tdT labeling in cholinergic neurons in a P60 adult mouse. Left panel depicts the

laterodorsal tegmentum (LDTg), and caudal region of pedunculopontine tegmentum (PPTg), and the right panel shows the rostral PPTg, parabigeminal nucleus (PBG), and oculomotor nucleus (3N). Scale bars = 500 µm. **B.** High power views showing tdT fluorescence in cholinergic neurons of LDTg, PPTg, and PBG of an adult (P60, top) and neonate (P0, bottom). Scale bars = 50 µm. **C.** Coronal sections of adult (left) and neonate (right) dorsal thalamus showing tdT-labeled cholinergic projections and terminals arbors in ventral and dorsal lateral geniculate nuclei (vLGN, dLGN), lateral posterior nucleus (LP), and pretectum (PT). Dotted lines delineate the borders of the dLGN. In the adult, cholinergic fibers project extensively throughout the dorsal thalamus however, at P0 the dLGN is devoid of cholinergic input. Scale bars = 100 µm.

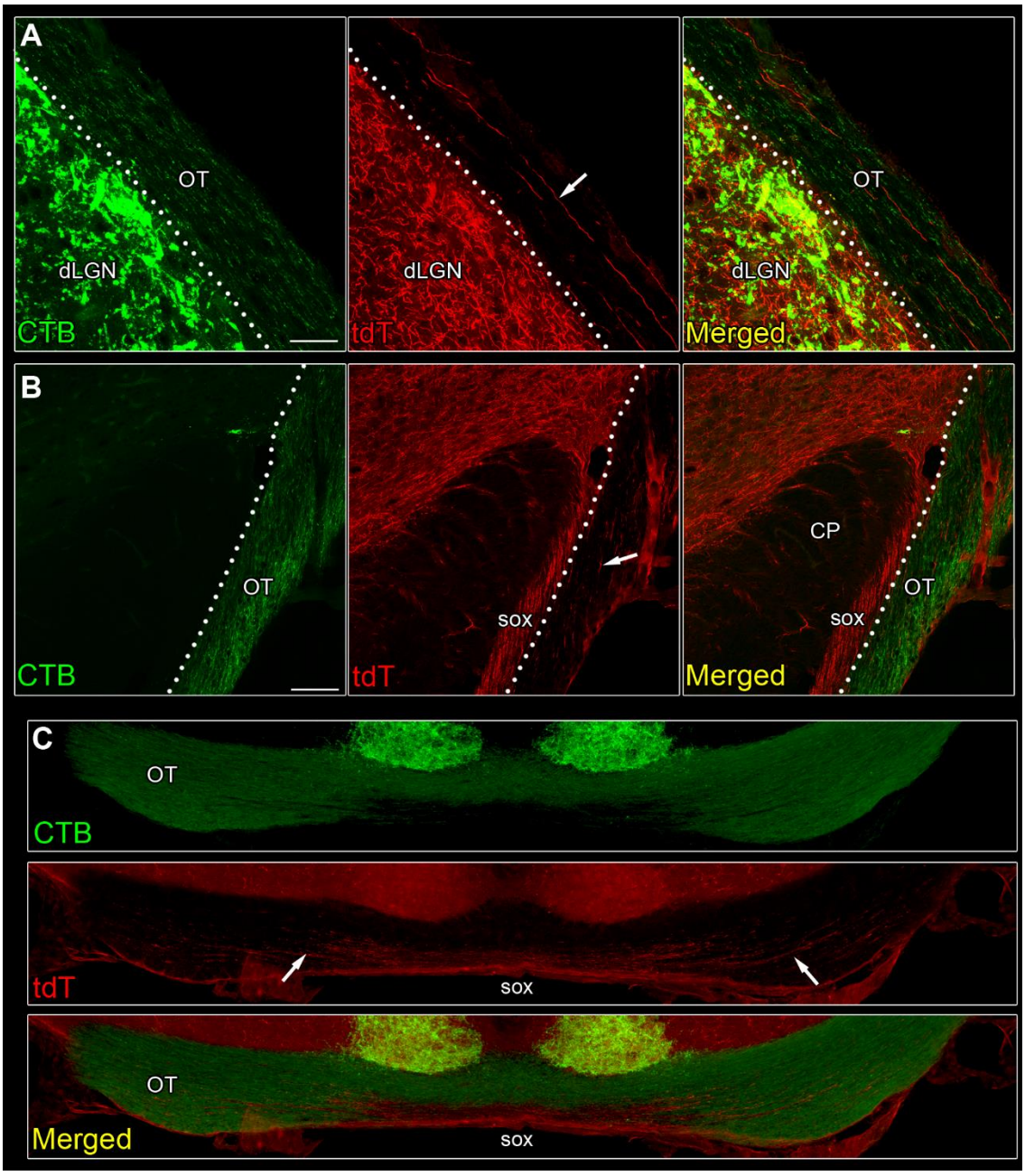

Figure 11. Relationship between cholinergic projections and the optic tract (OT). Coronal sections depicting OT (labeled with CTB-AF-488, green), cholinergic axons (labeled with tdT, red), and a merged image at the level of dLGN (A), cerebral peduncle (B), and optic chiasm (C). **A.** Cholinergic axons course within OT along the dorsolateral border of dLGN. Dotted line delineates the border between the OT and dLGN. Scale bar = 30 µm. **B.** Cholinergic axons travel

within the supraoptic decussation (SOX) along the lateral edge of the cerebral peduncle (CP). Lateral to SOX, cholinergic axons also are seen coursing through OT. Dotted line delineates the border between SOX and OT. Scale bar = 30 µm. **C.** Cholinergic axons are found along midline in SOX, just below the optic chiasm (OX) and also laterally in OT. Scale bar = 200 µm. In panels A-C, arrows depict location of cholinergic axons within OT.

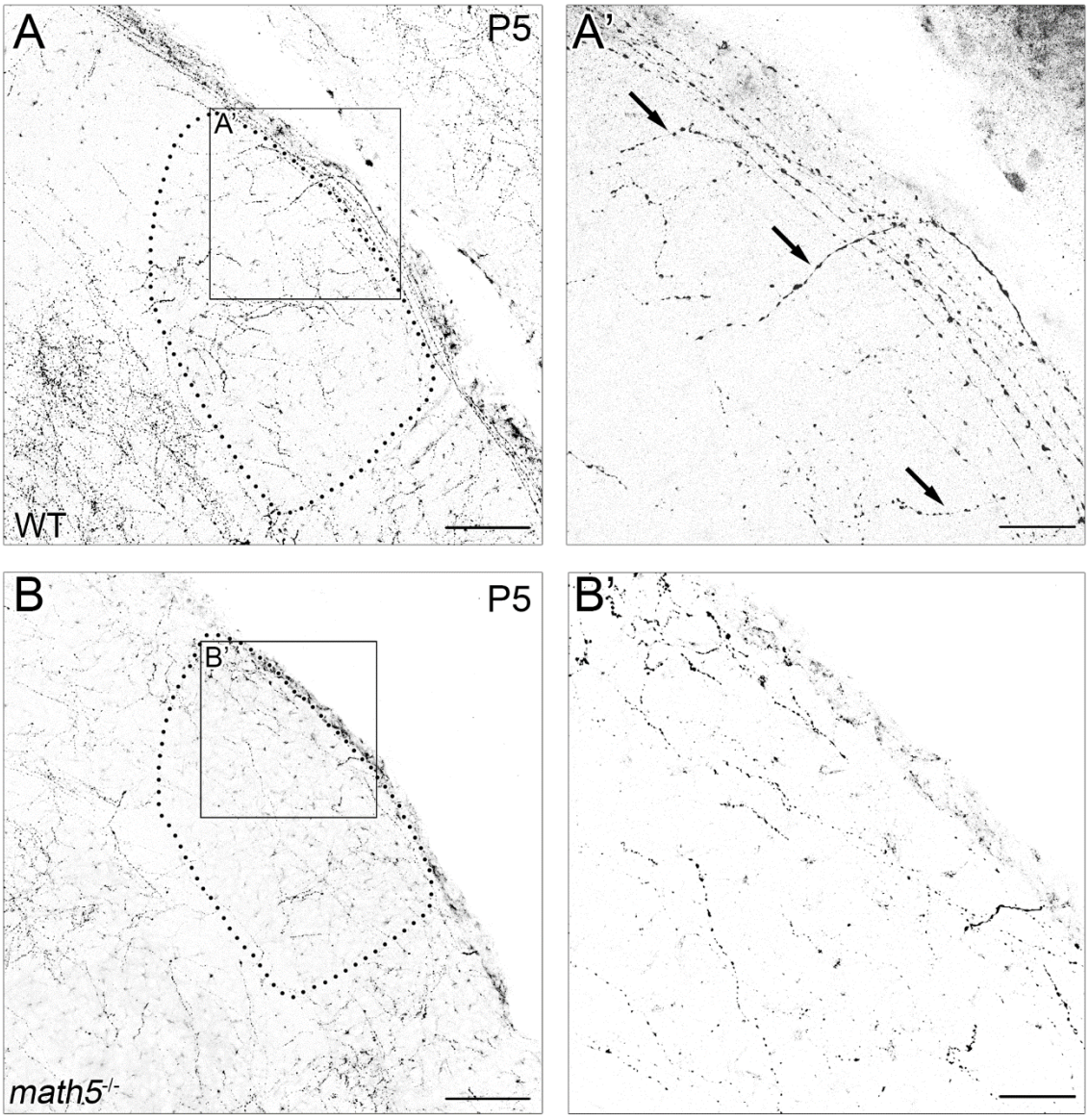

Figure 12. Arrival of cholinergic axons in dLGN during development in the presence and absence (*math5*$^{-/-}$) of retinal input. **A.** Coronal section of WT dLGN at P5, showing cholinergic axons coursing along the dorsolateral edge and entering the nucleus (Fig. 3A', arrows). **B.** Coronal section of P5 dLGN in

math5$^{-/-}$. Cholinergic fibers are present in *math5*$^{-/-}$ but are more widespread running through anteromedial aspect of dLGN (Fig. 3B'). Dotted lines outline the boundaries of dLGN. Scale bars = 100 μm (left panels), 30 μm (right panels).

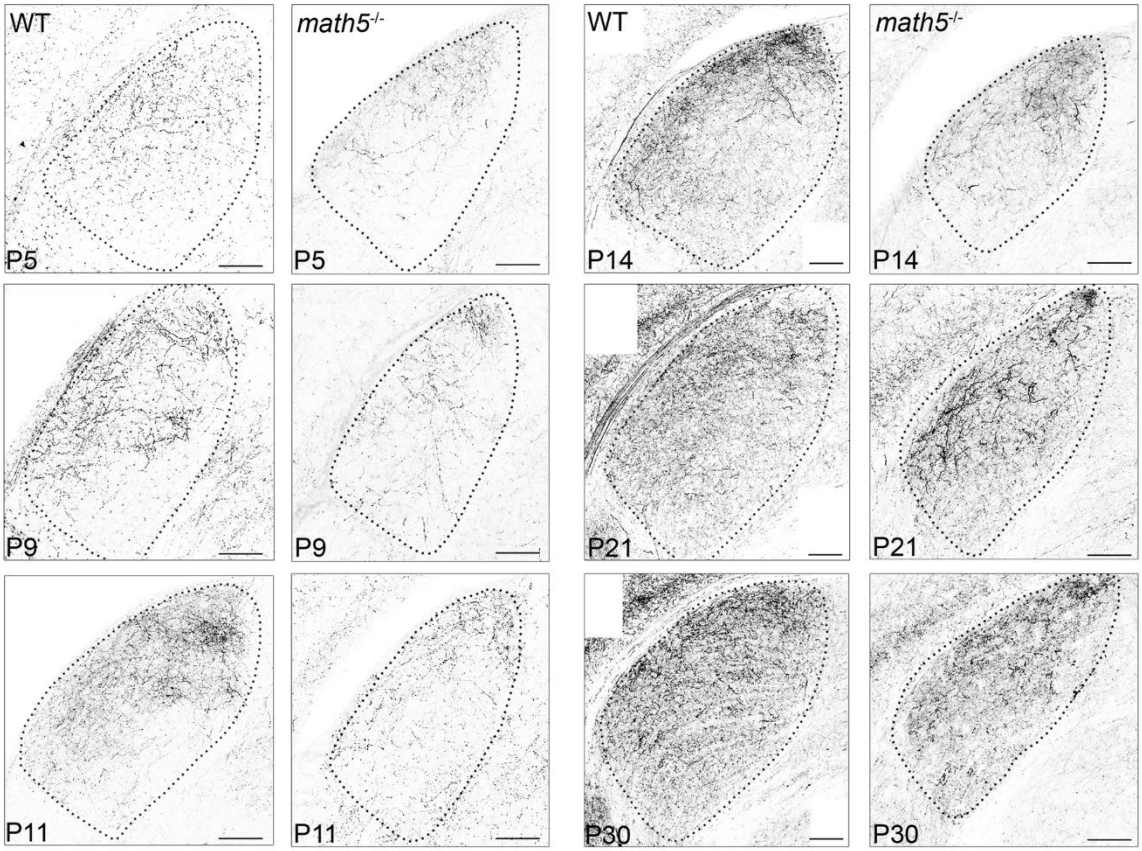

Figure 13. Cholinergic innervation of dLGN in the presence and absence (*math5*$^{-/-}$) of retinal input at different postnatal ages. Examples of coronal sections at P5, P9, P11, P14, P21, and P30, showing the extent of cholinergic innervation in dLGN of WT (left) and *math5*$^{-/-}$ mice (right). Dotted lines outline the boundaries of dLGN. Scale bars = 100 µm.

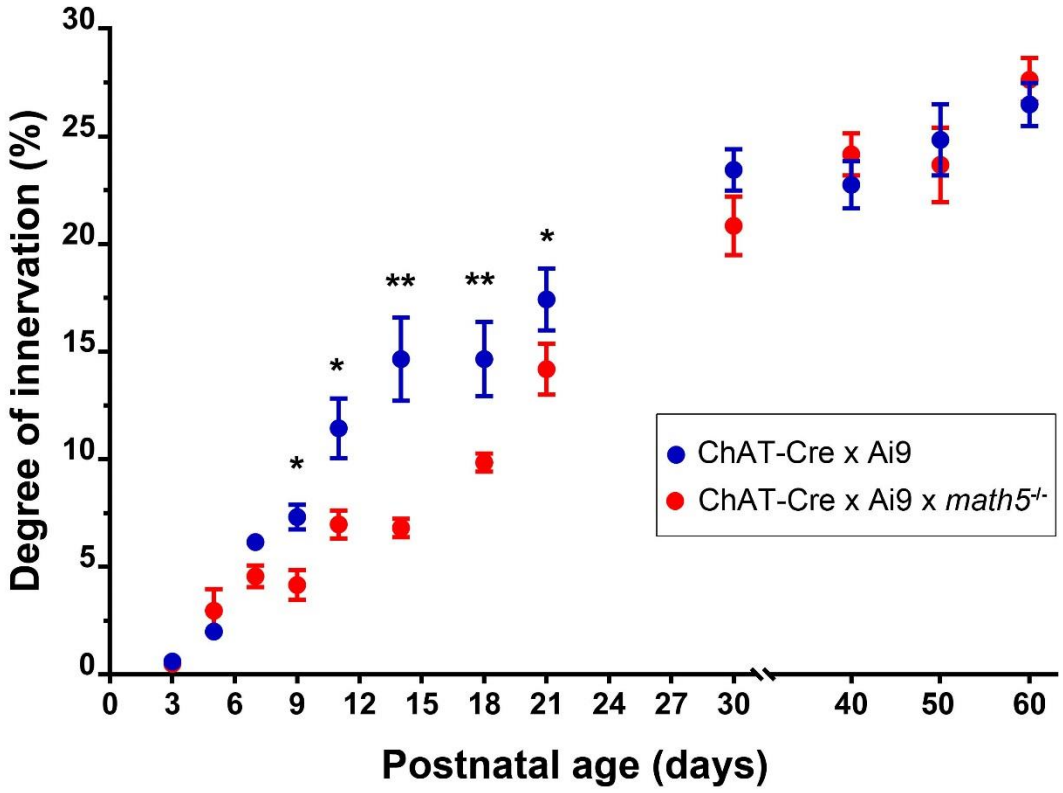

Figure 14. Summary plot depicting the degree of cholinergic innervation in dLGN as a function of postnatal age in WT (blue) and *math5*$^{-/-}$ (red) mice. Each data point represents the mean (±SEM) derived from a total of 4-6 hemispheres, using 3-5 successive sections through the middle of dLGN. Asterisks indicate statistically significant differences in innervation between WT and *math5*$^{-/-}$ (* $p < 0.05$, ** $p < 0.01$).

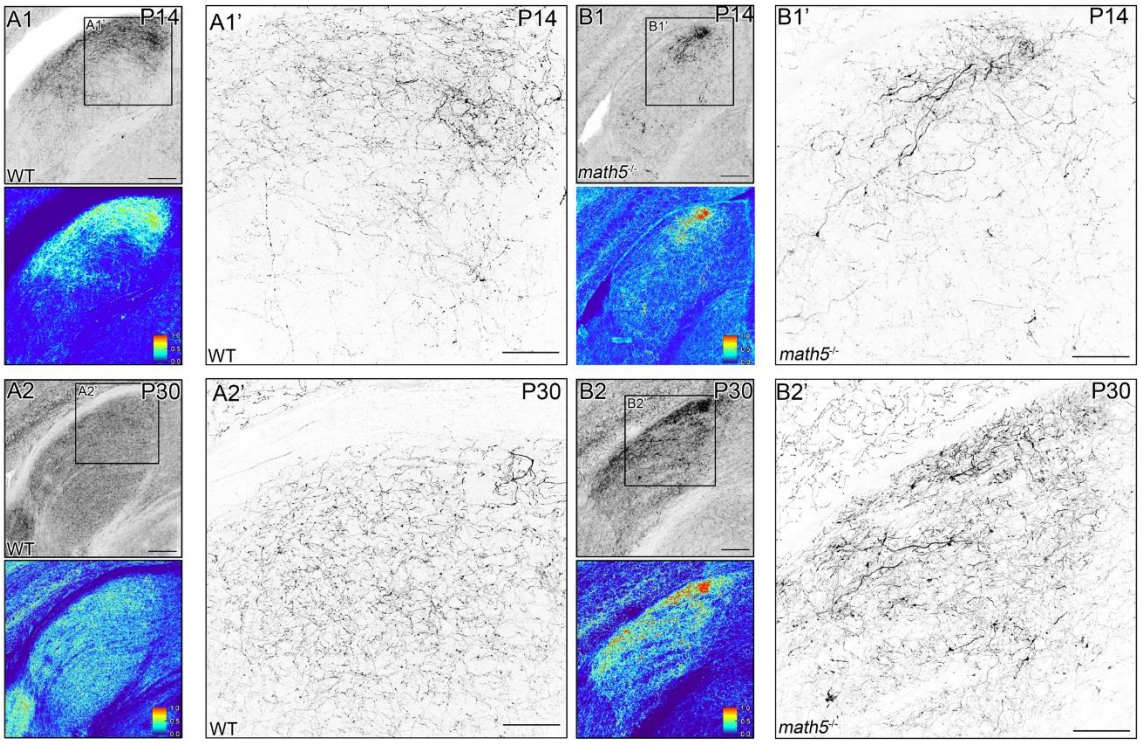

Figure 15. Terminal arbor organization of cholinergic fibers in dLGN in the presence and absence (*math5*$^{-/-}$) of retinal input. Examples of coronal sections through dLGN in WT (A1-2) and *math5*$^{-/-}$ (B1-2) mice at P14 and P30. Top left panels depict a low power image of dLGN. Bottom left panels are corresponding heat maps of fluorescence intensity, where red and blue colors correspond to relative signal intensity values, highest values in red, and lowest values in blue. Right panels show a high power view of the corresponding insets. **A1-2.** In P14 WT (A1), cholinergic fibers form a homogenous pattern of fluorescence in the dorsolateral sector of dLGN, which at P30 (A2) extends throughout the entire nucleus as innervation reaching adult levels. **B1-2.** In P14 (B1) and P30 (B2) *math5*$^{-/-}$ mice, the absence of retinal input leads to disruption of cholinergic terminal arbor organization forming ectopic patches of intense labeling consisting

of thick, tangled axonal processes. Scale bars = 100 µm (left panels), 50 µm (right panels).

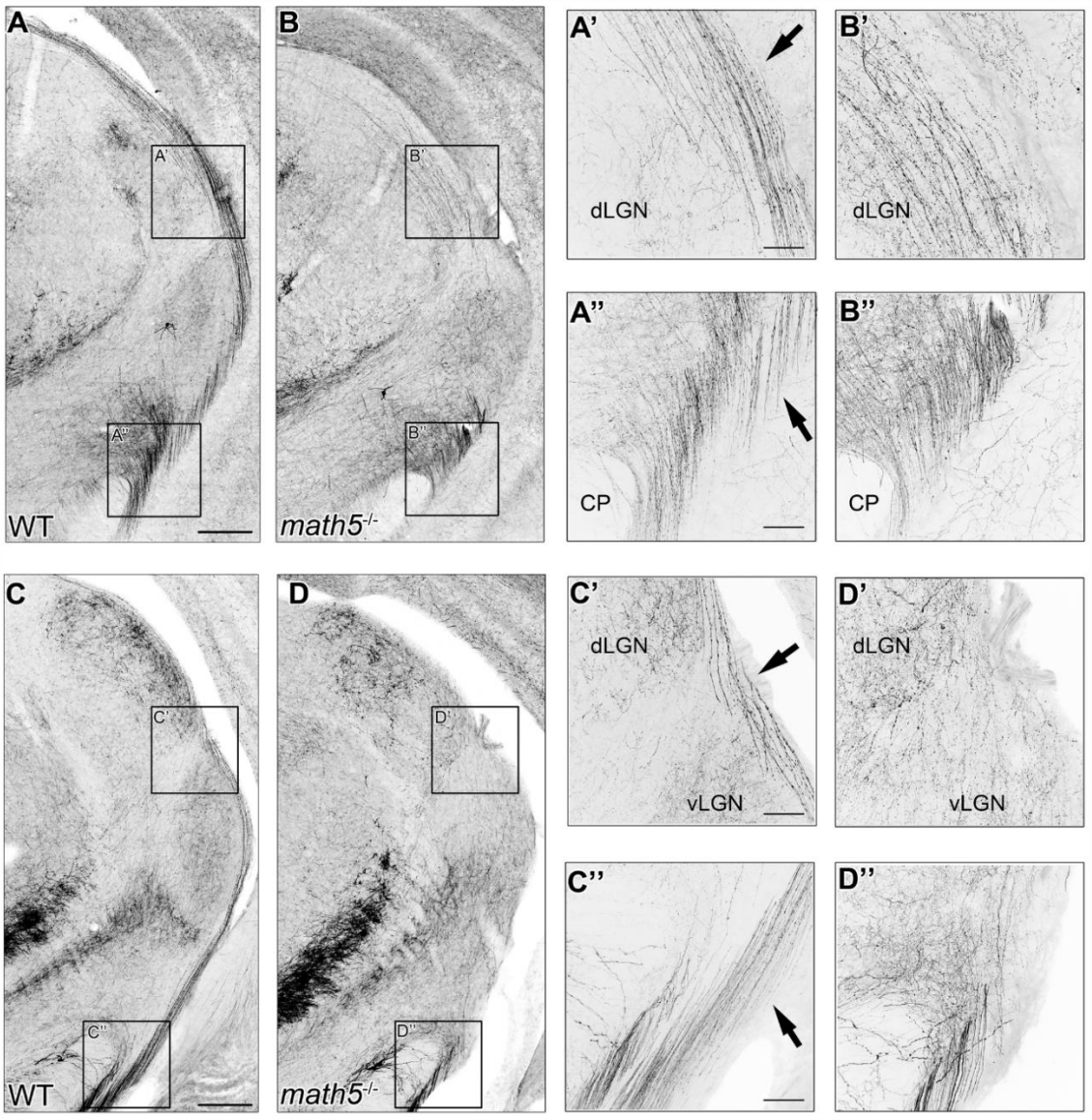

Figure 16. Routing of optic tract-traversing cholinergic axons in the presence and absence (*math5*$^{-/-}$) of retinal input. Example coronal sections through the thalamus are shown at the level of caudal dLGN (top panels) and middle dLGN (bottom panels) for WT (A & C) and *math5*$^{-/-}$ (B & D). High power views at the level of the cerebral peduncle and the border of dLGN/vLGN are shown in the right hand panels. In WT (A & C), cholinergic axons travel with the optic tract near the cerebral peduncle (A'' & C''), and continue dorsally along the outer

border of the vLGN and dLGN (A’ & C’). In *math5*$^{-/-}$ (B & D), cholinergic axons emerge near the cerebral peduncle (B’’ & D’’), but are displaced medially in the caudal dLGN (B’) and middle dLGN (D’). Scale bars = 200 μm (left panels), 50 μm (right panels).

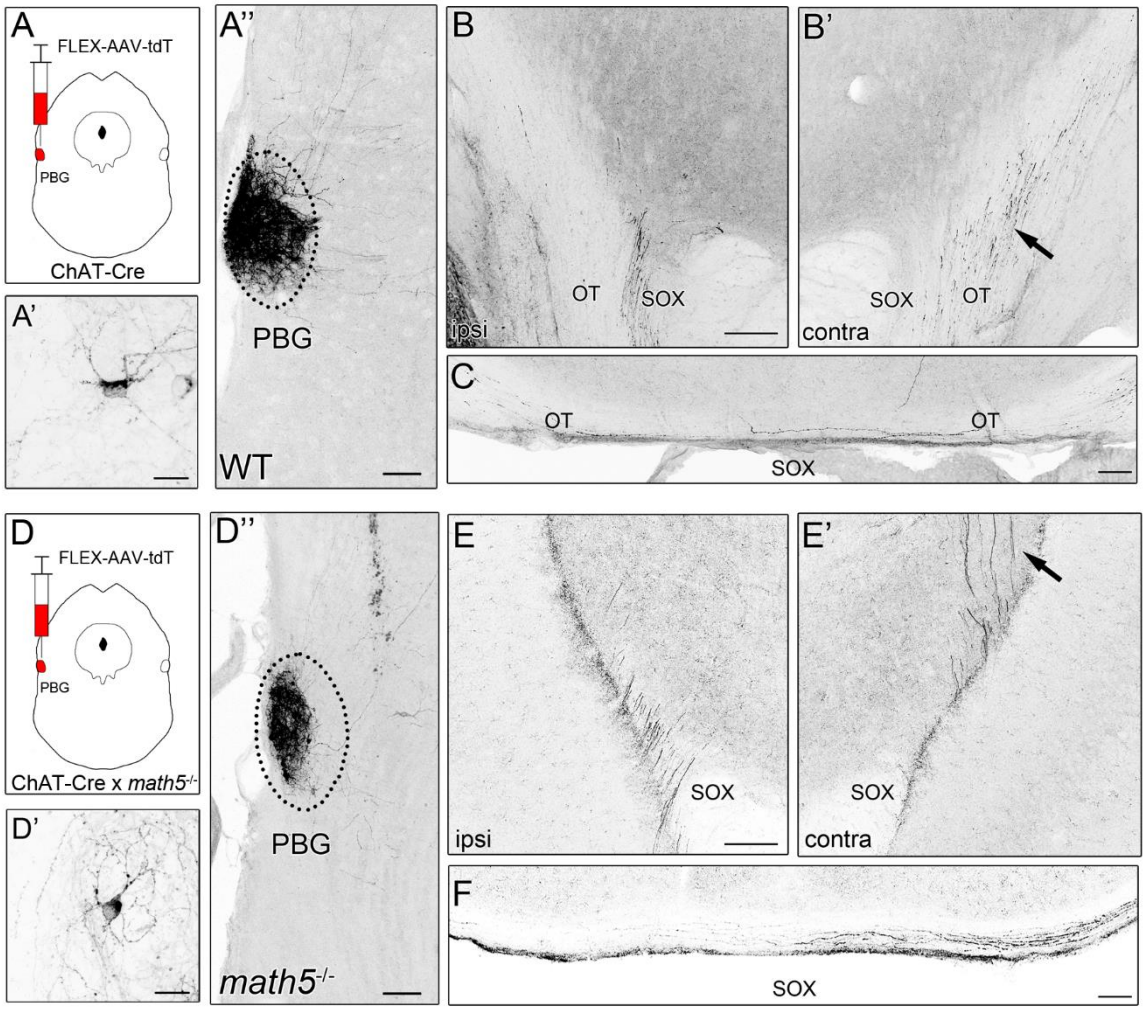

Figure 17. Routing of cholinergic PBG axons in the presence and absence (*math5*$^{-/-}$) of retinal input. Example cases show viral tracer (FLEX-AAV-ChIEF-tdT) injections into PBG of an adult WT (A-C) and *math5*$^{-/-}$ (D-F) ChAT-Cre mice, and the resulting axonal label in the supraoptic decussation (SOX) at the level of cerebral peduncle (CP) and ventral midline. **A.** Injection of viral tracer in WT ChAT-Cre mouse resulted in robust tdT labeling of neurons (A'), restricted to the left PBG (A''). **B.** View of the cerebral peduncles, showing PBG axons traveling in the ipsilateral supraoptic decussation (B), and running dorsally in the contralateral optic tract (B', arrow). **C.** View of the ventral midline showing PBG

axons crossing in the supraoptic decussation and running in the optic tract. **D.** Injection of viral tracer in *math5*$^{-/-}$ mouse resulted in robust tdT labeling of neurons of the left PBG. **E**. In *math5*$^{-/-}$ mice, PBG axons travel in the supraoptic decussation ipsilaterally (E), and run dorsally within the neuropil of the contralateral thalamus (E', arrow). **F.** View of the ventral midline showing PBG crossing in the supraoptic decussation and running laterally along the ventral aspect of the brain. Scale bars = 100 μm, 20 μm (A' & D').

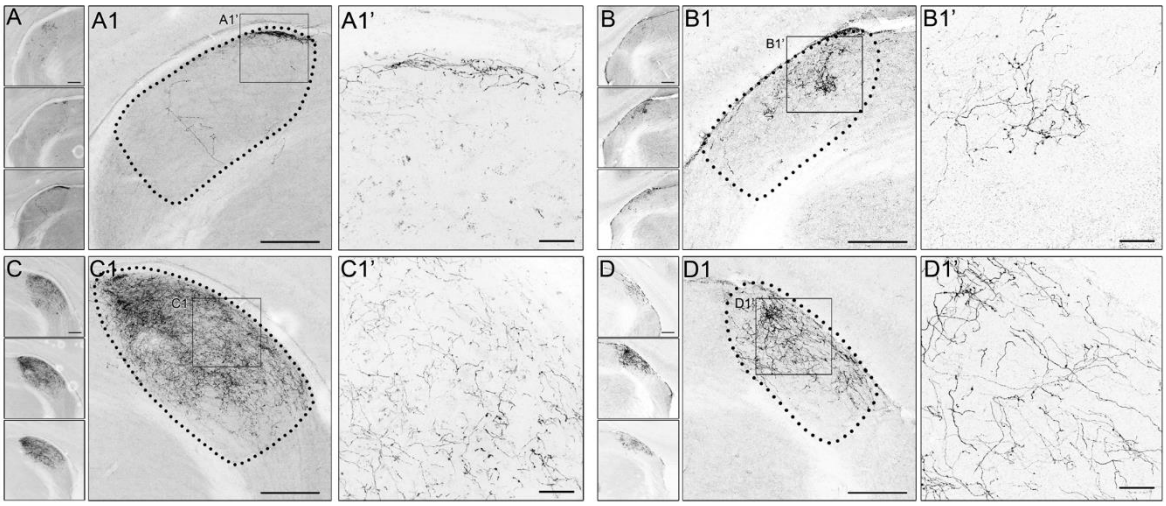

Figure 18. Patterning of PBG terminal arbors in dLGN in the presence and absence of retinal input (*math5*$^{-/-}$). Example coronal sections depicting tdT-labeled terminal arbors in dLGN after an injection of FLEX-AAV-ChIEF-tdT virus into the left PBG in a WT (A & C) and *math5*$^{-/-}$ (B & D) ChAT-Cre mouse. In the left panels, low power images show the distribution of PBG arbors in caudal (top panel), middle, and rostral (bottom panel) dLGN. Middle panels are high power views depicting PBG arbor distribution within an example section of dLGN. Dotted lines delineate the boundaries of dLGN. Right panels show high power views of PBG arbors. **A.** In ipsilateral dLGN of WT, arbors are restricted to a small region in the dorsomedial region of the middle and rostral dLGN, just beneath the optic tract (A1 & A1'). **B.** In the ipsilateral dLGN of *math5*$^{-/-}$, PBG arbors are were displaced into the medial regions of the nucleus (B1 & B1'). **C.** In the contralateral dLGN of WT, arbors are distributed throughout the caudo-rostral extent of dLGN (C1, C1'). **D.** In the contralateral dLGN of *math5*$^{-/-}$, arbors are

distributed throughout the caudo-rostral extent. Scale bars = 200 µm (left and middle panels), 30 µm (right panels).

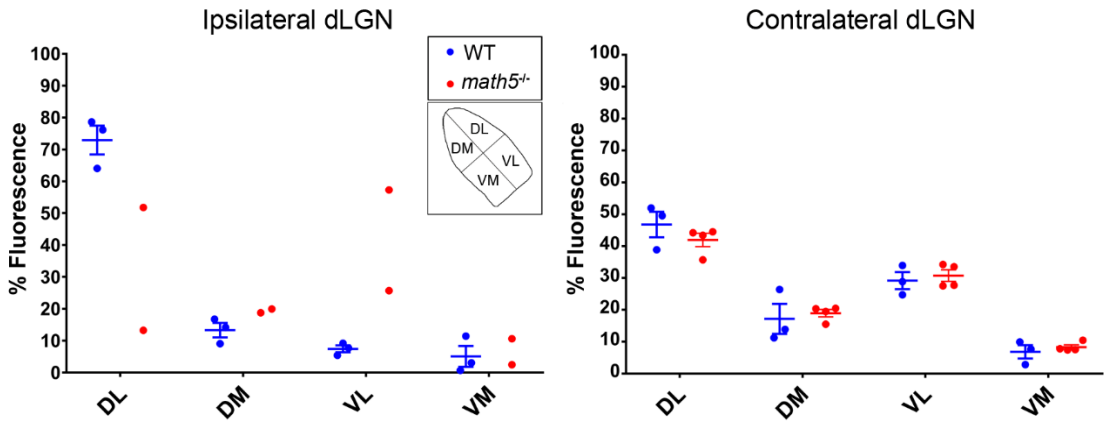

Figure 19. Scatter plot comparing the distribution of tdT-labeled PBG arbors in dLGN of WT and *math5*$^{-/-}$ mice after a unilateral injection of FLEX-AAV-ChIEF-tdT in PBG. Inset depicts the division of dLGN into 4 quadrants used in the analysis, including dorsolateral (DL), dorsomedial (DM), ventrolateral (VL), and ventromedial (VM). Values are expressed as percentage of labeling in each quadrant as a function of total fluorescence. Each data point depicts one dLGN hemisphere from each animal, based on quantification of 4-5 sections. In 2 cases of *math5*$^{-/-}$, no labeling was seen in the ipsilateral dLGN, and therefore were not included in the plot. Horizontal lines represent the mean and SEM.

Discussion

We used a ChAT-Cre mouse, crossed to a tdTomato reporter line (Ai9), to visualize and track the development of brainstem cholinergic projections to dLGN. Our results reveal that cholinergic brainstem innervation of mouse dLGN begins at the end of the first postnatal week, and increases slowly with age to reach an adult-like density by the end of the first postnatal month. Initially, cholinergic fibers appear in the dorsolateral region of dLGN just beneath the optic tract, then gradually progress in a ventromedial direction to form a homogeneous plexus of fibers throughout dLGN. This is consistent with earlier studies in cat and mouse, showing a slow but steady increase in ChAT immunoreactivity with postnatal age (Carden et al., 2000; Ballesteros et al., 2005). Thus, cholinergic innervation of dLGN occurs well after the establishment of the retinogeniculate pathway (Guido, 2008). Moreover, our results support the view that innervation of dLGN occurs in a sequential manner, with retinal projections arriving before nonretinal ones (Seabrook et al., 2013).

Although corticothalamic and cholinergic brainstem projections begin to arrive in dLGN at roughly the same time (P3-P5), their rate of innervation is vastly different. For example, cortical innervation of dLGN is nearly complete between P9-12 (Jacobs et al., 2007; Seabrook et al., 2013), yet brainstem cholinergic innervation is still sparse and restricted largely to the dorsolateral region, only reaching adult-like density of innervation by the end of the first postnatal month. Such timing indicates that the reciprocal connections between the dLGN and visual cortex are established prior to cholinergic brainstem input.

The onset of cholinergic brainstem innervation is consistent with the maturation of other reticular ascending arousal systems and expansion of behavioral repertoire during the late postnatal period (Breese & Traylor, 1972; Lidov & Molliver, 1982; Yamamoto et al., 2000; Cirelli & Tononi, 2015). Overall this suggests that network-wide, state-dependent modulation of sensory information becomes operational well after sensory connections are established.

Our results in *math5*$^{-/-}$ mice also support earlier studies underscoring the importance of retinal input in regulating the timing of nonretinal innervation of dLGN (Seabrook et al., 2013). The absence of retinal input slowed the rate of cholinergic innervation to dLGN, though the overall degree of innervation measured in adults was preserved. It is important to note that retinal input regulates timing of nonretinal input in a bidirectional manner. Whereas the current study showed a slower rate of cholinergic innervation of dLGN in *math5*$^{-/-}$ mice, previous studies in the same mutant demonstrate an acceleration of corticogeniculate innervation, suggesting that retinal input regulates nonretinal development through distinct molecular mechanisms. The accelerated arrival of corticogeniculate axons in *math5*$^{-/-}$ mice results from the disruption of aggrecan, a repellant extracellular matrix molecule that prevents the premature entry of cortical axons into dLGN (Brooks et al., 2013). While the molecular mechanism underlying retinal regulation of cholinergic innervation in dLGN is unresolved, the disruption in the rate of cholinergic innervation in *math5*$^{-/-}$ mice may reflect a reduction of trophic support during development. In other regions that receive cholinergic innervation, neurotrophins such as brain-derived neurotropic factor

(BDNF) and neurotrophin-3 (NT-3), have been shown to promote the growth of cholinergic neurites (Kishino et al., 1997; Mu et al., 1999; Robertson et al., 2006). In WT mice, BDNF and NT-3 are anterogradely transported from the retina to dLGN (Bartheld et al., 1996; Butowt & Bartheld, 2005). Therefore, it is possible that a reduction in the levels of these factors may underlie the dystrophic growth of cholinergic fibers observed in *math5*$^{-/-}$ mutants.

In addition to regulating the rate of cholinergic innervation of dLGN, we demonstrated that retinal input plays a role in establishing the thalamic trajectory of a subset of brainstem cholinergic axons. These axons, which arise from cholinergic neurons of PBG, normally run within the optic tract along the outer border of the thalamus en route to dLGN. However, in *math5*$^{-/-}$ mice PBG axons are displaced, traveling in a diffuse manner through thalamus. This indicates that during development, PBG axons use the retinal axons of the optic tract as a scaffold to navigate through the thalamus. Such axon-axon interactions are typically mediated by cell-adhesion molecules, which promote growth along the length of an existing axon (Pollerberg et al., 2013). Surprisingly, our tracing studies in *math5*$^{-/-}$ mice revealed that such interactions are not necessary for PBG axons to elongate and reach their appropriate target. We found that PBG axons continued to grow through thalamus and reach dLGN even in the absence of an optic tract. Furthermore, nuclei-specific targeting was preserved in *math5*$^{-/-}$ mice. PBG axons continued to innervate dLGN (and superior colliculus, unpublished observations) and were not found in neighboring structures within the lateral geniculate complex. In addition, the laterality of the projection did not

appear to be affected, as the bulk of PBG arbors targeted the contralateral dLGN in both WT and *math5*$^{-/-}$ mice. Therefore, it is likely that PBG axons rely on cues expressed within the thalamus to target, innervate, and arborize in dLGN. Future experiments are needed to fully elucidate the specific cues that govern PBG axon guidance.

Though retinal input does not appear to be necessary for nuclei-specific targeting of PBG input, it plays an important role in establishing the appropriate pattern and morphology of arbors within dLGN. In WTs, PBG arbors were consistently found within the dorsomedial pole of the ipsilateral dLGN, adjacent to the optic tract. However, in *math5*$^{-/-}$ mice this pattern was perturbed, with arbors either extending beyond their usual target in the dorsolateral quadrant of ipsilateral dLGN, or perhaps failing to reach the nucleus altogether. Interestingly, in both WT and *math5*$^{-/-}$ mice, PBG projections to the contralateral dLGN were similar in breadth and distribution.

In several mammals, inputs from PBG, superior colliculus, and certain types of RGCs convergence and target specific layers of dLGN (e.g., C-laminae of carnivores, koniocellular layers of primates), suggesting the existence of a conserved visual channel involved in the coordination of visuo-motor processing (Harting et al., 1986; Fitzpatrick et al., 1988; Harting et al., 1991; Diamond et al., 1992; Bickford et al., 2015). The rodent dLGN contains a homologous region, known as the dorsolateral shell (Reese, 1988), which receives input from direction selective retinal ganglion cells (DSGCs), as well as the superficial layers of the superior colliculus (Cruz-Martin et al., 2014; Bickford et al., 2015). In WT

mice we found an ipsilateral PBG projection to dLGN that targets the dorsolateral shell in a circumscribed area that appears to represent the upper nasal visual fields (Pfeiffenberger et al., 2006; Piscopo et al., 2013). While the presence of retinal input appears to be necessary for the proper targeting of PBG arbors ipsilateral dLGN it has little impact if any on contralateral projections. Thus, it is not yet clear how this is accomplished, or whether it involves interactions with other inputs that target the shell, such as those from DSGCs and/or the superior colliculus.

CHAPTER III

POSTNATAL DEVELOPMENT OF CHOLINERGIC INPUT TO THE THALAMIC RETICULAR NUCLEUS OF THE MOUSE

Introduction

The thalamic reticular nucleus (TRN) is a thin sheet of GABAergic neurons that surrounds the dorsolateral aspect of the mammalian thalamus (Jones, 1975, 2007; Guillery & Harting, 2003). While providing inhibitory input to thalamocortical relay neurons, TRN receives its primary excitatory drive from ascending thalamocortical (TC) and descending corticothalamic (CT) axon collaterals (Guillery et al., 1998; Pinault, 2004; Halassa & Acsády, 2016). Additionally, TRN receives input from several subcortical structures, including a large cholinergic projection from the brainstem and basal forebrain (Woolf & Butcher, 1986; Steriade et al., 1987; Hallanger et al., 1987; Jourdain et al., 1989). Together these projections work in concert to influence many aspects of sensory and motor processing, and play a critical role in the establishment of different cognitive states ranging from sleep and wakefulness, to attention and decision making (Crick, 1984; Pinault, 2004; Fogerson & Huguenard, 2016; Halassa & Acsády, 2016).

The study of adult TRN circuitry has been the topic of intense investigation, however remarkably little is known about when these elements are assembled during postnatal life. While both TC and CT projections begin to course through TRN at perinatal ages (Mitrofanis & Baker, 1993), the question of how and when other subcortical inputs innervate TRN and become operational remains unanswered. To address this, we focused on the development of cholinergic projections to the sensory sectors of TRN. In rodents, these inputs arise from two regions, the brainstem tegmental nuclei (i.e., Laterodorsal tegmentum, LDTg, and Pedunculopontine tegmentum, PPTg), and the cholinergic basal forebrain groups (i.e., nucleus of the horizontal diagonal band, HDB, and substantia innominata, SI) (Hallanger et al., 1987; Jourdain et al., 1989). When activated in sensory sectors of TRN, cholinergic projections evoke biphasic postsynaptic responses (Hu et al., 1989; Pinault & Deschenes, 1992; Sun et al., 2013; Pita-Almenar et al., 2014), modulating the signal transfer of TRN neurons in a state-dependent manner (Ni et al., 2016). Here we adopted a mouse model and utilized genetically modified strains (Madisen et al., 2010 & 2012) to assess the time course of cholinergic innervation and circuit formation within the sensory sectors of TRN.

Materials and Methods

Subjects

All breeding and experimental procedures were approved by the University of Louisville Institutional Animal Care and Use Committee. Cre recombinase expressing mouse lines ChAT-IRES-Cre (Jackson Labs, stock # 006410, strain B6;129S6-Chat$^{tm2(cre)Lowl}$/J) and Crh-Cre (MMRRC, stock # 030850-UCD, strain Tg(Crh-cre)^{KN282Gsat}/Mmucd) were bred to Cre-dependent reporter lines Ai9 (tdTomato; Jackson Labs, stock # 007905 B6;129S6-Gt(ROSA)$^{26Sortm9(CAG-tdTomato)Hze}$/J), or Ai32 (channelrhodopsin-2-eYFP; Jackson Labs, stock #012569, strain B6;129S-Gt(ROSA)$^{26Sortm32(CAG-COP4*H134R/EYFP)Hze}$/J). A total of 77 mice aged P1-P120 of either sex were used in experiments and included Crh-Cre$^{+/+}$ (*n* = 3), Crh-Cre$^{+/-}$ x Ai9$^{+/-}$ (*n* = 1), ChAT-Cre$^{+/-}$ x Ai9$^{+/-}$ (*n* = 18), and ChAT-Cre$^{+/-}$ x Ai32$^{+/-}$ (*n* = 55).

Histology

Brain tissue was harvested from mice that were deeply anaesthetized by hypothermia (<P5) or isoflurane vapors (4%). Animals were transcardially perfused with phosphate-buffered saline (PBS, 0.01 M phosphate buffer with 0.9% NaCl) followed by 4% paraformaldehyde (PFA) in 0.1 M phosphate buffer. Brains were removed and postfixed overnight in 4% PFA, then transferred to PBS. Brains were then blocked, and a vibratome (Leica VT1000S) was used to cut 70 µm-thick coronal sections containing TRN, dorsal thalamus, brainstem, and basal forebrain.

To amplify the inherent tdTomato (tdT) fluorescence in cholinergic processes within TRN, and to prevent photobleaching during confocal imaging, tissue was incubated in DsRed (Clontech) antibody. Sections were placed in blocking medium (10% normal goat serum (NGS), and 0.3% Triton X-100 in PBS) for 1 hour, and then incubated for 12 hours in rabbit anti-DsRed (1:1000) with 1% NGS in PBS. Treated sections were then incubated for 1 hour in 1:100 biotinylated goat anti-rabbit IgG antibody (Vector Labs) with 1% NGS in PBS, followed by 1 hour in 1:100 streptavidin Alexa Fluor (AF) 546 (Life Technologies) in PBS. NeuN antibody was used to visualize TRN neurons and outline the cytoarchitectural landmarks. Tissue was blocked (10% NGS 0.3% Triton X-100 in PBS) for 1 hour, incubated overnight in mouse monoclonal NeuN antibody (Chemicon, 1:100), then for one hour in 1:100 biotinylated goat anti-mouse IgG antibody (Vector Labs) in PBS, followed by 1 hour in 1:100 streptavidin AF-488 (SA AF-488; Life Technologies). All tissue was mounted onto gelatin-subbed glass slides using ProLong mounting medium containing DAPI (Life Technologies).

Viral tracing

To delineate sensory sectors of TRN, intracranial injections of a Cre-dependent adeno-associated viral tracer Flex-rev-oChIEF-tdTomato (Addgene plasmid #30541, serotype 9) were made in the thalamic relay nuclei of adult (P60-P120) Crh-Cre mice. Animals were deeply anesthetized using a ketamine (50mg/kg) /xylazine (10 mg/kg) mixture and placed in a stereotaxic frame. An incision was made along the scalp, and a hole was drilled in the skull above the

injection site. A 2% lidocaine gel was applied to the scalp incision. A Hamilton syringe attached to a nanopump was used to deliver 40 nL of the virus into vMGN (-3.4 AP, -2.0 ML, -3.2 DV; mm from Bregma), VB (-2.2 AP, -1.7 ML, -3.5 DV), or dLGN (-2.3 AP, -2.2 ML, -2.7 DV) of the left hemisphere. The scalp incision was sealed with Vetbond. Heart rate and breathing were continuously monitored and body temperature was maintained at 38 ºC throughout the procedure. After completion of the surgery, mice were monitored for 48 hours and given an analgesic (Carprofen, 5 mg/kg) every 12 hours. Thereafter, mice were monitored daily for a 14-17 day survival period. Mice were then euthanized, and sections containing thalamus and TRN were harvested using methods described above.

Slice preparation and in vitro recording

For *in vitro* electrophysiological recordings, ChAT-Cre x Ai32 mice aged P4-60 were deeply anesthetized with isoflurane (4%) and rapidly decapitated. The brains were removed and placed into cold (4 ºC) oxygenated sucrose cutting solution containing (in mM): Sucrose 234, glucose 11, KCl 2.5, $CaCl_2$ 0.5, $MgSO_4$ 10, NaH_2PO_4 1.25, $NaHCO_3$ 26. A vibratome was used to make 270 µm-thick coronal sections containing TRN. Slices were then incubated in oxygenated artificial cerebrospinal fluid (ACSF) containing (in mM): NaCl 126, $NaHCO_3$ 26, glucose 10, KCl 2.5, $MgCl_2$ 2, $CaCl_2$ 2, NaH_2PO_4 1.25 at 32 ºC for 30 minutes and then transferred to a recording chamber maintained at 32 ºC and perfused continuously at a rate of 2-3 ml/min with oxygenated ACSF.

During recordings, the tissue was visualized using DIC optics on a microscope equipped with a 10X objective, a 60X water immersion objective (Olympus), and a CCD camera (Olympus Y-150), using previously described methods (Dilger et al., 2011). EYFP was visualized with a fluorescent light source through a Chroma filter using a 10X or 60X objective. Borosillicate glass patch electrodes were pulled in two steps using a vertical puller (Narashige PC-10). Patch electrodes were filled with internal recording solution containing (in mM): K-gluconate 117, KCl 13, $MgCl_2$ 1, $CaCl_2$ 0.07, EGTA 0.1, HEPES 10. Biocytin (0.1-0.2% w/v; Molecular Probes) was incorporated in the recording solution and allowed to diffuse into neurons to allow for morphological reconstructions. After completion of recordings, slices containing biocytin-filled neurons were postfixed and incubated overnight in SA AF-647. The final tip resistance of patch electrodes was 8-12 MΩ. Whole-cell current and voltage clamp recordings were made using Multiclamp 700B amplifier (Molecular Devices), filtered at 3-10 kHz, and digitized (Digidata 1440A) using techniques described in detail elsewhere (Dilger et al., 2011; Jurgens et al., 2012; Seabrook et al., 2013). Recordings were conducted in neurons with resting membrane potential between -55 and -75 mV and series resistance between 10 and 25 MΩ. Pipette capacitance, series resistance, input resistance, and whole-cell capacitance were monitored throughout the recording session. To photoactivate ChR2-expressing cholinergic neurons or their processes, a light emitting diode (LED) (Prizmatix) was used to deliver blue light through the 60X objective. The illuminated spot was 0.45 mm in diameter, with light power of 300 mW/mm^2.

All light evoked responses were recorded in the presence of glutamate receptor antagonists (AMPA: 20 µM DNQX; NMDA: 10 µM (RS)-CPP). In some instances, (*n* = 3), GABA blockers ($GABA_A$: 10 µM SR-95531; $GABA_B$: 10 µM CGP-54626) were used to assess the pharmacology of light-evoked hyperpolarizing responses. To isolate nicotinic responses, recordings were done in the presence of the muscarinic blocker atropine (5 µM) or the M_2 muscarinic receptor antagonist, AF-DX 116 (5 µM). To examine muscarinic responses, recordings were conducted with the α4β2 nicotinic receptor antagonists DhβE (300 nm-5 µM) or the α7 antagonist MLA (5 µM). All drugs were dissolved in ACSF and bath-applied using methods described previously (Jurgens et al., 2012).

To quantify the incidence and amplitude of nicotinic and muscarinic receptor-mediated postsynaptic responses (Fig. 8 & 9), whole-cell recordings were conducted in ChAT-Cre x Ai32 mice between P4-P28 in voltage-clamp mode and at a holding potential of -70 mV. For photactivation, a short pulse (3 ms.) of blue light was presented over 5 consecutive trials. An inter-stimulus interval of 40 seconds between trials was used to avoid desensitization of cholinergic receptors and to account for long-lasting metabotropic muscarinic receptor-mediated currents. ClampFit analysis software (Molecular Devices) was used to measure the peak amplitude for postsynaptic nicotinic excitatory postsynaptic currents (nEPSC) or muscarinic inhibitory postsynaptic currents (mIPSC) on a trial-by-trial basis. Only trials where the peak amplitude of the nEPSC or mIPSC was above 2 standard deviations of root mean square (RMS)

peak-to-peak noise were considered as a response. For each neuron a mean peak amplitude was calculated that was based on 3-5 trials.

Image acquisition and analysis

All images were acquired using a laser scanning confocal microscope (FV 12000BX61) equipped with a 20X objective (0.75 NA). For clarity, the anatomical images displayed in Figs. 20-22, and 24-25 were digitally adjusted by inverting and enhancing their contrast. The images portrayed in Figs. 20B, 21C, 22, 24A-B were comprised of 2 or more sections that were digitally aligned and stitched together.

To quantify the degree of cholinergic innervation in TRN at different postnatal ages, three coronal sections through the rostro-caudal extent of sensory TRN were used (Figs. 20 , 22; AP -1.7 mm, -1.5 mm, and -1.3 mm from bregma; Paxinos & Franklin, 2004) (70 µm thickness, 1.14 µm optical sections). In order to maximize fluorescent signal detection while avoiding oversaturation, parameters for image acquisition were calibrated using the brightest and dimmest samples, and held constant for all analyzed sections. The images were collapsed in the Z-plane and imported into Photoshop (Adobe), where the area of TRN was outlined using DAPI staining. A threshold value (pixel intensity of 60) was chosen on the luminance histogram that provided a clear distinction between fluorescent signal and background, thereby generating a binarized image (Jaubert-Miazza et al., 2005; Demas et al., 2006; Seabrook et al., 2013; Dilger et al., 2015). ImageJ (NIH) was used to count the number of pixels comprising the signal and the total area of visual and nonvisual sectors of TRN (see Fig. 20D).

Based on anterograde tracing experiments, the visual sector of TRN (visTRN) was defined as the area above the apex and included the “head” of TRN, while nonvisual sector of TRN (non-visTRN) was defined as the area below the apex, and included the tail of TRN (see Results & Fig. 20C). This delineation is consistent with the divisions used by others (Kimura, 2014; Wimmer et al., 2015; Chen et al., 2015; Clemente-Perez et al., 2017). For each sector, the values were expressed as a percentage of the fluorescence signal in relation to the total area. Thus, in Figure 23 the degree of innervation is the area containing detectable fluorescence in relation to the total area of visTRN and non-visTRN. The percentages simply reflect an estimate of the density of cholinergic fibers innervating TRN.

In slices containing biocytin-filled TRN neurons, the location of responsive and non-responsive neurons to photoactivation of cholinergic terminals were mapped and plotted on a composite reconstruction of TRN (Figs. 26-27). For postnatal weeks 2-4, each TRN was digitally aligned using the apex as the reference point. For postnatal weeks 3 and 4, the size and shape of slices containing TRN were comparable. However, during postnatal week 2 (P7-13) TRN expanded in size, especially in the dorso-ventral extent. Thus, the slices comprising the composite plot for week 2 were calibrated to reflect the size and shape of TRN measured at P13.

Results

Previous studies in rat demonstrate that sensory thalamic nuclei project to TRN in a modality-specific, sectorial manner (Montero et al., 1977; Ohara & Lieberman, 1985; Coleman & Mitrofanis, 1996; Kimura et al., 2005). To confirm that such an arrangement exists in mouse, we used anterograde tracing techniques to label thalamocortical projections and their collaterals in TRN. To accomplish this, we utilized a mouse line that expresses Cre recombinase under the control of a promoter for corticotropin releasing hormone (Crh-Cre). In this strain, Cre is expressed in the thalamocortical neurons of first order sensory thalamic nuclei but not in higher order nuclei (e.g., ventral lateral geniculate nucleus, lateroposterior nucleus, posterior nucleus, etc), TRN, or the neocortex (Fig. 20A). When crossed with a tdTomato reporter line (Ai9), somatic labeling is present in ventral medial geniculate nucleus (vMGN), ventrobasal nucleus (VB; includes ventral posterolateral nucleus, VPL, and ventral posteromedial nucleus, VPM), and dorsal lateral geniculate nucleus (dLGN). The tdT-labeled axons of thalamocortical relay neurons can be seen coursing through TRN, internal capsule, and ultimately terminating in primary sensory areas of cortex, including auditory (A1), somatosensory (S1), and visual (V1) areas. By utilizing a Cre-dependent anterograde viral tracer FLEX-AAV-ChIEF-tdT, and making targeted injections into dLGN, VB, or vMGN of Crh-Cre mice, we were able to label thalamocortical projections in TRN. Staining with a neuronal marker NeuN (Fig. 20B) also reveals the cytoarchitecture and general shape of TRN in the coronal plane, including the dorsal “head”, the lateral “apex”, and the ventral “tail”

(Clemente-Perez et al., 2017). The viral tracing of thalamic inputs to TRN is summarized in Figure 20C. The left panels provide locations of targeted viral injections which resulted in tdT expression restricted to vMGN, VB, or dLGN. Corresponding panels on the right depict the location of tdT-labeled axonal projections arising from each sensory relay nucleus at three caudo-rostral levels of sensory TRN. In each case projections were arranged largely in a non-overlapping, sectorial manner. Projections from vMGN were found in the caudal-most regions of the TRN, and occupied a limited area of the “tail” in more rostral sections (Fig. 20 C1, right). Whereas, VB projected to more rostral areas of sensory TRN compared to vMGN, targeting regions below the apex and the ventral “tail” (Fig. 20 C2). Projections from dLGN were found in a similar rosto-caudal plane as those from VB, but innervated a region dorsal of the apex, including the “head” of the nucleus (Fig. 20 C3). Because vMGN and VB projections occupy regions below the apex, it is difficult to distinguish the caudo-rostral arrangement in the coronal plane. Therefore, we considered the region ventral to the apex, including the tail, as non-visual TRN (non-visTRN), and regions above the apex, including the head, as visual TRN (visTRN) (Fig. 20D; Kimura 2014; Wimmer et al., 2015; Clemente-Perez et al., 2017). Overall, these tracing experiments underscore the sectorial arrangement of sensory TRN, (Fig. 20D). Moreover, we used these demarcations to assess whether separate sensory sectors exhibit age-related differences in the progression of cholinergic innervation.

To visualize cholinergic neurons and their processes we crossed a ChAT-Cre mouse, which expresses Cre recombinase under the control of choline acetyltransferase (ChAT) promoter, to a tdTomato (tdT) reporter line (Ai9) (Madisen et al., 2010). Figure 21 shows the pattern of tdT labeling in the brainstem, basal forebrain, and TRN of an adult ChAT-Cre x Ai9 mice. In the brainstem (Fig. 21A-B), somatic tdT labeling was evident in TRN-projecting cholinergic neurons of the pedunculopontine tegmentum (PPTg) and laterodorsal tegmentum (LDTg) (Woolf & Butcher, 1986). Similarly, tdT labeling was present in cholinergic neurons of the basal forebrain (Fig. 21A, B top), including nucleus of the horizontal diagonal band (HDB), and substantia innominata (SI), which innervate TRN and the cortex (Woolf & Butcher, 1986; Hallanger et al., 1987). Together, brainstem and basal forebrain cholinergic nuclei give rise to a dense labeling pattern throughout the sensory regions of TRN (Fig. 21C). Moreover, tdT-labeled neurons in brainstem and BF were present at birth (Fig. 21B, bottom), indicating that their projections could be followed throughout early postnatal development.

To determine the time course of cholinergic innervation of sensory TRN, we examined ChAT-Cre x Ai9 mice at different postnatal ages from birth to adulthood. Figure 22 depicts examples of TRN sections of ChAT-Cre x Ai9 mice at selected ages between P1-P21. This series suggests that cholinergic innervation begins around the time of birth, proceeds in a ventral-to-dorsal manner, and becomes adult-like by the end of the third postnatal week. Between P1-P3, thin unbranched cholinergic axons were seen coursing in a medial-lateral

direction within the thalamus and entering the ventral, non-visTRN. At P5, a sparse field of cholinergic arbors was evident in non-visTRN. More dorsal regions corresponding to visTRN began to receive cholinergic input at P7, with the fibers extending to the dorsal tip of the head of TRN by P11. During the second and third week, cholinergic processes throughout TRN increased in density, and by P21, exhibited a reticular appearance that was especially prominent below the apex in non-visTRN. This progression is summarized in Figure 23, which quantifies the degree of cholinergic innervation in visual and non-visual regions of TRN throughout the first postnatal month. The scatter plot depicts the values of cholinergic innervation within visTRN and non-visTRN, expressed as the percentage of area containing tdT fluorescence. In non-visTRN, innervation increased rapidly during the first postnatal week, reaching maximal values by P11. However, cholinergic innervation of visTRN lagged considerably, showing a slower rate of innervation and reaching maximal values at P21. Both visTRN and non-visTRN showed a significant age-related increase in cholinergic innervation (two-way ANOVA, $F(8,54) = 80.4$, $p = 0.0001$). Moreover, between P1-P9, the degree of innervation of non-visTRN was significantly greater than visTRN (Bonferroni *post hoc* test, P1, $p = 0.035$; P3, $p = 0.021$; P5, $p = 0.015$; P7, $p = 0.002$; P9, $p = 0.003$). Between P11-14 values for the two regions were comparable. However, at P21 and P30, visTRN continued to show a substantial increase, whereas non-vis TRN stabilized (Bonferroni *post hoc* test, P21, $p = 0.001$; P30, $p = 0.001$). This difference is likely brought about by the formation of

the reticular pattern of cholinergic processes within ventral regions of TRN (Figs. 21C, Fig. 22).

To assess the synaptic properties of cholinergic transmission in TRN, we conducted *in vitro* whole-cell recordings from TRN neurons of acutely prepared thalamic slices while stimulating the release of Ach from synaptic terminals. To accomplish this, we took an optogenetic approach and selectively expressed channelrhodopsin-2 (ChR2) in cholinergic neurons by crossing ChAT-Cre mice to a Cre-dependent ChR2-eYFP reporter line (ChR2-eYFP; Ai32). Figure 24 portrays an acutely prepared coronal slice containing TRN from an adult ChAT-Cre x ChR2 mouse, as well as examples of light-evoked evoked cholinergic responses recorded throughout the visual and non-visual regions of TRN. In TRN, ChR2-eYFP fusion protein was present in cholinergic arbors, and resembled the pattern of tdT labeling pattern shown above (Fig. 24A vs. Figs. 21-22). Figure 24B depicts a typical recording experiment, where biocytin-filled electrodes were used to track the location of TRN neurons and their light-evoked responses. In adult TRN neurons (P30-45; n = 7) blue light stimulation (single pulse, 3 ms.) of cholinergic terminals evoked a biphasic, excitation-inhibition (E-I) response (Fig. 24B & C, left; see also Sun et al., 2013; Pita-Almenar et al., 2014). The E-I response consisted of a fast initial depolarization, followed by a long-lasting hyperpolarization. In some neurons, the initial excitatory response evoked spike firing (Fig. 24C, right). Figure 24D provides additional examples of light evoked responses and their underlying pharmacology. Bath application DhβE (5 μM), a nicotinic antagonist, abolished the excitatory component of the E-

I response, while atropine (5 µM), a muscarinic antagonist, blocked the inhibitory component. Taken together, these data confirm previous reports indicating that the biphasic E-I response is mediated by nicotinic and muscarinic receptor activation, respectively (Hu et al., 1989; Sun et al., 2013; Pita-Almenar et al., 2014; Ni et al., 2016).

To explore the development of cholinergic synaptic activity in TRN we conducted recordings in ChAT-Cre x ChR2-eYFP mice at early postnatal ages. To confirm that ChR2 is present in cholinergic neurons, we first recorded somatic light-evoked responses directly from cholinergic neurons of neonatal ChAT-Cre x ChR2-eYFP mice. Figure 25 depicts examples of responses from biocytin-filled cholinergic neurons of basal forebrain (Fig. 25 A1; HDB) and brainstem (Fig. 25 A2; PPTg) of a P4 ChAT-ChR2-eYFP mouse. Repetitive presentation of blue light pulses (1 ms., 1 or 5 Hz) evoked a train of depolarizations with spikes riding their peaks (Fig. 25 B1&B2). Stimulation with a sustained light pulse (100 ms.) evoked fast-onset, long-lasting, stable excitatory currents, showing little if any desensitization (Fig. 25 C1&C2). However, for TRN neurons recorded during the first postnatal week (P4-5), light-evoked cholinergic responses were extremely rare (2/9, 22.2%), purely excitatory, small in amplitude (2-3 mv), and found only in the non-visTRN. During week 2 cholinergic responses were more reliably evoked (29/39; 74.4%) with most exhibiting a biphasic profile.

To examine the development of each E-I component separately, we conducted voltage-clamp recordings during postnatal weeks 2-4, in the presence of muscarinic (5 µM atropine) or nicotinic antagonists (300 nM DhβE). The results

for excitatory nicotinic responses are summarized in Figure 26. Figure 26A depicts the location of TRN neurons during blue light stimulation (3 ms. pulse) of cholinergic terminals for postnatal weeks 2, 3 and 4. Each neuron was designated as residing in visTRN or non-visTRN, and as responsive or non-responsive to blue light stimulation. The location of each neuron within TRN was determined by biocytin reconstructions (n = 117; plotted in Fig. 26A), or through visualization of the pipette tip during recordings (n = 33, not shown but included in the analysis). Figure 26B summarizes the percentages of responsive and non-responsive neurons in visTRN and non-visTRN. Overall, there was an age-related increase in the incidence of responsive neurons (Chi square, week 2: 32/73, 43.8% *vs.* week 3: 34/51, 66.7%, χ^2 (1) = 6.26, p = 0.01; week 3: 34/51, 66.7% *vs.* week 4: 25/26, χ^2 (1) = 8.21, p = 0.004). During week 2, a significantly greater proportion of responsive neurons were located in non-visTRN, compared to visTRN (Chi square, visTRN 27.3%, n = 33 *vs.* non-visTRN 57.5%, n = 40, χ^2 (1) = 6.62, p = 0.01). For weeks 3 and 4, the proportions of responsive and non-responsive neurons were comparable between the two sectors (Chi-square, week 3: visTRN 70.4%, n = 27 *vs.* non-visTRN 62.5%, n = 24, χ^2 (1) = 0.35, p = 0.55; week 4: visTRN 90.9%, n = 11 *vs.* non-visTRN 100%, n = 15, χ^2 (1) = 1.36, p = 0.24). Examples of nicotinic responses recorded at different postnatal weeks are shown in Figure 26A, and the average response amplitudes for neurons located in visTRN and non-visTRN are summarized in Figure 26C. Overall, the amplitude of nicotinic responses increased significantly between postnatal weeks 2 and 4, (Kruskal-Wallis, H = 27.6, p = 0.001, Dunn’s comparison, week 2 vs. 3,

Q = 3.1 p = 0.005, week 2 vs. week 4, Q = 5.19, p = 0.001). While a 3-fold increase in amplitude was noted between weeks 2 and 4, there were no significant differences between visTRN and non-visTRN (Mann-Whitney, week 2: U = 99, p = 0.87; week: 3 U = 89, p = 0.11; week 4: U = 56, p = 0.30).

A similar analysis was conducted on muscarinic inhibitory responses of 71 neurons and the results are summarized in Figure 27. The plots in Figure 27A depict the locations of TRN neurons for each week (n = 66), along with representative examples of muscarinic responses in visTRN and non-visTRN. Overall, an age-related increase in the incidence of muscarinic responses occurred between week 2 and 4 (Chi-square, week 2 30.8%, n = 26 *vs.* week 4 90.9%, n = 22, χ^2 (1) = 17.4, p = 0.001). The incidence of responsive neurons located in visTRN and non-visTRN (Fig. 27B) was similar across each postnatal week (Chi square, week 2: visTRN 38.5%, n = 13 *vs.* non-visTRN 33.1%, n = 13, χ^2 (1) = 0.69, p = 0.40; week 3: visTRN 53.8%, n = 13 *vs.* non-visTRN 60%, n = 10, χ^2 (1) = 0.10, p = 0.76; week 4: visTRN 90%, n = 10 *vs.* non-visTRN 91.7%, n = 12, χ^2 (1) = 0.02, p = 0.89). The amplitude of muscarinic responses increased significantly between postnatal weeks 2 and 3 (Kruskal-Wallis, H = 17.32, p = 0.001, Dunn's comparison, week 2 *vs.* 3, Q = 2.68, p = 0.022; week 2 vs. 3, Q = 4.16, p = 0.001), and there were no significant differences between visTRN and non-visTRN values (Mann-Whitney, week 2: U = 6, p = 0.79; week 3: U = 17, p = 0.63; week 4: U = 48, p = 0.94).

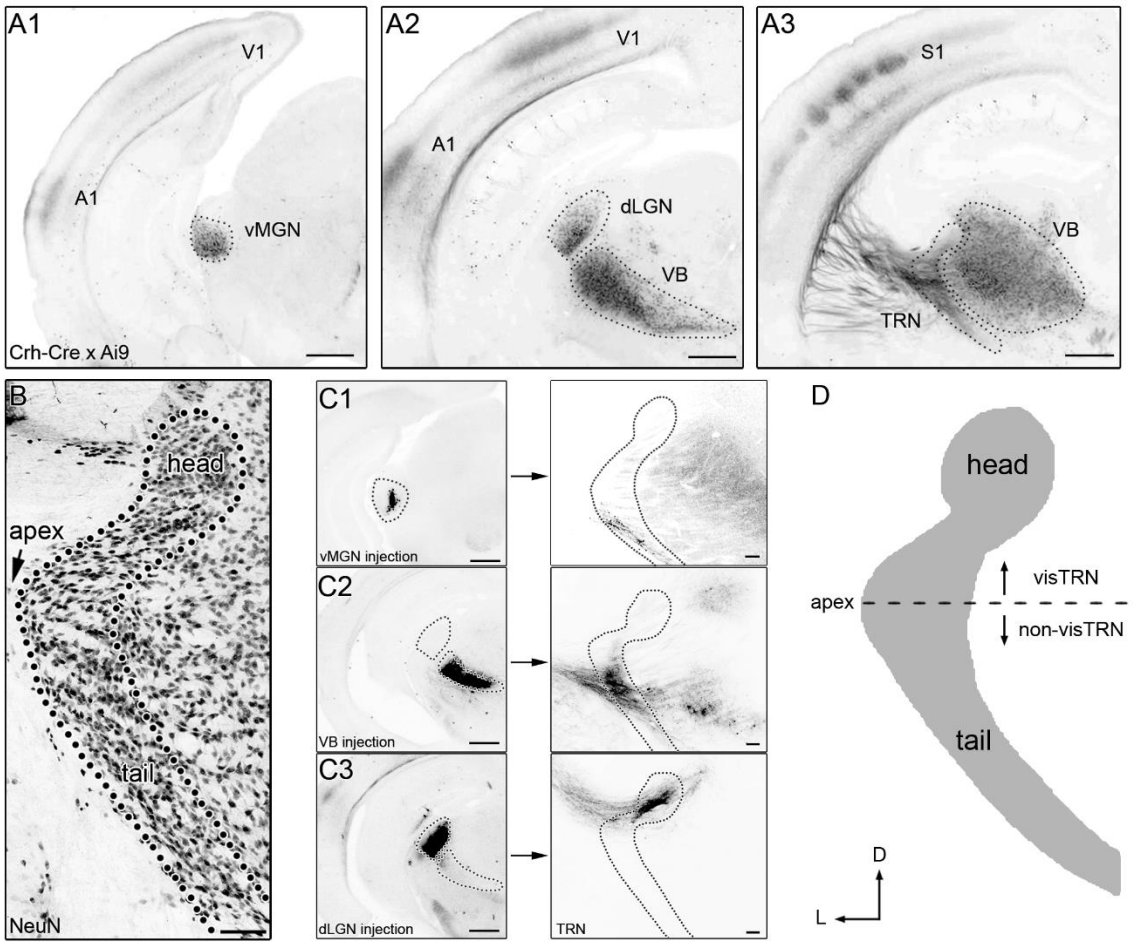

Figure 20: Delineation of sensory sectors in TRN. **A.** Coronal sections depict the pattern of tdTomato (tdT) labeling in sensory regions of thalamus and cortex of an adult Crh-Cre x Ai9 mouse. TdT labeling is expressed in thalamocortical (TC) neurons of 1st order thalamic relay nuclei ventral medial geniculate nucleus (vMGN; A1), ventrobasal complex (VB; A2 & A3), dorsal lateral geniculate nucleus (dLGN; A2), and their axonal projections coursing through the thalamic reticular nucleus (TRN) and terminating in sensory regions of cortex. Dotted lines delineate the borders of vMGN, VB, dLGN, and TRN. Scale = 500 µm. **B.** NeuN staining in a coronal section of TRN illustrates its cytoarchitectural boundaries and salient landmarks including the head, apex, and tail. Scale = 100 µm. **C1-3.**

Representative sections of thalamus in different Crh-Cre mice after targeted injections of the Cre-dependent anterograde viral tracer FLEX-AAV-ChIEF-tdT into vMGN, VB, or dLGN. Adjacent panels depict the sensory-specific sectorial pattern of labeled projections in TRN. vMGN (C1) and VB (C2) injections labeled TC afferents that were segregated in the caudo-rostral plane, in ventral TRN below the apex and within the tail of TRN. dLGN injections (C3) labeled projections above the apex in the head of TRN. Scale = 500 µm (left panels), 100 µm (right panels). Images of TRN (C1-C3) are in the same antero-posterior plane. **D.** Summary diagram illustrating the sectorial arrangement of TC projection within TRN. The horizontal line through the apex is used to separate dorsal visual TRN (visTRN) from ventral non-visual TRN (non-visTRN).

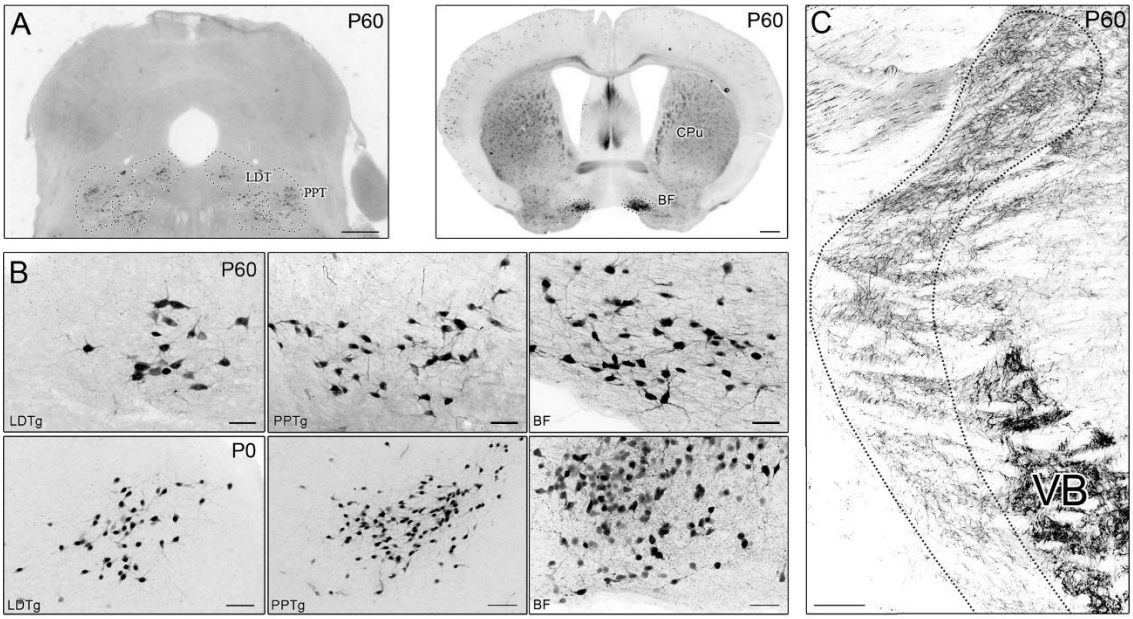

Figure 21. Pattern of tdT labeling in coronal sections of the brainstem, basal forebrain, and TRN of ChAT-Cre x Ai9 mouse. **A.** Coronal sections through the brainstem (left) and basal forebrain (right) showing tdT labeling of cholinergic neurons in an adult (P60) mouse. Low power views depict cholinergic neurons of the laterodorsal tegmentum (LDTg) and pedunculopontine tegmentum (PPTg) (left), and nucleus of the horizontal diagonal band (HDB) of the basal forebrain (BF) (right). TdT labeling is also present within cholinergic neurons of the caudate putamen (CPu), and ChAT-containing cortical interneurons (right). Scale = 500 µm. Dotted lines outline the approximate borders of brainstem and basal forebrain nuclei. **B.** High power views of tdT labeling in brainstem and basal forebrain cholinergic neurons of an adult (top, P60) and neonate (bottom, P0) mouse. Scale = 50 µm. **C.** Pattern of cholinergic projections in adult TRN, showing a prominent reticular pattern of innervation. Scale = 100 µm. Dotted lines show the borders of TRN. VB: Ventrobasal nucleus.

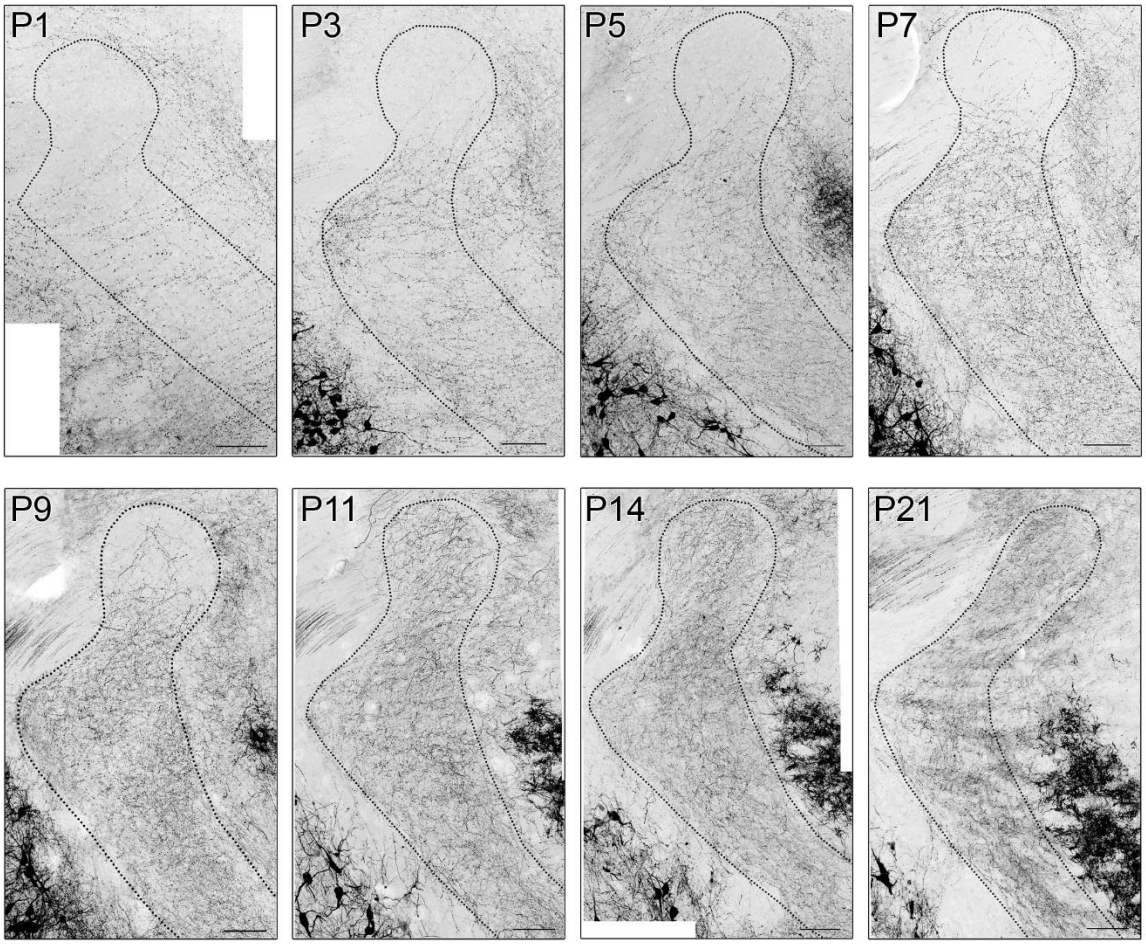

Figure 22. Cholinergic innervation of TRN. Examples of coronal sections through TRN of ChAT-Cre x Ai9 mice at different postnatal ages (P1, P3, P5, P7, P9, P11, P14, and P21). Between P1-5, cholinergic axons emerge within the ventral non-visTRN. Between P7-P11, cholinergic innervate the dorsal, visTRN. At P21, innervation resembles an adult-like pattern. For clarity, images were inverted and contrast-enhanced. Dotted lines outline the boundaries of TRN. Scale = 100 µm.

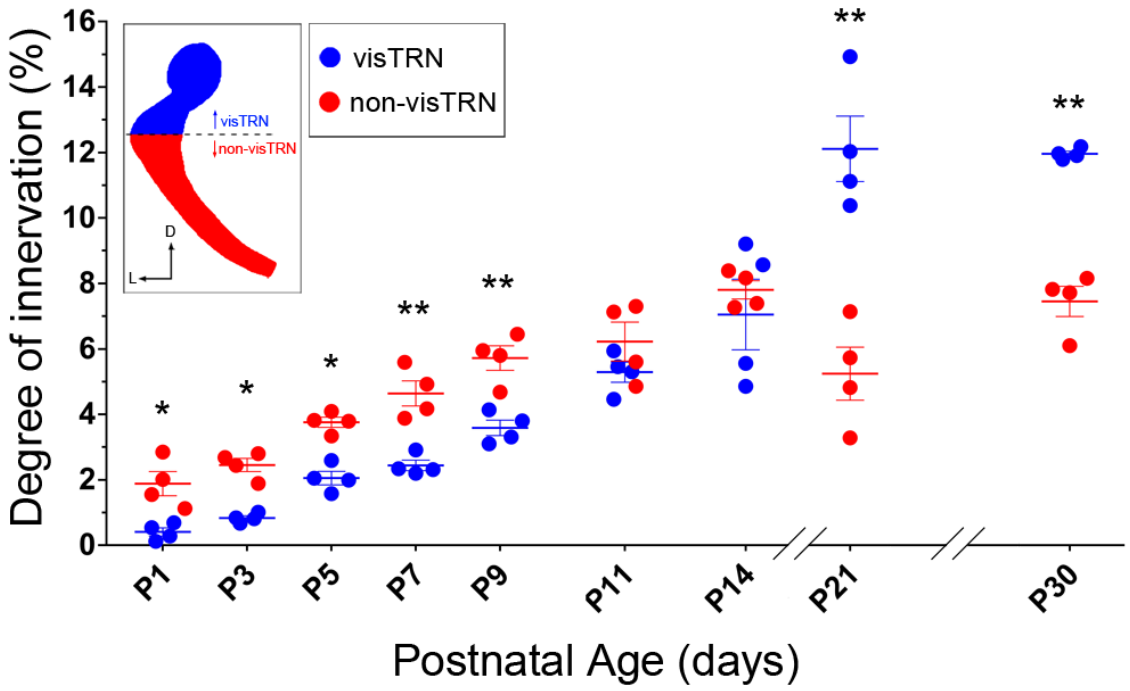

Figure 23. Age-related increase in the cholinergic innervation of TRN. Shown is a scatterplot that depicts the degree of cholinergic innervation in visTRN (blue), and non-visTRN (red) as a function of postnatal age in ChAT-Cre x Ai9 mice. Each point represents a single hemisphere, expressed as percentage of fluorescent signal compared to the total area of visTRN or non-visTRN. Horizontal lines depict mean and ± SEM values that are based on 4 hemispheres (three sections/hemisphere). Asterisks represent significant differences between visTRN and non-visTRN (* $p < 0.05$, ** $p < 0.01$).

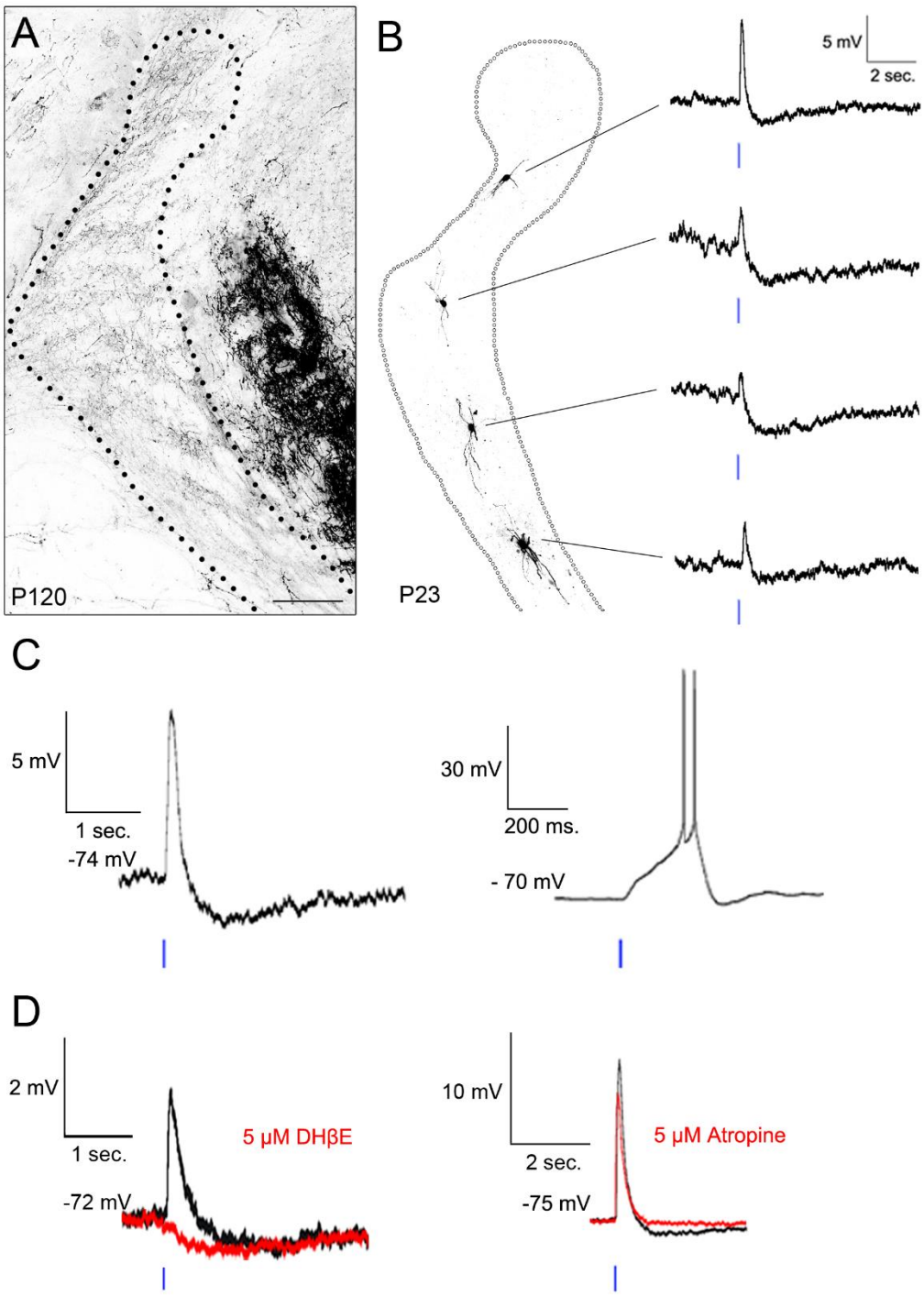

Figure 24. Optogenetic activation of cholinergic projections in TRN. **A.** Example of an acutely prepared coronal slice taken from an adult (P120) ChAT-Cre x ChR2-eYFP mouse showing the expression of ChR2-eYFP fusion protein in cholinergic arbors within TRN. **B.** Example of a typical slice recording experiment

in TRN of a P23 ChAT-Cre x ChR2-eYFP mouse. *Left:* Reconstructions of biocytin-filled TRN neurons recorded along the dorso-ventral extent of TRN. *Right:* Corresponding whole-cell voltage recordings showing postsynaptic responses evoked by blue light stimulation (single 3 ms. pulse). Light-evoked responses were biphasic, consisting of an initial rapid depolarization, followed by long-lasting hyperpolarization. **C.** *Left:* Example of light-evoked, biphasic excitation-inhibition response in TRN. *Right:* Example of light-evoked depolarization leading to the firing of action potentials. **D.** Underlying pharmacology of light-evoked cholinergic responses in TRN. Examples of light-evoked responses recorded before (black) and after (red) bath application of cholinergic receptor antagonists. The excitatory component was blocked by nicotinic antagonist DHβE (5 µM; left) and the inhibitory component was abolished by muscarinic antagonist atropine (5 µM; right). All responses were recorded at resting membrane potential (-60 to -70 mV) and in the presence of bath-applied glutamate receptor antagonists DNQX (20 µM, AMPA antagonist) and (RS)-CPP (10 µM, NMDA antagonist). Vertical blue lines represent the timing of blue light pulses.

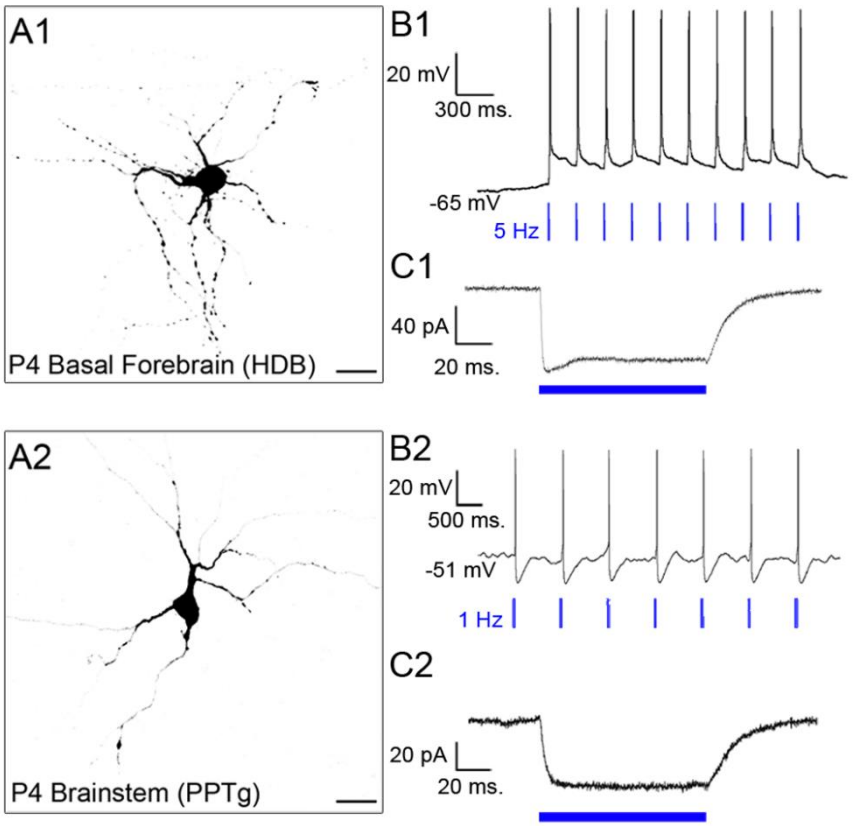

Figure 25. Light-evoked responses in cholinergic brainstem and basal forebrain neurons of neonatal (P4) ChAT-Cre x ChR2-eYFP mice. **A1-2.** Reconstructions of a biocytin-filled neurons in HDB of basal forebrain (A1), and PPTg of brainstem (A2). **B1-2.** Corresponding voltage responses evoked by blue light stimulation. Repetitive stimulation (1 ms. / 1 or 5 Hz) leads to a train of depolarizations with a spike riding their peaks. **C1-2.** A single 100 ms. pulse evokes a large, sustained inward current that shows little desensitization. Recordings were performed in current clamp (B1-2, V_M = -50 mV, -65 mV) or voltage clamp (C1-2, V_H = -70 mV), and in the presence of bath-applied glutamate receptor antagonists DNQX and (RS)-CPP.

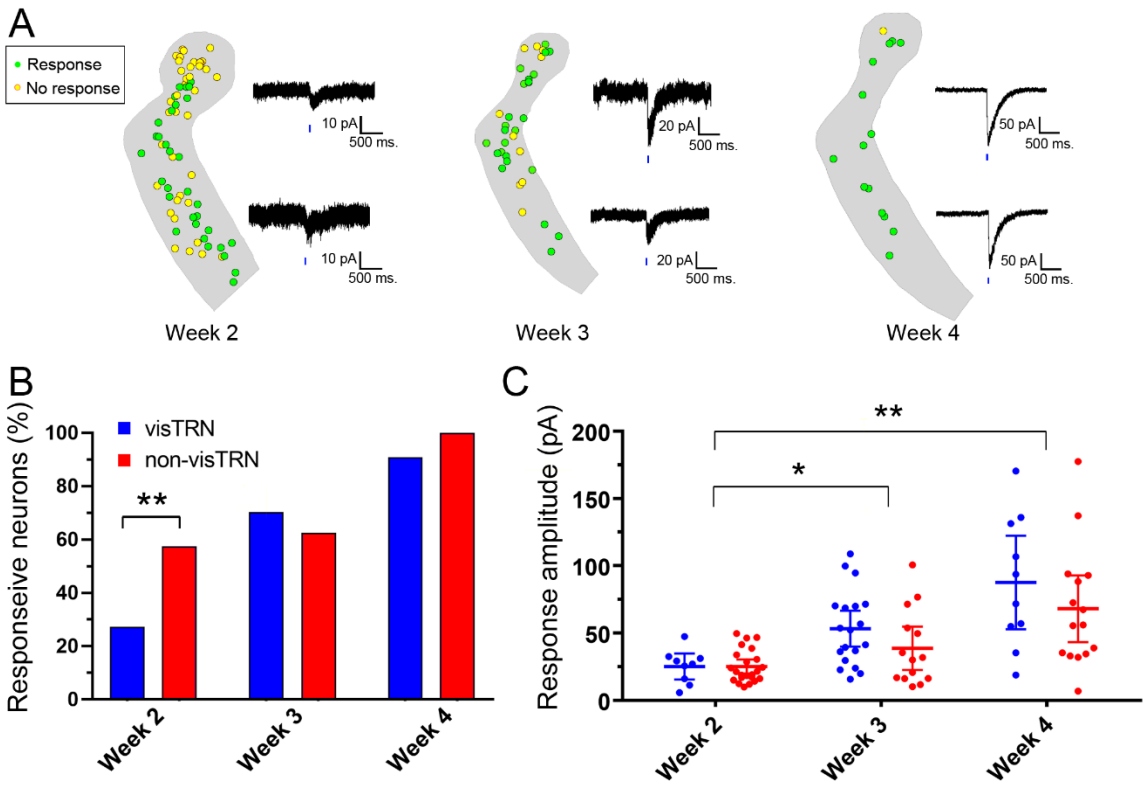

Figure 26. Development of light-evoked nicotinic responses in visTRN and non-visTRN. **A.** Composite plots depicting the relative location of light responsive (green dots) and non-responsive (yellow dots) neurons in TRN at postnatal weeks 2, 3, and 4. Adjacent to each plot are representative light-evoked (3 ms. pulse) nicotinic EPSCs in visTRN (top) and non-visTRN (bottom). Recordings were done in voltage clamp (V_H = -70 mV) and in the presence of glutamate (DNQX, (RS)-CPP) and muscarinic (atropine) receptor antagonists. **B.** Bar graphs depict the percentage of responsive and nonresponsive visTRN (blue) and non-visTRN (red) neurons at each postnatal week**.** Asterisks represent significant differences between visTRN and non-visTRN (** $p < 0.01$). **C.** Scatter plots showing the average peak response amplitude for neurons in visTRN and non-visTRN at each postnatal week. Each point represents the response of a

single neuron. Horizontal lines depict mean values and 95% confidence intervals. Asterisks represent significant age-related differences (* $p < 0.05$, ** $p < 0.01$).

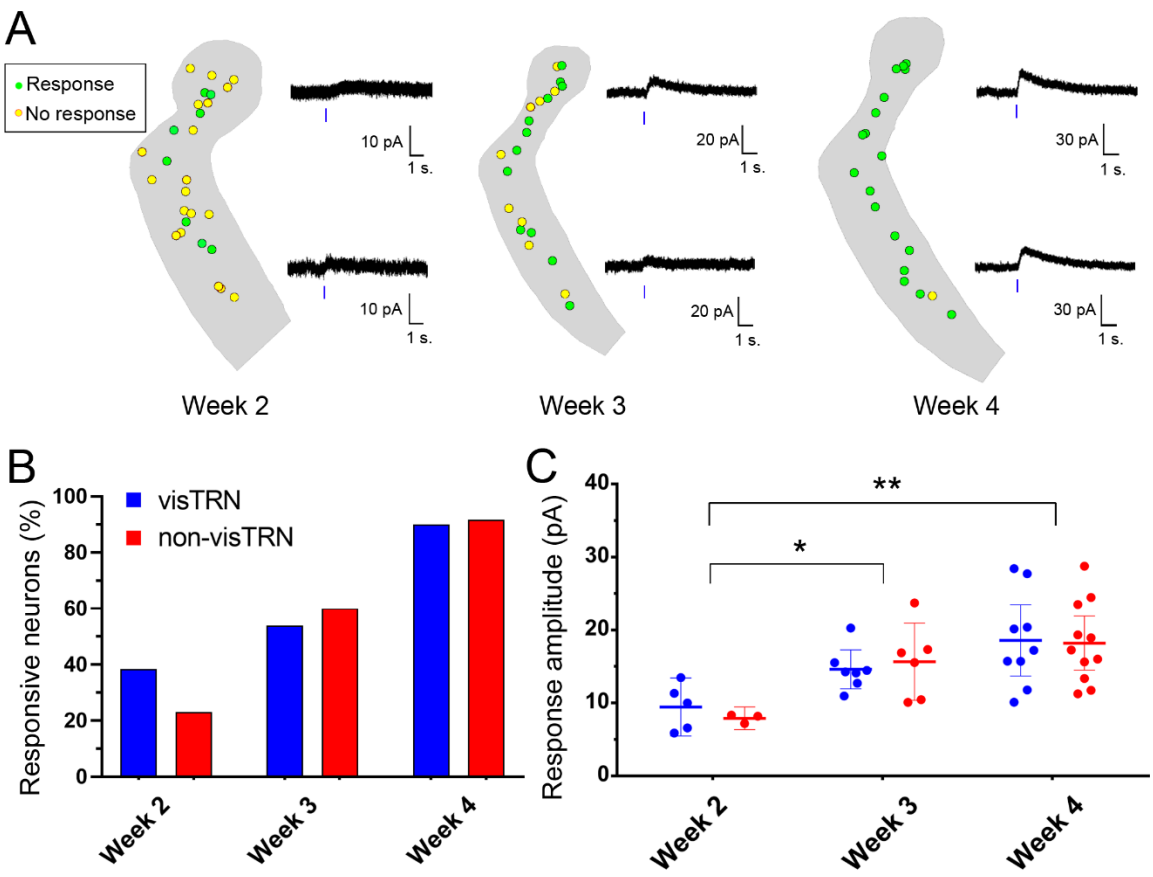

Figure 27. Development of light-evoked muscarinic responses in visTRN and non-visTRN. **A.** Composite plots depicting the relative location of light responsive (green dots) and non-responsive (yellow dots) neurons in TRN at postnatal weeks 2, 3, and 4. Adjacent to each plot are representative light-evoked (3 ms. pulse) muscarinic IPSCs in visTRN (top) and non-visTRN (bottom). Recordings done in voltage clamp (V_H = -70 mV) in the presence of glutamate (DNQX, (RS)-CPP) and nicotinic (DHβE) receptor antagonists. **B.** Bar graphs depict the percentage of responsive and nonresponsive visTRN (blue) and non-visTRN (red) neurons at each postnatal week**. C.** Scatter plots showing the average peak response amplitude for neurons in visTRN and non-visTRN at each postnatal

week. Each point represents the response of a single neuron. Horizontal lines depict mean values and 95% confidence intervals. Asterisk represents significant age-related differences (* $p < 0.05$, ** $p < 0.01$).

Discussion

We took advantage of genetically modified mouse lines to examine the development of cholinergic projections to the sensory sectors of TRN. To fully understand the patterning of cholinergic input to TRN and to test whether there was a systematic progression of innervation across different sensory regions of TRN, we first conducted anterograde tracing experiments to delineate the location of these regions. While the sectorial arrangement of sensory regions in TRN has been established in a number of mammals, including rodents (Jones, 1975; Montero et al., 1977; Ohara & Lieberman, 1985; Conley et al., 1991; Harting et al., 1991; Crabtree 1992a, 1992b; Coleman & Mitrofanis, 1996; Kimura et al., 2005; Fitzgibbon et al., 2007), studies in the mouse have been limited largely to the analysis of a single modality (Wimmer et al., 2015; Chen et al., 2015; Clemente-Perez et al., 2017). Here we used a mouse line that expresses Cre recombinase in the thalamocortical neurons of first-order thalamic sensory nuclei (Crh-Cre), and performed Cre-dependent anterograde viral tracing to confirm that like other rodents, the TRN of the mouse exhibits a modality-specific sectorial arrangement. In the coronal plane, auditory and somatosensory sectors are located ventral to the apex and in the tail of TRN, while the visual sector resides dorsal to the apex and within the head of TRN. While TC projections from sensory thalamic nuclei are largely segregated within TRN, it does not preclude the possibility of cross-modal interactions (Crabtree & Isaac, 2002; Kimura, 2014). Indeed, TRN neurons are not bound by cytoarchitectural laminae, have dendritic arbors that span across multiple sectors (Pinault, 2004; Kimura, 2014;

see Fig. 24B) and are themselves, electrically and synaptically coupled (Landisman et al., 2002; Long et al., 2004).

In assessing the progression of cholinergic projections within sensory sectors of TRN, we compared visual and non-visual (auditory & somatosensory) sectors, as these regions could be reliably defined in a coronal plane by conventional designations that outline its shape (e.g., apex, head, and tail). Using a Cre-dependent mouse line to visualize cholinergic projections, we found that cholinergic axons follow a ventral to dorsal progression during development, with non-visual sectors receiving innervation earlier than visual ones. During the first week, axons target the non-visual ventral sectors of TRN, with processes growing into the visual sector over the course of the second postnatal week. Thereafter, the density of innervation increases throughout the TRN and forms a reticular profile by the third postnatal week, which is especially conspicuous in the non-visual regions of TRN. The timing and progression of cholinergic innervation in sensory TRN seems consistent with observations made in other sensory thalamic nuclei. For example, cholinergic projections seem to innervate somatosensory thalamic structures (e.g., VB, and posterior nucleus) before visual ones (e.g., dLGN, and lateroposterior nucleus). In ChAT-Cre x Ai9 mice, we found that brainstem cholinergic projections are evident throughout all of VB by P0, yet dLGN remains devoid of fibers until the end of the first postnatal week (unpublished observations, see also Ballesteros et al., 2005). Perhaps this sequence is related to a general principle of sensory thalamic development whereby the somatosensory system and develops sooner than the visual system

(Schlaggar & O'Leary, 1994; O'Leary et al., 1994; Molnár & Blakemore, 1996; Bayer & Altman, 1991; Hevner et al., 2002; Molnár et al., 2003; Fox & Wong, 2005; Jacobs et al., 2007). Moreover, projections that convey sensory information seem to be established prior to those that serve a modulatory role. While TRN does not receive direct sensory inputs from the periphery, thalamocortical projections from first-order nuclei pass through the TRN at early perinatal ages (Mitrofanis and Baker, 1993), before the arrival of cholinergic projections. A similar sequence occurs in dLGN, in which the arrival and establishment retinofugal projections occurs well before the emergence of modulatory inputs from brainstem and layer VI of visual cortex (Ballesteros et al., 2005; Seabrook et al., 2013). Together, these observations suggest highly orchestrated development plan for thalamic circuit development in which nonvisual structures mature before visual ones, and where sensory projections are established before modulatory ones.

Our optogenetic experiments reveal that the emergence of functional cholinergic connections also follows the same ventral-to-dorsal progression. Light-evoked postsynaptic responses first emerge in non-visTRN during week 1, becoming more prevalent and stronger during week 2. By contrast, a comparable proportion of responsive cells was not detected in visTRN until week 3. It is also important to note that adult TRN, responses are biphasic in nature, having both a fast nicotinic excitatory component and a slower muscarinic inhibitory one (Hu et al., 1989; Sun et al., 2013). Typically, activation of metabotropic receptors requires repetitive stimulation, however we and others show that muscarinic

responses in TRN are reliably evoked with single electrical or optogenetic pulses. (Sun et al., 2013; Pita-Almenar et al., 2014). In thalamus, such an arrangement is unique to TRN neurons, and helps shape oscillatory activity during different behavioral states (Pita-Almenar et al., 2014; Ni et al., 2016). Our recordings suggest these elements develop in sequential fashion. Initially, responses are purely excitatory, with biphasic excitation-inhibition responses emerging later. Indeed, inhibitory responses were rarely encountered though week 2 and were not prevalent until week 4.

Cholinergic inputs to the TRN play an important role in sleep, including the regulation of oscillatory rhythms during slow wave sleep (e.g., sleep spindles), and sleep-wake transitions (Steriade, 2004; Han et al., 2014; Ni et al., 2016; Kroeger et al., 2017). During development, the emergence of distinct sleep-wake patterns of cortical activity appears to coincide with formation of functional cholinergic synapses in TRN. While state-dependent modulation is largely absent before P10, rodents exhibit distinct patterns of cortical activity by the end of the second postnatal week (Khazipov & Luhmann, 2006; Cirelli & Tononi, 2015; Shen & Colonnese, 2016). This is characterized by an alternation between synchronous low frequency activity during slow wave sleep, and asynchronous high frequency activity during rapid eye movement (REM) sleep and wakefulness. While an adult-like pattern of cortical activity is already evident by P17, further changes in the duration of REM and NREM (non-rapid eye movement) sleep occur as late as the end of the first postnatal month (Jouvet-Mournier et al., 1970; Daszuta & Gambarelli, 1985; Mirmiran et al., 2003). Thus

the protracted development of cholinergic inputs to TRN, which occurs largely after the circuits mediating thalamocortical transmission are established, likely contributes to the modulation of sleep-wake states.

SUMMARY AND CONCLUSIONS

In this dissertation, we examined the anatomical organization and developmental progression of cholinergic input to the mouse visual thalamus, focusing primarily on dLGN and TRN. In Chapter I we used neural tracers to show that dLGN receives extensive cholinergic innervation from the contralateral PBG, a dense but restricted projection from the ipsilateral PBG, and a sparse projection from the ipsilateral PPTg. Furthermore, we observed cholinergic projections to TRN arising from LDTg, PPTg, and the basal forebrain. In Chapter II we used a genetically modified mouse line to visualize cholinergic innervation of the visual thalamus during early postnatal development. Cholinergic fibers arrived in dLGN by the end of the first postnatal week, and the density of innervation increased gradually to reach adult-like levels by the end of the first month. In the absence of retinogeniculate pathway (*math5*$^{-/-}$), we saw a disruption in the rate, pattern, and trajectory of cholinergic input to dLGN. Finally, in Chapter III, we examined the anatomical and functional development of cholinergic input to TRN. Cholinergic innervation of TRN began in the ventral non-visual sectors during the first postnatal week, progressed into the dorsal visual sector during week 2, and reached an adult-like pattern by week 3. The emergence of cholinergic postsynaptic responses followed a similar ventral-to-dorsal developmental progression. By the end of the first postnatal month, the

entire TRN exhibited an adult-like reticular pattern of innervation, with nearly all neurons exhibiting mature biphasic responses to stimulation of cholinergic afferents.

We performed anterograde viral tracing experiments using ChAT-Cre mouse in order to selectively target expression of tdTomato in cholinergic brainstem and basal forebrain nuclei. A Cre-dependent viral tracing approach was advantageous since it avoids problems associated with conventional molecular tracers (e.g., WGA, BDA), including uptake of tracer by fibers of passage, or labeling of neighboring non-cholinergic neuronal populations. We found that in mouse, dLGN receives cholinergic projections from PBG and PPTg, Previous tracing studies in several species have also shown the same brainstem nuclei innervate dLGN, but suggested that is PPTg is the main contributor of cholinergic input to dLGN, with only a small projection arising from PBG. For instance, lesioning of PBG did not appear to significantly reduce the density of ChAT labeling in dLGN of tree shrews (Fitzpatrick et al., 1988). Furthermore, previous tracing studies in rat found that PBG projections are restricted to the dorsolateral regions of the rostral contralateral dLGN (Harting et al., 1991). However, our studies in mice showed that PPTg neurons contributed only a sparse and diffuse projection to dLGN. By contrast, PBG projections targeted dLGN extensively, with fibers extending throughout the caudo-rostral extent of the nucleus and well beyond the dorsolateral regions. There was also a small ipsilateral PBG projection which targeted the mediodorsal dLGN. While the functional significance of PBG inputs to dLGN is not well understood, several

studies have shown that activity of PBG neurons is associated with eye movements, detection of moving stimuli, and visuo-motor escape responses (Graybiel, 1978; Watanabe & Kawana, 1979; Cui & Malpeli 2003; Ma et al., 2013; Shang et al., 2015; Shang et al., 2018).

In dLGN of several species, there is are areas which receive converging input from PBG, DSGCs, and SC (e.g., C-lamina in cats, koniocellular layers in tree shrews). These areas are thought to comprise a visual channel involved in processing motion and coordination of eye movements. In the rodent dLGN, a homologous region, known as the dorsolateral shell, has been shown to receive converging input from DSGCs and SC (Harting et al., 1986; Fitzpatrick et al., 1988). In our studies, we found that the contralateral PBG projection is expansive, extending beyond the dorsolateral areas of dLGN. A recent study has shown that some DSGC subtypes also project beyond the dorsolateral shell, therefore there may be overlap with PBG projections which is not anatomically confined to the shell (Kay et al., 2011). The ipsilateral PBG projection targeted the area that represents the upper visual field (i.e., dorsomedial dLGN) and could therefore be involved in processing of looming stimuli. As part of our studies in Chapter I, we also traced cholinergic projections to TRN. Consistent with reports in other species (Woolf & Butcher, 1986; Hallanger et al., 1987), our tracing studies showed that cholinergic projections to TRN originated from both brainstem (LDTg & PPTg) and basal forebrain (HDB & SI). What remains to be seen is how the inputs from these two areas compare in terms of projection pattern, density of innervation, arbor morphology, and synaptic ultrastructure.

To track the development of cholinergic input to dLGN, we crossed the ChAT-Cre mouse to a Cre-dependent reporter line (Ai9) to drive expression tdTomato in cholinergic neurons from an early age. This allowed for robust fluorescent protein labeling of cholinergic fibers within dLGN and TRN, especially at perinatal ages when low expression of relevant biomarkers (e.g., ChAT) makes immunohistochemical detection of fibers difficult. In Chapter II, we showed that cholinergic fibers arrive in dLGN at P5, increase in density gradually, and reach adult-like levels by the end of the first postnatal month. Such protracted onset places cholinergic projections as the last input to reach maturity within dLGN, well after those arising from the retina, cortex, or TRN (Godement et al., 1984; Jacobs et al., 2007; Seabrook et al., 2013; Campbell et al., 2016). Such slow onset of cholinergic innervation in the visual dorsal thalamus and TRN, compared to non-visual thalamic regions, may be relate to the slow development of the visual pathways in the rodent. For instance, while evoked somatosensory and auditory activity can be observed by the end of the first postnatal week, visually-evoked activity emerges largely during the second week, just before the time of natural eye-opening (Khazipov & Luhmann, 2006; Cirelli & Tononi, 2015; Shen & Colonnese, 2016).

The main finding in our developmental studies was the observed disruptions in the rate, trajectory, and pattern of cholinergic projections to dLGN in the absence of retinal input. For these studies we utilized a genetic knock-out mouse (*math5*$^{-/-}$), in which 95% of RGCs fail to differentiate, leaving the central nervous system devoid of retinofugal projections. Conventionally, neonatal eye

enucleations have been the standard manipulation used to eliminate retinal projections in the developing visual system. However, we used a genetic model of visual deafferentation to avoid the confounding influence of retinal axons and the inflammatory signaling associated with retinal axon degeneration. Compared to WT mice, in *math5*$^{-/-}$ we found a delay in cholinergic innervation of dLGN. Similar disruptions in developmental timing have been previously demonstrated in the corticogeniculate (CG) pathway, where *math5*$^{-/-}$ mice exhibited an acceleration in the rate of CG innervation (Seabrook et al., 2013). Together, these findings suggest that the retinogeniculate pathway plays a critical regulatory role, orchestrating the timely arrival of various nonretinal input to dLGN as part of a conserved developmental mechanism. While the mechanisms behind retinal regulation of cortical dLGN innervation have been explored (Brooks et al., 2011), the molecular cues involved in cholinergic input development are yet to be determined.

In addition to the developmental studies, we performed anterograde tracing of PBG projections in *math5*$^{-/-}$ mice. Since cholinergic axons of PBG travel within the OT and cross the midline near the optic chiasm, we speculated that PBG projections depend on retinal projections and would be disrupted in absence of retinal input. We found that the trajectory of PBG axonal tracts was altered in *math5*$^{-/-}$, traveling medially through the neuropil of the thalamus rather than the normal route along the dorsolateral edge of the thalamus. While we saw a disruption in the projection to the ipsilateral dLGN, the contralateral projection pattern resembled that of WT mice. Though PBG axons and retinal axons

traverse together in the OT, the retinal pathway does appear to be necessary for targeting of dLGN by the main, contralateral PBG projection. However, the retinal pathway is required for targeting of PBG arbors to specific regions (i.e., mediodorsal) of the ipsilateral dLGN.

Finally, we explored cholinergic development within TRN, a GABAergic thalamic nucleus which provides inhibitory input to TC relay neurons of dLGN and other sensory relay nuclei. To our knowledge, this was the first study to examine the anatomical and functional maturation of cholinergic input to TRN. By utilizing the same transgenic approach to label cholinergic neurons from an early age (ChAT-Cre x Ai9 mouse), we showed cholinergic fibers arrive in the ventral non-visual sectors at perinatal ages. However, innervation of the dorsal visual sector occurred later, during the second postnatal week. By taking an optogenetic approach (ChAT-Cre x ChR2 mice), we showed that formation of functional cholinergic connections in the non-visual sectors of TRN preceded that of the visual sector. Immature postsynaptic responses, consisting of low amplitude nicotinic depolarizations, were seen in the ventral non-visual TRN sectors during week 1, and appeared in the visual sector by the end of week 2. By the end of the first month, nearly all TRN neurons exhibited adult-like biphasic responses consisting of brief nicotinic excitation, followed by long-lasting muscarinic inhibition (E-I; Sun et al., 2013; Beierlein, 2014). Such sequence mirrors the developmental progression in the rest of the dorsal thalamus, where cholinergic innervation of non-visual relay nuclei (e.g., MGB & VB) occurs before that of dLGN. What remains unknown is whether there are developmental and/or

functional differences between the inputs from various cholinergic brainstem (LDTg & PPTg), and basal forebrain (SI, HDB, & NBM) nuclei.

Overall, our studies show the organizational pattern and developmental time course of cholinergic innervation in the visual thalamus of the mouse. Future work can build on these results and explore other facets of cholinergic input formation and function in thalamic circuits. A particularly appealing avenue for future research is optogenetic stimulation or suppression of the brainstem and basal forebrain inputs in awake behaving mice. Such approach can broaden our understanding of the modulatory effects exerted by cholinergic inputs on thalamic circuits during various behaviors or cognitive states.

REFERENCES

Ahlsen, G. (1984). Brain stem neurones with differential projection to functional subregions of the dorsal lateral geniculate complex in the cat. *Neuroscience* 12(3), 817-838.

Ahlsen, G., Lindstrom, S., & Lo, F. S. (1984). Inhibition from the brain stem of inhibitory interneurones of the cat's dorsal lateral geniculate nucleus. *Journal of Physiology* 347, 593-609.

Anderson, J. C., da Costa, N. M., & Martin, K. A. (2009). The W cell pathway to cat primary visual cortex. *Journal of Comparative Neurology* 516(1), 20-35.

Antal, M., Acuna-Goycolea, C., Pressler, R. T., Blitz, D. M., & Regehr, W. G. (2010). Cholinergic activation of M2 receptors leads to context-dependent modulation of feedforward inhibition in the visual thalamus. *PLoS Biology* 8(4), e1000348.

Arroyo, S., Bennett, C., & Hestrin, S. (2014). Nicotinic modulation of cortical circuits. *Frontiers in Neural Circuits* 8(30).

Baleydier, C., & Magnin, M. (1979). Afferent and efferent connections of the parabigeminal nucleus in cat revealed by retrograde axonal transport of horseradish peroxidase. *Brain Research* 161(2), 187-198.

Bickford, M. E., Zhou, N., Krahe, T. E., Govindaiah, G., & Guido, W. (2015). Retinal and Tectal "Driver-Like" Inputs Converge in the Shell of the Mouse Dorsal Lateral Geniculate Nucleus. *Journal of Neuroscience* 35(29), 10523-10534.

Bigl, V., Woolf, N. J., & Butcher, L. L. (1982). Cholinergic projections from the basal forebrain to frontal, parietal, temporal, occipital, and cingulate cortices: a combined fluorescent tracer and acetylcholinesterase analysis. *Brain Research Bulletin* 8(6), 727-749.

Ballesteros, J. M., Van Der List, D. A., & Chalupa, L. M. (2005). Formation of eye-specific retinogeniculate projections occurs prior to the innervation of the dorsal lateral geniculate nucleus by cholinergic fibers. *Thalamus & Related Systems* 3(2), 157-163.

Bartheld, C. S., Byers, M. R., Williams, R., & Bothwell, M. (1996). Anterograde transport of neurotrophins and axodendritic transfer in the developing visual system. *Nature* 379, 830-833.

Bayer, S.A., & Altman, J. (1991). *Neocortical Development.* Raven, New York.

Beierlein, M. (2014). Synaptic mechanisms underlying cholinergic control of thalamic reticular nucleus neurons. *Journal of Physiology* 592(19), 4137-4145.

Bickford, M. E., Slusarczyk, A., Dilger, E. K., Krahe, T. E., Kucuk, C., & Guido, W. (2010). Synaptic development of the mouse dorsal lateral geniculate nucleus. *Journal of Comparative Neurology* 518(5), 622-635.

Bickford, M. E., Zhou, N., Krahe, T. E., Govindaiah, G., & Guido, W. (2015). Retinal and tectal "driver-like" inputs converge in the shell of the mouse dorsal lateral geniculate nucleus. *Journal of Neuroscience* 35(29), 10523-10534.

Bickford, M. E., Gunluk, A. E., Van Horn, S. C., & Sherman, S. M. (1994). GABAergic projection from the basal forebrain to the visual sector of the thalamic reticular nucleus in the cat. *Journal of Comparative Neurology* 348(4), 481-510.

Bickford, M. E., Ramcharan, E., Godwin, D. W., Erisir, A., Gnadt, J., & Sherman, S. M. (2000). Neurotransmitters contained in the subcortical extraretinal inputs to the monkey lateral geniculate nucleus. *Journal of Comparative Neurology* 424(4), 701-717

Bickford, M. E., Slusarczyk, A., Dilger, E. K., Krahe, T. E., Kucuk, C., & Guido, W. (2010). Synaptic development of the mouse dorsal lateral geniculate nucleus. *Journal of Comparative Neurology* 518(5), 622-635.

Bigl, V., Woolf, N. J., & Butcher, L. L. (1982). Cholinergic projections from the basal forebrain to frontal, parietal, temporal, occipital, and cingulate cortices: a combined fluorescent tracer and acetylcholinesterase analysis. *Brain Research Bulletin* 8(6), 727-749.

Bista, P., Meuth, S. G., Kanyshkova, T., Cerina, M., Pawlowski, M., Ehling, P., Landgraf, P., Borsotto, M., Heurteaux, C., Pape, H. C., Baukrowitz, T., & Budde, T. (2012). Identification of the muscarinic pathway underlying cessation of sleep-related burst activity in rat thalamocortical relay neurons. *Pflügers Archiv* 463(1), 89-102.

Bouabe, H., & Okkenhaug, K. (2013). Gene targeting in mice: a review. *Methods in Molecular Biology* 1064, 315-336.

Breese, G. R., & Traylor, T. D. (1972). Developmental characteristics of brain catecholamines and tyrosine hydroxylase in the rat: effects of 6-hydroxydopamine. *British Journal of Pharmacology* 44(2), 210-222.

Broadwell, R. D., & Bleier, R. (1976). A cytoarchitectonic atlas of the mouse hypothalamus. *Journal of Comparative Neurology* 167(3), 315-339.

Brooks, J. M., Su, J., Levy, C., Wang, J. S., Seabrook, T. A., Guido, W., & Fox, M. A. (2013). A molecular mechanism regulating the timing of corticogeniculate innervation. *Cell Reports* 5(3), 573-581.

Brown, N. L., Kanekar, S., Vetter, M. L., Tucker, P. K., Gemza, D. L., & Glaser, T.

(1998). Math5 encodes a murine basic helix-loop-helix transcription factor expressed during early stages of retinal neurogenesis. *Development* 125(23), 4821-4833.

Budd, J. M. (2004). How much feedback from visual cortex to lateral geniculate nucleus in cat: a perspective. *Visual Neuroscience* 21(4), 487-500.

Butowt, R., & Bartheld, C. S. (2005). Anterograde axonal transport of BDNF and NT-3 by retinal ganglion cells: roles of neurotrophin receptors. *Molecular and Cellular Neuroscience* 29(1), 11-25.

Campbell, P. W., & Guido, W. Development of feed-forward and feedback connections between dLGN and TRN. Program No. 529.21. 2016. San Diego, CA. Society for Neuroscience, 2016. Online.

Carden, W. B. D., A.; Guido, W., Godwin, D. W., & Bickford, M. E. (2000). Development of the cholinergic, nitrergic, and GABAergic Innervation of the cat dorsal lateral geniculate nucleus. *Journal of Comparative Neurology* 418, 65-80.

Chen, C., & Regehr, W. G. (2000). Developmental remodeling of the retinogeniculate synapse. *Neuron* 28(3), 955-966.

Chen, Z., Wimmer, R. D., Wilson, M. A., & Halassa, M. M. (2015). Thalamic circuit mechanisms link sensory processing in sleep and attention. *Frontiers in Neural Circuits* 9, 83.

Cirelli, C., & Tononi, G. (2015). Cortical development, electroencephalogram rhythms, and the sleep/wake cycle. *Biological Psychiatry* 77(12), 1071-1078.

Clemente-Perez, A., Makinson, S. R., Higashikubo, B., Brovarney, S., Cho, F. S., Urry, A., Holden, S. S., Wimer, M., Dávid, C., Fenno, L. E., Ascády, L., Deisseroth, K., & Paz, J. T. (2017). Distinct thalamic reticular cell types differentially modulate normal and pathological cortical rhythms. *Cell Reports* 19, 2130-2142.

Coleman, K. A., & Mitrofanis, J. (1996). Organization of the visual reticular thalamic nucleus of the rat. *European Journal of Neuroscience* 8, 388-404.

Conley, M., Kupersmith, A. C., & Diamond, I. T. (1991). The organization of projections from subdivisions of the auditory cortex and thalamus to the auditory sector of the thalamic reticular nucleus in galago. *European Journal of Neuroscience* 3, 1089-1103.

Crabtree, J. W. (1992a). The somatotopic organization within the cat's thalamic reticular nucleus. *European Journal of Neuroscience* 4, 1352-1361.

Crabtree, J. W. (1992b). The somatotopic organization within the rabbit's thalamic reticular nucleus. *European Journal of Neuroscience* 4, 1343-1351.

Crabtree, J. W., & Isaac, J. T. (2002). New intrathalamic pathways allowing modality-related and cross-modality switching in the dorsal thalamus. *Journal of Neuroscience* 22, 8754-8761.

Crick, F. (1984) Function of the thalamic reticular complex: the searchlight hypothesis. *Proceedings of the National Academy of Sciences* 81, 4586-4590.

Crunelli, V., Lightowler, S., & Pollard, C. E. (1989). A T-type Ca2+ current underlies low-threshold Ca2+ potentials in cells of the cat and rat lateral geniculate nucleus. *Journal of Physiology* 413, 543-561.

Cruz-Martin, A., El-Danaf, R. N., Osakada, F., Sriram, B., Dhande, O. S., Nguyen, P. L., Callaway, E. M., Ghosh, A., & Huberman, A. D. (2014). A dedicated circuit links direction-selective retinal ganglion cells to the primary visual cortex. *Nature* 507(7492), 358-361.

Cui, H., & Malpeli, J. G. (2003). Activity in the parabigeminal nucleus during eye movements directed at moving and stationary targets. *Journal of Neurophysiology* 89(6), 3128-3142.

Curro Dossi, R., Pare, D., & Steriade, M. (1991). Short-lasting nicotinic and long-lasting muscarinic depolarizing responses of thalamocortical neurons to stimulation of mesopontine cholinergic nuclei. *Journal of Neurophysiology* 65(3), 393-406.

Daszuta, A., & Gambarelli, F. (1985). Early postnatal development of EEG and sleep-waking cycle in two inbred mouse strains. *Developmental Brain Research* 354, 39-47.

Demas, J., Sagdullaev, B. T., Green, E., Jaubert-Miazza, L., McCall, M. A., Gregg, R., Wong, R. O., & Guido, W. (2006). Failure to maintain eye-specific segregation in nob, a mutant with abnormally patterned retinal activity. *Neuron* 50(2), 247-259.

Deschenes, M., Paradis, M., Roy, J. P., & Steriade, M. (1984). Electrophysiology of neurons of lateral thalamic nuclei in cat: resting properties and burst discharges. *Journal of Neurophysiology* 51(6), 1196-1219.

Diamond, I. T., Fitzpatrick, D., & Conley, M. (1992). A projection from the parabigeminal nucleus to the pulvinar nucleus in galago. *Journal of Comparative Neurology* 316(3), 375-382.

Dilger, E. K., Shin, H. S., & Guido, W. (2011). Requirements for synaptically evoked plateau potentials in relay cells of the dorsal lateral geniculate nucleus of the mouse. *Journal of Physiology* 589, 919-937.

Dilger, E., K., Krahe, T. E., Morhardt, D. R., Seabrook, T. A., Shin, H., S, & Guido, W. (2015). Absence of plateau potentials in dLGN cells leads to a breakdown in retinogeniculate refinement. *Journal of Neuroscience* 35(8), 3652-3662.

Do, P. J., Xu, M., Lee, S., Chang, W., Zhang, S., Chung, S., Yung, T. J., Fan, J.

L., Miyamichi, K., Luo, L., & Dan, Y. (2016). Cell type-specific long-range connections of basal forebrain circuit. *eLife* 5, e13214.

El-Danaf, R. N., Krahe, T. E., Dilger, E. K., Bickford, M. E., Fox, M. A., & Guido, W. (2015). Developmental remodeling of relay cells in the dorsal lateral geniculate nucleus in the absence of retinal input. *Neural Development* 10(19).

Erisir, A., Van Horn, S. C., Bickford, M. E., & Sherman, S. M. (1997). Immunocytochemistry and distribution of parabrachial terminals in the lateral geniculate nucleus of the cat: a comparison with corticogeniculate terminals. *Journal of Comparative Neurology*, 377(4), 535-549.

Erisir, A., Van Horn, S. C., & Sherman, S. M. (1997b). Relative numbers of cortical and brainstem inputs to the lateral geniculate nucleus. *Proceedings of the National Academy of Sciences* 94(4), 1517-1520.

Fitzpatrick, D., Carey, R. G., & Diamond, I. T. (1980). The projection of the superior colliculus upon the lateral geniculate body in Tupaia glis and Galago senegalensis. *Brain Research* 194(2), 494-499.

Fitzpatrick, D., Conley, M., Luppino, G., Matelli, M., & Diamond, I. T. (1988). Cholinergic projections from the midbrain reticular formation and the parabigeminal nucleus to the lateral geniculate nucleus in the tree shrew. *Journal of Comparative Neurology* 272(1), 43-67.

Fitzpatrick, D., Diamond, I. T., & Raczkowski, D. (1989). Cholinergic and monoaminergic innervation of the cat's thalamus: comparison of the lateral geniculate nucleus with other principal sensory nuclei. *Journal of Comparative Neurology* 288(4), 647-675.

Fitzgibbon, T., Szmajda, B. A. & Martin, P. R. (2007). First order connections of the visual sector of the thalamic reticular nucleus in marmoset monkeys (Callithrix jacchus). *Visual Neuroscience* 24, 857–874.

Fogerson, P. M., & Huguenard, J. R. (2016). Tapping the brakes: cellular and synaptic mechanisms that regulate thalamic oscillations. *Neuron* 92, 687-704.

Fox, K., & Wong, R. O. L. (2005). A comparison of experience-dependent plasticity in the visual and somatosensory systems. *Neuron* 48, 465-477.

Godement, P., Salaun, J., & Imbert, M. (1984). Prenatal and postnatal development of retinogeniculate and retinocollicular projections in the mouse. *Journal of Comparative Neurology* 230(4), 552-575.

Godwin, D. W., Vaughan, J. W., & Sherman, S. M. (1996). Metabotropic glutamate receptors switch visual response mode of lateral geniculate nucleus cells from burst to tonic. *Journal of Neurophysiology* 76(3), 1800-1816.

Grant, E., Hoerder-Suabedissen, A., & Molnar, Z. (2016). The regulation of corticofugal fiber targeting by retinal inputs. *Cerebral Cortex* 26(3), 1336-

1348.

Graybiel, A. M. (1978). A satellite system of the superior colliculus: the parabigeminal nucleus and its projections to the superficial collicular layers. *Brain Research* 145(2), 365-374.

Grubb, M. S., & Thompson, I. D. (2003). Quantitative characterization of visual response properties in the mouse dorsal lateral geniculate nucleus. *Journal of Neurophysiology* 90(6), 3594-3607.

Guido, W. (2008). Refinement of the retinogeniculate pathway. *Journal of Physiology London* 586(18), 4357-4362.

Guillery, R. W., Feig, S. L., & Lozsadi, D. A. (1998). Paying attention to the thalamic reticular nucleus. *Trends in Neuroscience* 21, 28-32.

Guillery, R. W., & Harting, J. K. (2003). Structure and connections of the thalamic reticular nucleus: advancing views over half a century. *Journal of Comparative Neurology* 463, 360-371.

Gut, N. K., & Winn, P. (2016). The pedunculopontine tegmental nucleus-A functional hypothesis from the comparative literature. *Movement Disorders* 31(5), 615-624.

Halassa, M. M., & Acsády, L. (2016). Thalamic inhibition: diverse sources, diverse scales. *Trends in Neuroscience* 39, 680-693.

Hallanger, A. E., Levey, A. I., Lee, H. J., Rye, D. B., & Wainer, B. H. (1987). The origins of cholinergic and other subcortical afferents to the thalamus in the rat. *Journal of Comparative Neurology* 262(1), 105-124.

Hallanger, A. E., & Wainer, B. H. (1988). Ascending projections from the pedunculopontine tegmental nucleus and the adjacent mesopontine tegmentum in the rat. *Journal of Comparative Neurology* 274(4), 483-515.

Hallanger, A. E., Price, S. D., Lee, H. J., Steininger, T. L., & Wainer, B. H. (1990). Ultrastructure of cholinergic synaptic terminals in the thalamic anteroventral, ventroposterior, and dorsal lateral geniculate nuclei of the rat. *Journal of Comparative Neurology* 299(4), 482-492.

Han, Y., Shi, Y. F., Xi, W., Zhou, R., Tan, Z. B., Wang, H., Li, X. M., Chen, Z., Feng, G., Luo, M., Huang, Z. L., Duan S., & Yu, Y. Q. (2014). Selective activation of cholinergic basal forebrain neurons induces immediate sleep-wake transitions. *Current Biology*, 24, 693-698.

Harting, J. K., Hall, W. C., Diamond, I. T., & Martin, G. F. (1973). Anterograde degeneration study of the superior colliculus in tupaia glis: evidence for a subdivision between superficial and deep layers. *Journal of Comparative Neurology* 148(3), 361-386.

Harting, J. K., Hashikawa, T., & Van Lieshout, D. (1986). Laminar distribution of tectal, parabigeminal and pretectal inputs to the primate dorsal lateral geniculate nucleus: connectional studies in galago crassicaudatus. *Brain Research* 366(1-2), 358-363.

Harting, J. K., Van Lieshout, D. P. & Feig, S. (1991). Connectional studies of the primate lateral geniculate nucleus: distribution of axons arising from the thalamic reticular nucleus of galago crassicaudatus. *Journal of Comparative Neurology* 310, 411–427.

Harting, J. K., Van Lieshout, D. P., Hashikawa, T., & Weber, J. T. (1991). The parabigeminogeniculate projection: connectional studies in eight mammals. *Journal of Comparative Neurology* 305(4), 559-581.

Hashikawa, T., Van Lieshout, D., & Harting, J. K. (1986). Projections from the parabigeminal nucleus to the dorsal lateral geniculate nucleus in the tree shrew Tupaia glis. *Journal of Comparative Neurology* 246(3), 382-394.

Henver, R. F., Miyashita-Lin, E., & Rubenstein, J. I. R. (2002). Cortical and thalamic axon pathfinding defects in Tbr1, Gbx2, and Pax6 mutant mice: Evidence that cortical and thalamic axons interact and guide each other. *Journal of Comparative Neurology* 447, 8-17.

Herrera, C. G., Cadavieco, M. C., Jego, S., Ponomarenko, A., Korotkova, T., & Adamantidis, A. (2016). Hypothalamic feedforward inhibition of thalamocortical network controls arousal and consciousness. *Nature Neuroscience* 19(2), 290-298.

Hong, Y. K., & Chen, C. (2011). Wiring and rewiring of the retinogeniculate synapse. *Current Opinion in Neurobiology* 21(2), 228-237.

Hu, B., Steriade, M., & Deschenes, M. (1989). The effects of brainstem peribrachial stimulation on perigeniculate neurons: the blockage of spindle waves. *Neuroscience* 31, 1-12.

Hu, B., Steriade, M., & Deschenes, M. (1989b). The effects of brainstem peribrachial stimulation on neurons of the lateral geniculate nucleus. *Neuroscience* 31(1), 13-24.

Huberman, A. D., Wei, W., Elstrott, J., Stafford, B. K., Feller, M. B., & Barres, B. A. (2009). Genetic identification of an on-off direction-selective retinal ganglion cell subtype reveals a layer-specific subcortical map of posterior motion. *Neuron* 62(3), 327-334.

Huberman, A. D., Feller, M. B., & Chapman, B. (2008). Mechanisms underlying development of visual maps and receptive fields. *Annual Reviews in Neuroscience* 31, 479-509.

Jacobs, E. C., Campagnoni, C., Kampf, K., Reyes, S. D., Kalra, V., Handley, V., Xie, Y. Y., Hong-Hu Y., Spreur, V., Fisher, R.S., & Campagnoni, A. T. (2007). Visualization of corticofugal projections during early cortical development in a tau-GFP-transgenic mouse. *European Journal of Neuroscience* 25(1), 17-30.

Jaubert-Miazza, L., Green, E., Lo, F. S., Bui, K., Mills, J., & Guido, W. (2005). Structural and functional composition of the developing retinogeniculate pathway in the mouse. *Visual Neuroscience* 22(5), 661-676.

Jones, E. G. (1975). Some aspects of the organization of the thalamic reticular complex. *Journal of Comparative Neurology* 162, 285-308.

Jones, E. G. (2007). *The Thalamus, Vol 1*. Cambridge University Press, Cambridge.

Jones, E. G. (2009). Synchrony in the interconnected circuitry of the thalamus and cerebral cortex. *Annals of the New York Academy of Sciences* 1157, 10-23.

Jourdain, A., Semba, K., & Fibiger, H. C. (1989). Basal forebrain and mesopontine tegmental projections to the reticular thalamic nucleus: an axonal collateralization and immunohistochemical study in the rat. *Brain Research* 505, 55-65.

Jouvet-Mounier D., Astic L., & Lacote D. (1970). Ontogenesis of the states of sleep in rat, cat, and guinea pig during the first postnatal month. *Developmental Psychobiology* 2, 216-239.

Jurgens, C. W., Bell, K. A., McQuiston, A. R., & Guido, W. (2012). Optogenetic stimulation of the corticothalamic pathway affects relay cells and GABAergic neurons differently in the mouse visual thalamus. *PLoS One* 7, e45717.

Kay, J. N., De la Huerta, I., Kim, I. J., Zhang, Y., Yamagata, M., Chu, M. W., Meister, M., & Sanes, J. R. (2011). Retinal ganglion cells with distinct directional preferences differ in molecular identity, structure, and central projections. *Journal of Neuroscience* 31(838), 7753-7762.

Kerschensteiner, D., & Guido, W. (2017). Organization of the dorsal lateral geniculate nucleus in the mouse. *Visual Neuroscience* 34, e008.

Kim, I. J., Zhang, Y., Yamagata, M., Meister, M., & Sanes, J. R. (2008). Molecular identification of a retinal cell type that responds to upward motion. *Nature* 452(7186), 478-482.

Kim, I. J., Zhang, Y., Meister, M., & Sanes, J. R. (2010). Laminar restriction of retinal ganglion cell dendrites and axons: subtype-specific developmental patterns revealed with transgenic markers. *Journal of Neuroscience* 30(4), 1452-1462.

Kimura, A., Donishi, T., Okamoto, K., & Tamai, Y. (2005). Topography of projections from the primary and non-primary auditory cortical areas to the medial geniculate body and thalamic reticular nucleus in the rat. *Journal of Neuroscience* 135, 1325-1342.

Kimura, A. (2014). Diverse subthreshold cross-modal sensory interactions in the thalamic reticular nucleus: implications for new pathways of cross-modal attentional gating function. *European Journal of Neuroscience* 39, 1405-1418.

Kishino, A., Ishige, Y., Tatsuno, T., Nakayama, C., & Noguchi, H. (1997). BDNF prevents and reverses adult rat motor neuron degeneration and induces

axonal outgrowth. *Experimental Neurology*, 144(2), 273-286.

Khazipov, R., & Luhmann, H. J. (2006). Early patterns of electrical activity in the developing cerebral cortex of humans and rodents. *Trends in Neuroscience* 29, 414-418.

Kroeger, D., Ferrari, L. L., Petit, G., Mahoney, C. E., Fuller, P. M., Arrigoni, E., & Scammell, T. E. (2017). Cholinergic, glutamatergic, and GABAergic neurons of the pedunculopontine tegmental nucleus have distinct effects on sleep/wake behavior in mice. *Journal of Neuroscience* 37, 1352-1366.

Landisman, C. E., Long, M. A., Beierlein, M., Deans, M. R., Paul, D. L., & Connors, B. W. (2002). Electrical synapses in the thalamic reticular nucleus. *Journal of Neuroscience* 22, 1002-1009.

Lee, S. H., & Dan, Y. (2012). Neuromodulation of brain states. *Neuron* 76(1), 209-222.

LeVay, S., & Ferster, D. (1977). Relay cell classes in the lateral geniculate nucleus of the cat and the effects of visual deprivation. *Journal of Comparative Neurology* 172(4), 563-584.

Lidov, H. G., & Molliver, M. E. (1982). Immunohistochemical study of the development of serotonergic neurons in the rat CNS. *Brain Research Bulletin* 9(1-6), 559-604.

Lo, F. S., Lu, S. M., & Sherman, S. M. (1991). Intracellular and extracellular in vivo recording of different response modes for relay cells of the cat's lateral geniculate nucleus. *Experimental Brain Research* 83(2), 317-328.

Long, M. A., Landisman, C. E., & Connors, B. W. (2004). Small clusters of electrically coupled neurons generate synchronous rhythms in the thalamic reticular nucleus. *Journal of Neuroscience* 24, 341-349.

Lu, S. M., Guido, W., & Sherman, S. M. (1993). The brain-stem parabrachial region controls mode of response to visual stimulation of neurons in the cat's lateral geniculate nucleus. *Visual Neuroscience* 10(4), 631-642.

Luo, L., Callaway, E. M., & Svoboda, K. (2008). Genetic dissection of neural circuits. *Neuron* 57(5), 634-660.

Ma, R., Cui, H., Lee, S. H., Anastasio, T. J., & Malpeli, J. G. (2013). Predictive encoding of moving target trajectory by neurons in the parabigeminal nucleus. *Journal of Neurophysiology* 109(8), 2029-2043.

Madisen, L., Zwingman, T. A., Sunkin, S. M., Oh, S. W., Zariwala, H. A., Gu, H., Ng, L. L., Palmiter, R. D., Hawrylycz, M. J., Jones, A. R., Lein, E. S., & Zeng, H. (2010). A robust and high-throughput Cre reporting and characterization system for the whole mouse brain. *Nature Neuroscience* 13, 133-140.

Madisen, L., Mao, T., Koch, H., Zhuo, J. M., Berenyi, A., Fujisawa, S., Hsu, Y. W., Garcia, A. J., Gu, X., Zanella, S., Kidney, J., Gu, H., Mao, Y., Hooks, B. M., Boyden, E. S., Buzsaki, G., Ramirez, J. M., Jones, A. R., Svoboda, K.,

Han, X., Turner, E., & Zeng, H. (2012). A toolbox of cre-dependent optogenetic transgenic mice for light-induced activation and silencing. *Nature Neuroscience* 15, 793-802.

Masland, R. H., & Martin, P. R. (2007). The unsolved mystery of vision. *Current Biology* 17(15), 577-582.

McCormick, D. A., & Prince, D. A. (1986). Acetylcholine induces burst firing in thalamic reticular neurones by activating a potassium conductance. *Nature* 319(6052), 402-405.

McCormick, D. A., & Prince, D. A. (1987). Actions of acetylcholine in the guinea-pig and cat medial and lateral geniculate nuclei, in vitro. *Journal of Physiology* 392, 147-165.

McCormick, D. A., & Pape, H. C. (1988). Acetylcholine inhibits identified interneurons in the cat lateral geniculate nucleus. *Nature* 334(6179), 246-248.

McCormick, D. A., & Feeser, H. R. (1990). Functional implications of burst firing and single spike activity in lateral geniculate relay neurons. *Neuroscience* 39(1), 103-113.

McCormick, D. A. (1992). Cellular mechanisms underlying cholinergic and noradrenergic modulation of neuronal firing mode in the cat and guinea pig dorsal lateral geniculate nucleus. *Journal of Neuroscience* 12(1), 278-289.

McCormick, D. A., McGinley, M. J., & Salkoff, D. B. (2015). Brain state dependent activity in the cortex and thalamus. *Current Opinion in Neurobiology* 31, 133-140.

Mena-Segovia, J., & Bolam, J. P. (2017). Rethinking the Pedunculopontine nucleus: from cellular organization to function. *Neuron* 94(1), 7-18.

Mesulam, M. M., Mufson, E. J., Wainer, B. H., & Levey, A. I. (1983). Central cholinergic pathways in the rat: an overview based on an alternative nomenclature (Ch1-Ch6). *Neuroscience* 10(4), 1185-1201.

Mirmiran, M., Maas, Y. G., & Ariagno, R. L. (2003). Development of fetal and neonatal sleep and circadian rhythms. *Sleep Medicine Reviews* 7, 321-334.

Mitrofanis, J., & Baker, G. E. (1993). Development of the thalamic reticular and perireticular nuclei in rats and their relationship to the course of growing corticofugal and corticopetal axons. *Journal of Comparative Neurology* 338, 575-587.

Molnár, Z., & Blakemore C. (1996). How do thalamic axons find their way to the cortex? *Trends in Neuroscience* 18, 389-397.

Molnár, Z., Higashi, S., & López-Bendito G. (2003). Choreography of early thalamic development. *Cerebral Cortex* 13, 661-669.

Montero, V. M., Guillery, R. W., & Woolsey, C. N. (1977). Retinotopic organization within the thalamic reticular nucleus demonstrated by a double label autoradiographic technique. *Brain Research* 138, 407-421.

Montero, V. M. (1991). A quantitative study of synaptic contacts on interneurons and relay cells of the cat lateral geniculate nucleus. *Experimental Brain Research* 86(2), 257-270.

Mu, J. S., Li, W. P., Yao, Z. B., & Zhou, X. F. (1999). Deprivation of endogenous brain-derived neurotrophic factor results in impairment of spatial learning and memory in adult rats. *Brain Research* 835(2), 259-265.

Ni, K. M., Hou, X. J., Yang, C. H., Dong, P., Li, Y., Zhang, Y., Jiang, P., Berg, D. K., Duan, S., & Li, X. M. (2016). Selectively driving cholinergic fibers optically in the thalamic reticular nucleus promotes sleep. *eLife* 5, e10382.

Ohara, P. T., & Lieberman, A. R. (1985). The thalamic reticular nucleus of the adult rat: experimental anatomical studies. *Journal of Neurocytology* 14, 365-411.

O'Leary, D. D., Ruff, N. L., & Dyck, R. H. (1994). Development, critical period plasticity, and adult reorganizations of mammalian somatosensory systems. *Current Opinion in Neurobiology* 4, 535-544.

Ozaki, T., & Kaplan, E. (2006). Brainstem input modulates globally the transmission through the lateral geniculate nucleus. *International Journal of Neuroscience* 116(3), 247-264.

Pare, D., Smith, Y., Parent, A., & Steriade, M. (1988). Projections of brainstem core cholinergic and non-cholinergic neurons of cat to intralaminar and reticular thalamic nuclei. *Neuroscience* 25(1), 69-86.

Parent, A., Pare, D., Smith, Y., & Steriade, M. (1988). Basal forebrain cholinergic and noncholinergic projections to the thalamus and brainstem in cats and monkeys. *Journal of Comparative Neurology* 277(2), 281-301.

Pasquier, D. A., & Villar, M. J. (1982). Subcortical projections to the lateral geniculate body in the rat. *Experimental Brain Research* 48(3), 409-419.

Paxinos, G., & Franklin, K. (2004). *The mouse brain in stereotaxic coordinates.* Elsevier Science, Oxford.

Pfeiffenberger, C., Yamada, J., & Feldheim, D. A. (2006). Ephrin-As and patterned retinal activity act together in the development of topographic maps in the primary visual system. *Journal of Neuroscience* 26(50), 12873-12884.

Pinault, D. (2004). The thalamic reticular nucleus: structure, function and concept. *Brain Research Reviews* 46, 1-31.

Pinault, D., & Deschenes, M. (1992). Muscarinic inhibition of reticular thalamic cells by basal forebrain neurones. *Neuroreport* 3, 1101-1104.

Piscopo, D. M., El-Danaf, R. N., Huberman, A. D., & Niell, C. M. (2013). Diverse visual features encoded in mouse lateral geniculate nucleus. *Journal of Neuroscience* 33(11), 4642-4656.

Pita-Almenar, J. D., Yu, D., Lu, H. C., & Beierlein, M. (2014). Mechanisms underlying desynchronization of cholinergic-evoked thalamic network activity. *Journal of Neuroscience* 34, 14463-14474.

Pollerberg, G. E., Thelen, K., Theiss, M. O., & Hochlehnert, B. C. (2013). The role of cell adhesion molecules for navigating axons: density matters. *Mechanisms of Development* 130(6-8), 359-372.

Reese, B. E. (1988). 'Hidden lamination' in the dorsal lateral geniculate nucleus: the functional organization of this thalamic region in the rat. *Brain Research* 472(2), 119-137.

Robertson, R. T., Baratta, J., Yu, J., & Guthrie, K. M. (2006). A role for neurotrophin-3 in targeting developing cholinergic axon projections to cerebral cortex. *Neuroscience* 143(2), 523-539.

Rousso, D. L., Qiao, M., Kagan, R. D., Yamagata, M., Palmiter, R. D., & Sanes, J. R. (2016). Two Pairs of ON and OFF Retinal Ganglion Cells Are Defined by Intersectional Patterns of Transcription Factor Expression. *Cell Reports* 15(9), 1930-1944.

Scarnati, E., Gasbarri, A., Campana, E., & Pacitti, C. (1987). The organization of nucleus tegmenti pedunculopontinus neurons projecting to basal ganglia and thalamus: a retrograde fluorescent double labeling study in the rat. *Neuroscience Letters* 79(1-2), 11-16.

Schlaggar, B. L., & O'Leary, D. D. (1994). Early development of the somatotopic map and barrel patterning in rat somatosensory cortex. *Journal of Comparative Neurology* 346, 80-96.

Seabrook, T. A., El-Danaf, R. N., Krahe, T. E., Fox, M. A., & Guido, W. (2013). Retinal input regulates the timing of corticogeniculate innervation. *Journal of Neuroscience* 33(24), 10085-10097.

Sefton, A. J., & Martin, P. R. (1984). Relation of the parabigeminal nucleus to the superior colliculus and dorsal lateral geniculate nucleus in the hooded rat. *Experimental Brain Research* 56(1), 144-148.

Shang, C., Chen, Z., Liu, A., Li, Y., Zhang, J., Qu, B., Yan, F., Zhang, Y., Liu, W., Guo, X., Li, D., Wang, Y., & Cao, P. (2018). Divergent midbrain circuits orchestrate escape and freezing responses to looming stimuli in mice. *Nature Communications* 9(1), 1232.

Shang, C., Liu, Z., Chen, Z., Shi, Y., Wang, Q., Liu, S., Li, D., & Cao, P. (2015). A parvalbumin-positive excitatory visual pathway to trigger fear responses in mice. *Science* 348(6242), 1472-1477.

Shen, J., & Colonnese, M. T. (2016). Development of activity in the mouse visual Cortex. *Journal of Neuroscience* 36, 12259-12275.

Sherk, H. (1978). Visual response properties and visual field topography in the cat's parabigeminal nucleus. *Brain Research* 145(2), 375-379.

Sherk, H. (1979). A comparison of visual-response properties in cat's parabigeminal nucleus and superior colliculus. *Journal of Neurophysiology* 42(6), 1640-1655.

Sherman, S. M., & Koch, C. (1986). The control of retinogeniculate transmission in the mammalian lateral geniculate nucleus. *Experimental Brain Research* 63(1), 1-20.

Sherman, S. M. (1996). Dual response modes in lateral geniculate neurons: mechanisms and functions. *Visual Neuroscience* 13(2), 205-213.

Sherman, S. M., & Guillery, R. W. (1996). Functional organization of thalamocortical relays. *Journal of Neurophysiology* 76(3), 1367-1395.

Sherman, S. M., & Guillery, R. W. (1998). On the actions that one nerve cell can have on another: distinguishing "drivers" from "modulators". *Proceedings of the National Academy of Sciences* 95(12), 7121-7126.

Sherman, S. M. (2001). Tonic and burst firing: dual modes of thalamocortical relay. *Trends in Neuroscience* 24(2), 122-126.

Sherman, S. M., & Guillery, R. W. (2002). The role of the thalamus in the flow of information to the cortex. *Philosophical Transactions of the Royal Society of London Britain Biological Sciences* 357(1428), 1695-1708.

Sherman, S. M. (2005). Thalamic relays and cortical functioning. *Progress in Brain Research* 149, 107-126.

Smith, Y., Pare, D., Deschenes, M., Parent, A., & Steriade, M. (1988). Cholinergic and non-cholinergic projections from the upper brainstem core to the visual thalamus in the cat. *Experimental Brain Research* 70(1), 166-180.

Sokhadze, G., Campbell, P. W., & Guido, W. (2018). Postnatal development of cholinergic input to the thalamic reticular nucleus of the mouse. *European Journal of Neuroscience, In Press.*

Stanford, L. R., Friedlander, M. J., & Sherman, S. M. (1983). Morphological and physiological properties of geniculate W-cells of the cat: a comparison with X- and Y-cells. *Journal of Neurophysiology* 50(3), 582-608.

Steriade, M., Parent, A., Pare, D., & Smith, Y. (1987). Cholinergic and non-cholinergic neurons of cat basal forebrain project to reticular and mediodorsal thalamic nuclei. *Brain Research* 408(1-2), 372-376.

Steriade, M., Pare, D., Parent, A., & Smith, Y. (1988). Projections of cholinergic and non-cholinergic neurons of the brainstem core to relay and associational thalamic nuclei in the cat and macaque monkey. *Neuroscience* 25(1), 47-67.

Steriade, M. (1990). Cholinergic control of thalamic function. *Archives Internationales de Physiologie et de Biochemie* 98(3), 11-46.

Steriade, M., Datta, S., Pare, D., Oakson, G., & Curro Dossi, R. C. (1990). Neuronal activities in brain-stem cholinergic nuclei related to tonic activation processes in thalamocortical systems. *Journal of Neuroscience* 10(8), 2541-2559.

Steriade, M. (1993). Cholinergic blockage of network- and intrinsically generated slow oscillations promotes waking and REM sleep activity patterns in thalamic and cortical neurons. *Progress in Brain Research* 98, 345-355.

Steriade, M. (2004). Acetylcholine systems and rhythmic activities during the waking-sleep cycle. *Progress in Brain Research* 145, 179-196.

Stevenson, J. A., & Lund, R. D. (1982). Alterations of the crossed parabigeminotectal projection induced by neonatal eye removal in rats. *Journal of Comparative Neurology* 207(2), 191-202.

Stevenson, J. A., & Lund, R. D. (1982). A crossed parabigemino-lateral geniculate projection in rats blinded at birth. *Experimental Brain Research* 45, 95-100.

Sun, Y. G., Pita-Almenar, J. D., Wu, C. S., Renger, J. J., Uebele, V. N., Lu, H. C., & Beierlein, M. (2013). Biphasic cholinergic synaptic transmission controls action potential activity in thalamic reticular nucleus neurons. *Journal of Neuroscience* 33, 2048-2059.

Torborg, C. L., & Feller, M. B. (2005). Spontaneous patterned retinal activity and the refinement of retinal projections. *Progress in Neurobiology* 76(4), 213-235.

Uhlrich, D. J., Tamamaki, N., & Sherman, S. M. (1990). Brainstem control of response modes in neurons of the cat's lateral geniculate nucleus. *Proceedings of the National Academy of Sciences* 87(7), 2560-2563.

Van Horn, S. C., Erisir, A., & Sherman, S. M. (2000). Relative distribution of synapses in the A-laminae of the lateral geniculate nucleus of the cat. *Journal of Comparative Neurology* 416(4), 509-520.

Wang, S. W., Kim, B. S., Ding, K., Wang, H., Sun, D., Johnson, R. L., Klein, W.H., & Gan, L. (2001). Requirement for math5 in the development of retinal ganglion cells. *Genes & Development* 15(1), 24-29.

Wang, H. L., & Morales, M. (2009). Pedunculopontine and laterodorsal tegmental nuclei contain distinct populations of cholinergic, glutamatergic and GABAergic neurons in the rat. *European Journal of Neuroscience* 29(2), 340-358.

Watanabe, K., & Kawana, E. (1979). Efferent projections of the parabigeminal nucleus in rats: a horseradish peroxidase (HRP) study. *Brain Research* 168(1), 1-11.

Webster, M. J., & Rowe, M. H. (1984). Morphology of identified relay cells and

interneurons in the dorsal lateral geniculate nucleus of the rat. *Experimental Brain Research* 56(3), 468-474.

Wimmer, R. D., Schmitt, L. I., Davidson, T. J., Nakajima, M., Deisseroth, K., & Halassa, M. M. (2015). Thalamic control of sensory selection in divided attention. *Nature* 526, 705-709.

Woolf, N. J., & Butcher, L. L. (1986). Cholinergic systems in the rat brain: III. Projections from the pontomesencephalic tegmentum to the thalamus, tectum, basal ganglia, and basal forebrain. *Brain Research Bulletin* 16(5), 603-637.

Woolf, N. J., Hernit, M. C., & Butcher, L. L. (1986). Cholinergic and non-cholinergic projections from the rat basal forebrain revealed by combined choline acetyltransferase and Phaseolus vulgaris leucoagglutinin immunohistochemistry. *Neuroscience Letters* 66(3), 281-286.

Yamamoto, Y., Ueta, Y., Hara, Y., Serino, R., Nomura, M., Shibuya, I., Shirahara A., & Yamashita, H. (2000). Postnatal development of orexin/hypocretin in rats. *Brain Research Molecular Brain Research* 78(1-2), 108-119.

Yang, Y. C., Hu, C. C., & Lai, Y. C. (2015). Non-additive modulation of synaptic transmission by serotonin, adenosine, and cholinergic modulators in the sensory thalamus. *Frontiers in Cellular Neuroscience* 9, 60.

Zeater, N., Buzas, P., Dreher, B., Grunert, U., & Martin, P. R. (2018). Projections of three subcortical visual centers to marmoset lateral geniculate nucleus. *Journal of Comparative Neurology*, *In Press.*

Zhan, X. J., Cox, C. L., Rinzel, J., & Sherman, S. M. (1999). Current clamp and modeling studies of low-threshold calcium spikes in cells of the cat's lateral geniculate nucleus. *Journal of Neurophysiology* 81(5), 2360-2373.

Zhao, S., Ting, J. T., Atallah, H. E., Qiu, L., Tan, J., Gloss, B., Augustine, G. J., Deisseroth, K., Luo, M., Graybiel, A. M., & Feng, G. (2011). Cell type-specific channelrhodopsin-2 transgenic mice for optogenetic dissection of neural circuitry function. *Nature Methods* 8(9), 745-752.

Zhu, J. J., & Uhlrich, D. J. (1997). Nicotinic receptor-mediated responses in relay cells and interneurons in the rat lateral geniculate nucleus. *Neuroscience* 80(1), 191-202.

Zhu, J. J., & Uhlrich, D. J. (1998). Cellular mechanisms underlying two muscarinic receptor-mediated depolarizing responses in relay cells of the rat lateral geniculate nucleus. *Neuroscience* 87(4), 767-781.

Zhu, J. J., Uhlrich, D. J., & Lytton, W. W. (1999). Properties of a hyperpolarization-activated cation current in interneurons in the rat lateral geniculate nucleus. *Neuroscience* 92(2), 445-457.

Zhu, J., & Heggelund, P. (2001). Muscarinic regulation of dendritic and axonal outputs of rat thalamic interneurons: a new cellular mechanism for uncoupling distal dendrites. *Journal of Neuroscience* 21(4), 1148-1159.

Ziburkus, J., & Guido, W. (2006). Loss of binocular responses and reduced retinal convergence during the period of retinogeniculate axon segregation. *Journal of Neurophysiology* 96(5), 2775-2784.

APPENDIX

LIST OF ABBREVIATIONS

3N: Oculomotor nucleus
A1: Primary auditory cortex
AAV: Adeno-associated virus
ACh: acetylcholine
ACSF: Artificial cerebrospinal fluid
AF: Alexa Fluor
ANOVA: Analysis of variance
AP: Antero-posterior
Aq: Cerebral aqueduct
BDNF: Brain-derived neurotrophic factor
BF: Basal forebrain
ChAT: Choline acetyltransferase
ChR2: channelrhodopsin-2
CP: Cerebral peduncle
Crh: Corticotropin releasing hormone
CT: Corticothalamic
CTB: Cholera toxin subunit B
dLGN: Dorsal lateral geniculate nucleus
DSGC: Direction-selective ganglion cell
DV: Dorso-ventral
E-I: Excitation-inhibition
eYFP: enhanced yellow fluorescent protein
HDB: Nucleus of the horizontal diagonal band
HSV: Herpes simplex virus
IGL: intergeniculate leaflet
IPSC: Inhibitory postsynaptic current
LDTg: Laterodorsal tegmentum
LED: Light-emitting diode
LP: Lateral posterior nucleus
MCPO: magnocellular nucleus
ML: Medio-lateral
MLA: Methyllycacontine
Mo5: Motor nucleus of the trigeminal nerve
NGS: Normal goat serum
non-visTRN: Non-visual TRN
NT-3: Neurotrophin-3
OT: Optic tract
OX: Optic chiasm
P: Postnatal day
PBG: Parabigeminal nucleus
PBS: Phosphate-buffered saline
PCR: polymerase chain reaction
PFA: Paraformaldehyde
Po: Posterior nucleus
PPTg: Pedunculopontine tegmentum
PT: Pretectum
RGC: Retinal ganglion cell
RMS: Root mean squared
S1: Primary somatosensory cortex
SA: Streptavidin
SC: Superior colliculus
SI: Substantia innominata
SOX: supraoptic decussation
TC: thalamocortical
tdT: tdTomato
TRN: Thalamic reticular nucleus
V1: Primary visual cortex
VB: Ventrobasal complex
visTRN: visual TRN
vLGN: Ventral lateral geniculate nucleus
vMGN: ventral medial geniculate nucleus
VPM: ventral posteromedial nucleus
VPL: Ventral posterolateral nucleus
WT: Wild type

CURRICULUM VITA

NAME:	Guela Sokhadze
ADDRESS:	Department of Anatomical Sciences & Neurobiology
	511 South Floyd Street, Room 111
	Louisville, KY, 40202
EDUCATION	
& TRAINING:	B.S., Psychology
	University of Louisville, Kentucky
	2008 - 2011
	M.S./Ph.D., Anatomical Sciences and Neurobiology
	University of Louisville, Kentucky
	2012 - present

AWARDS

2010	Summer Research Opportunity Program Award, University of Louisville, Louisville, KY. (Mentor: Dr. Ayman El-Baz).
2010	Undergraduate Research Grant, University of Louisville, Louisville, KY. (Mentor: Dr. Ayman El-Baz)
2011	Student Research Grant, San Diego Autism Research Institute (ARI), San Diego, CA.
2011	Best Student Poster Award, AAPB Annual meeting, New Orleans, LA.
2011	Student Travel Award, ISNR annual meeting, Phoenix, AZ.
2012	AAPB Citation Paper Award (*Effects of TMS on Autonomic Nervous System in Children with Autism).*

PROFESSIONAL SOCIETIES

2009- present	Member, Association for Psychological Sciences (APS)
2010- present	Member, Society for Psychophysiological Research (SPR)
2010- present	Member, Association for Applied Psychophysiology & Biofeedback (AAPB)
2010- present	Member, International Society for Neurofeedback Research (ISNR)
2013- present	Member, Society for Neuroscience (SFN)

SELECTED PUBLICATIONS

Nitzken, M., Casanova, M. F., Khalifa, F., Sokhadze, G., & El-Baz, A. S. (2011). Shape-based detection of cortex variability for more accurate discrimination between autistic and normal brains. In A. S. El-Baz, R. Acharya U, A. F. Laine & J. Suri (Eds.), *Multimodality state-of-the-art medical image segmentation and registration methodologies, II* (pp. 161-185). New York, NY: Springer-Verlag.

Gross, E., El-Baz, A. S., Sokhadze, G., Sears, L., Casanova, M. F., & Sokhadze, E. M. (2012). Induced EEG gamma oscillation alignment improves differentiation between autism and ADHD group responses in a facial categorization task. *Journal of Neurotherapy* 16(2), 78-91.

Sokhadze, E. M., Baruth, J. M., Sears, L., Sokhadze, G., El-Baz, A. S., Williams, E., Klapheke, R., & Casanova, M. F. (2012). Event-related potential study of attention regulation during illusory figure categorization task in ADHD, autism spectrum disorder, and typical children. *Journal of Neurotherapy* 16(1), 12-31.

Sokhadze, G., Campbell, P. W., & Guido, W. (2018). Postnatal development of cholinergic input to the thalamic reticular nucleus of the mouse. *European Journal of Neuroscience*. doi:10.111/ejn.13942.

Sokhadze, G., Seabrook, T. A., & Guido, W. (2018). The absence of retinal input disrupts the development of cholinergic brainstem projections in the mouse dorsal lateral geniculate nucleus. *Journal of Neural Development, in revision.*

SELECTED PRESENTATIONS

Sokhadze, G., Sears, L., & Sokhadze, E. M. (2010). Neurofeedback training to improve attention and control alertness in ADHD. *The 18th International Society Neurofeedback Research Annual Conference*. Denver, CO.

Sokhadze, G., & Carroll, T. (2010). Monitoring of peripheral physiological parameters during repetitive transcranial stimulation (TMS) treatment in autism. The *9th Annual Posters-at-the-Capitol Undergraduate Conference.* Frankfort, KY, January 26.

Sokhadze, G., El-Baz, A., Sokhadze, E., Sears, L., & Casanova, M. F. (2012). Effects of TMS on autonomic nervous system in children with autism. *The Association Applied Psychophysiology Biofeedback Annual Meeting*. Baltimore, MD.

Sokhadze, G., Sears, L., El-Baz, A., Sokhadze, E. M., & Casanova, M. F. (2012). An event-related potential study of visual spatial attention deficits in autism. *The International Society Neurofeedback Research 20th Annual Conference.* Orlando, FL.

Sokhadze, G., Zhou, N., Bickford, M. E., & Guido, W. The organization and development of cholinergic brainstem input to the mouse visual thalamus. Program No. 817.02. 2014 Neuroscience Meeting Planner. Washington D.C. Society for Neuroscience, 2014. Online.

Sokhadze, G., Govindaiah, G., & Guido, W. Developmental regulation of cholinergic input to the visual thalamus. Program No. 148.10. 2015. Chicago, IL. Society for Neuroscience, 2015. Online.

Sokhadze, G., & Guido, W. Postnatal development of cholinergic input to the thalamic reticular nucleus. Program No. 529.25. 2016. San Diego, CA. Society for Neuroscience, 2016. Online.